Ultra Wideband Ranging and Link Budget Design for Naval Crane Applications

Haris I. Volos

Thesis submitted to the Faculty of the
Virginia Polytechnic Institute and State University
in partial fulfillment of the requirements for the degree of

Master of Science
in
Electrical Engineering

R. Michael Buehrer, Chair
Jeffrey H. Reed
Steven W. Ellingson

June 1, 2006
Blacksburg, Virginia

Keywords: UWB, Ranging, Link Budget

Ultra Wideband Ranging and Link Budget Design for Naval Crane Applications

Haris I. Volos

(ABSTRACT)

In this thesis a UWB-based ranging scheme is designed, simulated, implemented and tested. This system was designed to address the problem of safely unloading cargo crates to ships in the open seas. UWB antennas are placed on the four corners of the cargo crate, providing the information needed to a ranging/positioning algorithm that estimates the orientation and distance of the ship's deck from the crate. Furthermore, the system is successfully tested in a 1/24 scale demonstration. In addition to the UWB ranging application, this thesis evaluates an already proposed modification to the traditional narrowband link budget based on the Friis transmission formula. The proposed modification replaces frequency-domain parameters with time-domain values to handle the wide bandwidth of UWB systems. The proposed approach is shown via measurements to be much more accurate than the traditional technique.

Acknowledgments

First of all, I would like to express my gratitude to my advisor, Dr. R. Michael Buehrer, for his constant support and encouragement which have inspired and motivated me throughout the course of the writing of this thesis. I would also like to thank the other members of my thesis committee, Dr. Jeffrey Reed and Dr. Steven Ellingson, for their willing participation in the process.

I must also thank the Fulbright Commission of Cyprus for selecting me to be one of the recipients of the Cyprus America Scholarship Program (CASP). Further, I greatly appreciate the people of AMIDEAST who have been very helpful and understanding in their administering of my scholarship, especially Quincy Demordy, my scholarship advisor. This scholarship has made my studies at Virginia Tech possible.

I wish to acknowledge Joseph Gaeddert for sharing his knowledge with me on all the white boards we filled up during our fruitful discussions. I can't forget to thank my office mate, Haesoo Kim, for his help as well in many ways. I would also like to acknowledge the contributions and support of Chris Anderson, Swaroop Venkatesh, Natalia Rivera, and Rekka Mennon. The staff of MPRG has also provided timely help and support. Furthermore, I would like to thank Randall Nealy, staff engineer of VTAG, for all his help with the UWB antennas and crate. In addition, I thank Nader A. Nayfeh for his cooperation for the development of the UWB ranging demo.

Among my many friends I want especially to thank Alexandros Arsalis, Vasilis Vlachakis, Martin Holzer, and Scott Russell for being there for me. Of course I must thank my parents and my sisters for all their love and support. Finally I thank God for being by my side.

Contents

List of Figures

List of Tables

Chapter 1

Introduction

Ultra Wideband is a technology that until February 2002 was only used for radar, sensing, military communications and other niche applications. In February 2002, the FCC allowed UWB to be used for commercial data communications, radar and safety applications [1].

The FCC's ruling to allow UWB usage created a wide unlicensed band of spectrum (3.1-10.6 GHz [5]) with the potential for extremely high data rate (Gbps). However, because the allocated bandwidth overlaps with frequencies that are already used by other licensed systems, the FCC limited the maximum power transmitted in the whole band to approximately 0.5 mW, therefore limiting UWB for short range communications. However, data rate can always be traded for distance [1].

The FCC defines UWB as a signal with either a *fractional bandwidth* of 20% of the center frequency or an absolute bandwidth of 500 MHz when the center frequency is above 6 GHz [5]. This requirement can be satisfied using techniques like direct sequence (DS), spread spectrum (SS), multicarrier (MC), and impulse radio signals. The latter is the most promising method because systems utilizing it can have potentially low complexity and low cost, a noise-like signal, resistant to severe multipath fading and jamming, and have very good time domain resolution allowing for location and tracking applications [1].

This thesis will only consider impulse based UWB (I-UWB) and will examine two aspects of UWB, each in its own part: First UWB based Ranging for naval crane applications including theoretical development and demonstration, and second, UWB Link Budget design proposing a modification to the traditional narrow band link budget to make it more suitable for UWB systems.

Part I: Ultra Wideband Ranging An UWB pulse is a good candidate for ranging applications because of its short duration which can provide a resolution of millimeters. UWB is already being used in ranging applications for determining the location of objects [2, 3]. In a ranging application, a UWB pulse is transmitted, reflected, and received. By

knowing the pulse's round-trip travel time and propagation velocity, the distance between the UWB ranging device and the object that reflects the pulse back can be calculated.

An application that addresses the problem of safely and smoothly unloading crate cargo to ships that fluctuate because of sea waves will be examined both in theory and with a 1/24 scale demonstration.

Part II: Ultra Wideband Link Budget Design With the introduction of UWB systems for communications, engineers need to be able to estimate the performance of a communications system when designed. The performance of a communications link is directly related to the ratio of the received signal power to the system noise power. The procedure of estimating the signal-to-noise ratio of the link is often termed calculating a link budget. In order to calculate the signal power to noise power ratio the received power has to estimated. For traditional narrow band systems the Friis transmission formula is used. However, as will be demonstrated in this part of the thesis the Friis formula is not the optimal choice for an I-UWB system. This part of the thesis presents a suggested modification to the Friis formula which was first presented in [5] followed by a validation section evaluating the proposed link budget by taking necessary frequency and time domain measurements.

Part I

Ultra Wideband Ranging

Chapter 2

UWB Ranging Theoretical Development

2.1 Objective

In this part of this thesis an application of UWB ranging will be examined. The scenario, as is shown in Figure 2.1 includes a crane located on land or on a ship that is trying to unload a crate to a ship as smoothly as possible. The ship is expected to move up and down and to have a slope as well. In order for the crane to accommodate for the ship's fluctuations the crate is to be equipped with UWB receivers and transmitters in order to determine the relative ship's distance and orientation to the crate.

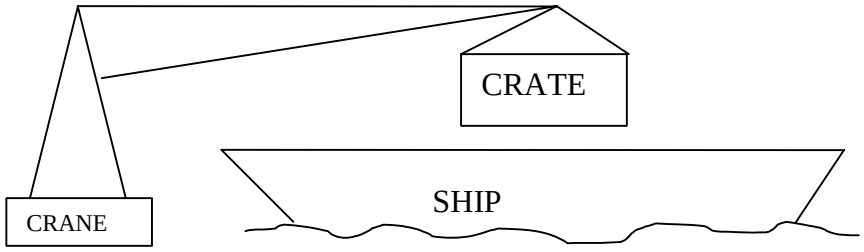

Figure 2.1: Problem Scenario

2.2 Using UWB Pulses for ranging

UWB pulses can be used in ranging applications. A UWB pulse is sent, reflected, and received back, and by knowing the pulse's travel time (assuming that the pulse travels at the speed of light) the distance between the UWB ranging device and the object that reflects the pulse back can be calculated. However, this task is not always easy because the pulse might not take the expected path, and/or strong reflections of other paths might confuse the ranging device. Therefore, a careful design of a ranging device that will be as immune to unwanted conditions as possible is desired.

The proposed design suggests that the crate has four ranging devices at its four corners that aim to find the distance of each side of the crate to the ship's deck. This design is illustrated in Figure 2.2.

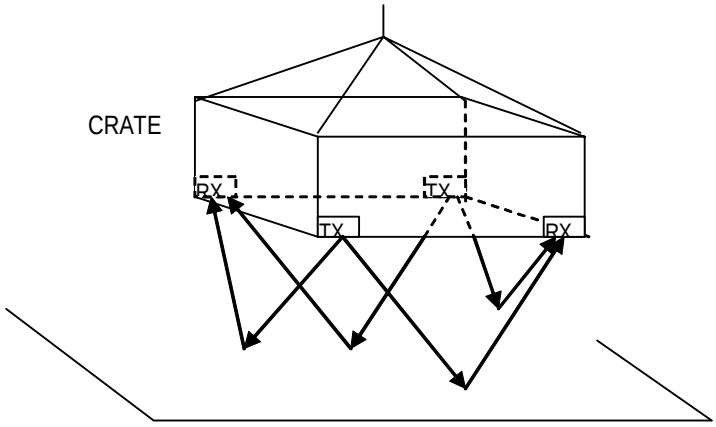

Figure 2.2: Ranging Sensors' Location

2.3 Estimating Crate Orientation

2.3.1 Estimating Height above a Level Deck

For this problem the path traveled by the pulse must be predicted, in order to estimate its traveled distance. When a pulse is sent, usually the receiver also observes copies of the same pulse shifted in time (due to multiple reflections). Because of this, it is of interest to predict the path of the first arriving pulse, which is also the shortest path. The predicted travel path for this application is a simple reflection from the ship's deck. Furthermore, it is known from physics that the angle of incidence of wave is equal to the angle of reflection. The travel path of a reflected pulse is a triangle with sides d (the base of the triangle which is equal to the separation distance between the transmitter and the receiver), and $a \,\&\, b$ as the other

two sides as shown in Figure 2.3. This path of the pulse will be useful if it is proven that the distance $a + b$ is minimum when $a = b$.

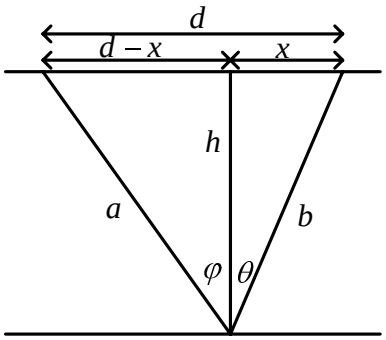

Figure 2.3: Reflected Path Distance Estimation

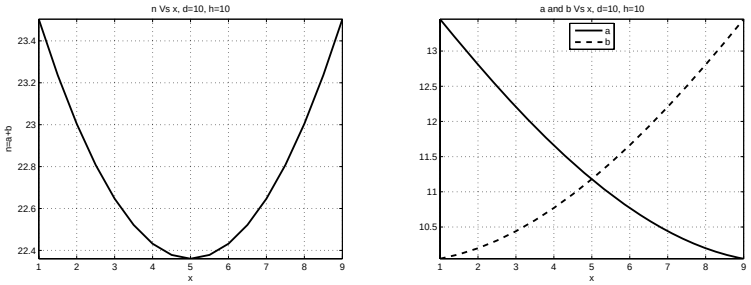

(a) $n = a + b$ Vs x (b) a and b Vs x

Figure 2.4: $n = a + b$ Minimum Point

Referring to Figure 2.3, from trigonometry:

$$sin\varphi = \frac{d - x}{a} \tag{2.1}$$

$$sin\theta = \frac{x}{b} \tag{2.2}$$

n is defined as:

$$n = a + b \tag{2.3}$$

Substituting a and b:

$$n = \frac{d - x}{sin\varphi} + \frac{x}{sin\theta} \tag{2.4}$$

Taking the first derivative with respect to x:

$$\frac{dn}{dx} = -\frac{1}{sin\varphi} + \frac{1}{sin\theta} \tag{2.5}$$

Setting the first derivative to zero:

$$\frac{1}{sin\theta} = \frac{1}{sin\varphi} \Leftrightarrow sin\varphi = sin\theta \Leftrightarrow \varphi = \theta \tag{2.6}$$

$\frac{d^2n}{dx^2} = 0$, therefore, a plot (Figure 2.4) is required that there is a minimum point at $\varphi = \theta$.

Also it's known that:

$$a = \frac{h}{cos\varphi} \tag{2.7}$$

$$b = \frac{h}{cos\theta} \tag{2.8}$$

Therefore, if $\varphi = \theta$, then $a = b$ as well as shown in Figure 2.4(b).

2.3.2 Estimating Height Above Deck with slope φ

The ship's deck is assumed to not only vary its distance from the crate, but also to have a slope φ (illustrated in Figure 2.5). Essentially what is needed is a procedure to find h given d, $n = a + b$ and φ. That procedure will be developed below.

Referring to Figure 2.5, φ is the slope of the ship's deck, the top line is the crate (d), and $n = a + b$ is the distance traveled by the pulse. Let

$$a = a_1 + a_2 \tag{2.9}$$

as shown in Figure 2.5, using Law of Sines (On the triangle with sides a, b and d)

$$\frac{sin(\varphi + \theta)}{a} = \frac{sin(180 - 2\theta)}{d}$$

$$a = \frac{dsin(\varphi + \theta)}{sin(2\theta)} \tag{2.10}$$

$$\frac{sin(\theta - \varphi)}{b} = \frac{sin(180 - 2\theta)}{d}$$

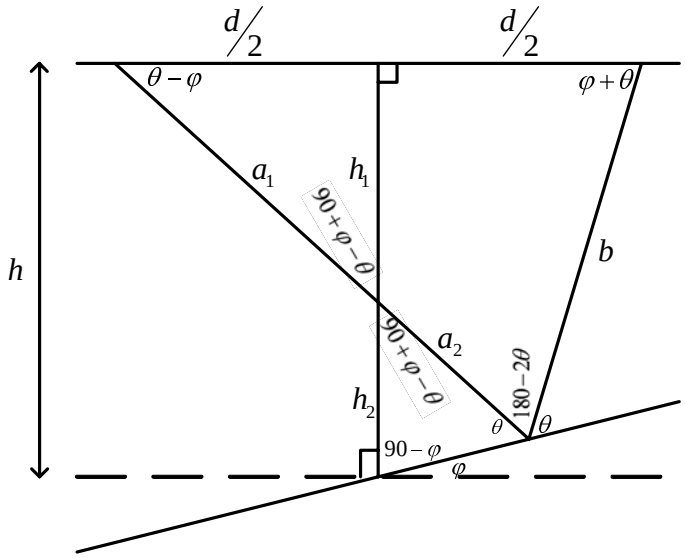

Figure 2.5: Reflection With a Slope φ

$$b = \frac{dsin(\theta - \varphi)}{sin(2\theta)} \tag{2.11}$$

Substituting a and b:

$$\begin{aligned} n &= a + b \\ &= \frac{d}{sin(2\theta)} \left[sin(\varphi - \theta) + sin(\varphi + \theta)\right] \\ &= \frac{d}{2sin\theta cos\theta} \left[sin\theta cos\varphi - cos\theta sin\varphi + sin\theta cos\varphi + cos\theta sin\varphi\right] \\ &= \frac{2dsin\theta cos\varphi}{2sin\theta cos\varphi} \\ &= \frac{dcos\varphi}{cos\theta} \end{aligned} \tag{2.12}$$

$$\begin{aligned} cos\theta = \frac{d}{n} cos\varphi \Leftrightarrow \\ \theta = \arccos(\frac{d}{n} cos\varphi) \end{aligned} \tag{2.13}$$

Using the law of sines (On the triangle with sides a_1, h_1 & $d/2$):

$$\frac{\sin\left(90-(-\varphi+\theta)\right)}{d/2}=\frac{\sin(90)}{a_1}\Leftrightarrow$$
$$a_1=\frac{d}{2\cos(\theta-\varphi)} \tag{2.14}$$

From Pythagorean Theorem (On the same triangle):

$$h_1=\sqrt{a_1^2-\frac{d^2}{4}} \tag{2.15}$$

$$a_2=a-a_1 \tag{2.16}$$

Using the law of sines (On the triangle with sides a_2, h_2 & labeled deck side):

$$\frac{\sin\left(90-\varphi\right)}{a_2}=\frac{\sin(\theta)}{h_2}\Leftrightarrow$$
$$h_2=\frac{a_2\sin(\theta)}{\cos(\varphi)} \tag{2.17}$$

$$h=h_1+h_2=\sqrt{a_1^2-\frac{d^2}{4}}+\frac{a_2\sin(\theta)}{\cos(\varphi)} \tag{2.18}$$

An expression for h given $a+b$, d and φ was just found. However, a mathematical expression to give $a+b$ given h, d, and φ was not found. A MATLAB function that can find the exact $a+b$ that gives a specific h was written instead. This is useful for creating data for testing the algorithm by means of simulation.

2.3.3 Determining Height and Orientation Relative to Deck

In the actual application the only available information is the separation distance between the transmitter and the receiver (d), and the traveled distance ($n=a+b$), but there is no information about the slope (φ). However, the d's and traveled distances $a+b$ from the ranges taken on each of the four sides are available which can be used in order to estimate the actual slope φ. Below is a procedure to find h, given d and $n=a+b$ for each of the four sides but not φ.

Referring to the Figure 2.6, the sides are numbered 1 to 4, and the corners are numbered c_1 to c_4. Further,

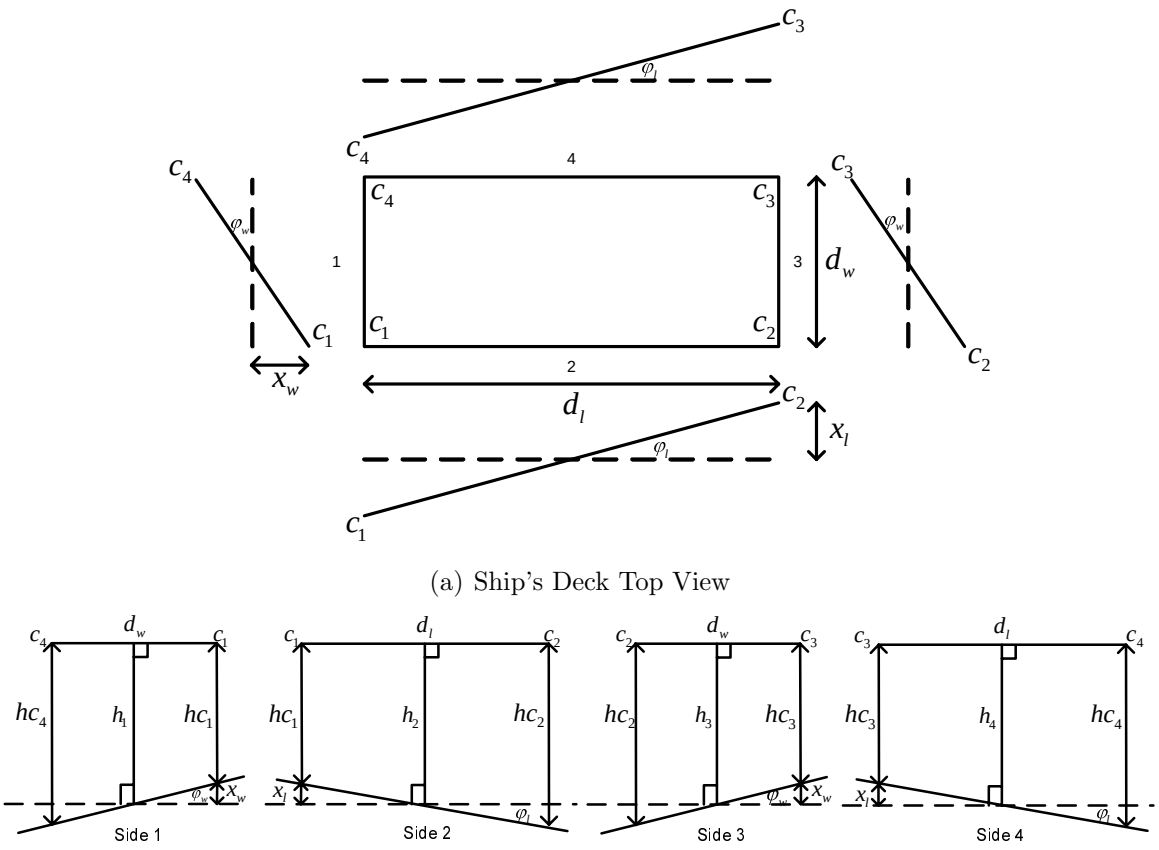

(a) Ship's Deck Top View

(b) Crate's Sides

Figure 2.6: Crate's Dimensions, Heights, and Slopes

$h_1 - h_4$ are the heights of the center of the sides 1 to 4 to the deck respectively, and
$hc_1 - hc_4$ are the heights of the corners 1 to 4 to the deck respectively.
d_w and d_l are the distances between the transmitter and receiver for the width and length side respectively.
Finally, φ_w and φ_l are the slope of the ship's deck at the width's side and length's side respectively.

Assuming that the heights $h_1 - h_4$ and the slopes φ_w & φ_l are known, the difference x between the corner heights and the center heights can be found as follows:

$$x_w = \frac{d_w}{2} \tan(\varphi_w) \tag{2.19}$$

$$x_l = \frac{d_l}{2} \tan(\varphi_l) \tag{2.20}$$

If $h_1 > h_3$

$$\begin{aligned} hc_1 &= h_2 + x_l \\ hc_2 &= h_2 - x_l \\ hc_3 &= h_4 - x_l \\ hc_4 &= h_4 + x_l \end{aligned}$$

If $h_1 < h_3$ the sign of x_l is reversed and the above operations are performed. This is because the φ's are assumed to be always positive and the only way to tell the exact orientation is the difference between the heights of the different sides.

If $h_2 > h_4$

$$\begin{aligned} hc_1 &= h_1 + x_w \\ hc_2 &= h_3 + x_w \\ hc_3 &= h_3 - x_w \\ hc_4 &= h_1 - x_w \end{aligned}$$

If $h_2 < h_4$ the sign of x_w is reversed and the above operations are performed.

$$\varphi_w = \arctan\left(\frac{|hc_1 - hc_4|}{d_w}\right) = \arctan\left(\frac{|hc_2 - hc_3|}{d_w}\right) \tag{2.21}$$

$$\varphi_l = \arctan\left(\frac{|hc_1 - hc_2|}{d_l}\right) = \arctan\left(\frac{|hc_3 - hc_4|}{d_l}\right) \tag{2.22}$$

To find the heights of the corners the following procedure is performed:

1. Assume $\varphi_l = \varphi_w = 0$
2. Find the center heights of sides 1 and 3 using Equation (2.18).
3. Find the center heights of sides 2 and 4 using Equation (2.18).
4. Find the height to corner 1 coming from the center of side 1 and coming from the center of side 2. Do the same for the other corners. [Equations (2.19) and (2.20)]
5. Average the two heights for each corner.
6. Find two new vlaues of φ_l and φ_w using the four corners.
7. Average the new φ angles.

8. Repeat from 2, until the calculated angle φ values don't change.

On more than 10000 tests with h in the range 0.5 to 10.5, $d_w = 20$, $d_l = 20$ and angles from 0 to 20, the maximum % error found was 0.002391 which is attributed to rounding errors. This indicates that algorithm given a set of valid data, assuming specific heights and slopes, converges to the assumed heights and slopes. Additional tests will follow in the next section.

Using the corner heights, the ship's deck can be plotted as shown at Figure 2.7. The top rectangle represents the crate and the rectangle below represents the ship's deck.

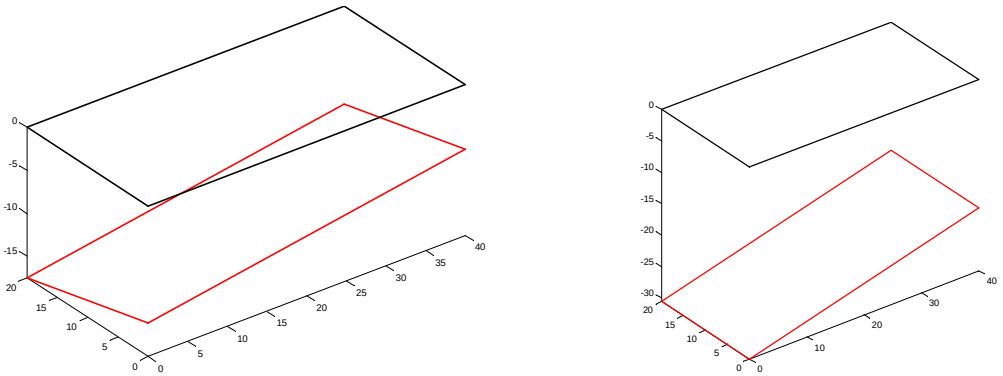

(a) $\varphi_l = 8.38^o$, $\varphi_w = 10.64^o$ (b) $\varphi_l = 14.09^o$, $\varphi_w = 0^o$

Figure 2.7: Sample Plots

2.4 Simulation Tests

The proposed algorithm for estimating the height and orientation of the crate is now evaluated by means of computer simulation.

The simulation was done for two arbitrarily chosen scenarios that roughly represent potentially actual dimensions. First, the dimensions of the crate are assumed 5x5x5 m (Figure 2.8(a)) and the maximum distance from the crate to the deck is 5 m (approximately two floors high); therefore, the maximum distance from the deck to the tx/rx antennas is 10 m. Thus the working range for the range estimator is 5 to 10 m. For the second scenario the crate was no longer assumed to be a cube, but to have the length side (d_l) equal to 10 m, instead of 5 m (Figure 2.8.)

For each case the height of one of the sides was assumed, and based on that height and the assumed slopes, the rest of the heights were calculated. Based on the assumed heights the

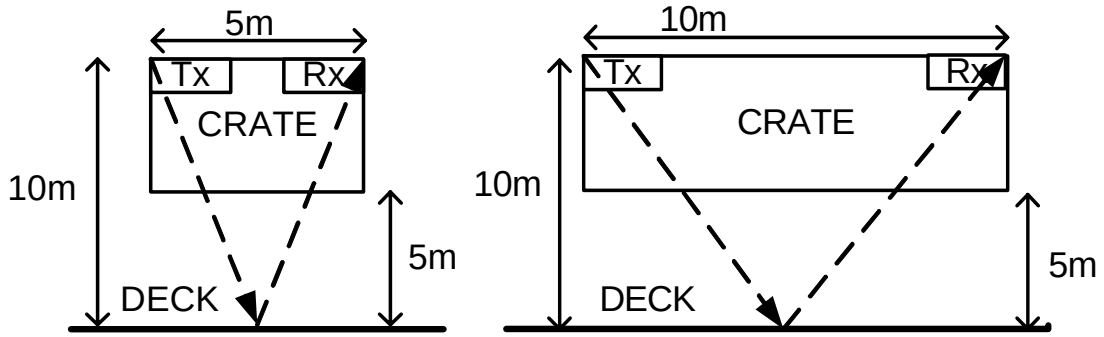

(a) 5m Side (b) 10m Side

Figure 2.8: Crate Dimensions Used for the Simulation

respective traveled distances were also calculated. Finally, a zero mean Gaussian noise was added to the assumed traveled distances before passing them to the estimation algorithm.

The simulation cases for each scenario were:

- 15 different input variances from 5 dBm^2 to -30 dBm^2 (i.e. SNR values)
- 11 different heights from 5m to 10m.
- 6 different slopes for each side from 0 to 20degrees.
- 4 different cases for each slope pair $[(\varphi_w, \varphi_l)$,$(-\varphi_w, \varphi_l)$,$(\varphi_w, -\varphi_l)$,$(-\varphi_w, -\varphi_l).]$
- All the above were repeated for each of the four different sides.

The total was 95,040 different cases for each scenario, repeated twice for improving the results.

From the results two plots were created for each side. The first plot is the estimation variance (output of the algorithm) vs the assumed height (Figures 2.9 and 2.11), and the second set of plots show the estimation variance against the input noise's variance (Figure 2.10 and 2.12.) For the variance calculations the results from all φ were included.

The estimation variance against the height for the the first dimension scenario (all sides equal to 5 m) is shown in Figure 2.9. It can be observed that the estimation variance does not vary significantly with the assumed height. Furthermore, it can be seen that for each input variance case the estimation variance is reduced. Additionally, the results for each side are almost identical. Moreover, Figure 2.10 shows the estimation variance against the input variance for the 5 m and 10 m height cases which are found to be almost identical. The estimation variance was found to have a linear relationship with the input variance to

the algorithm. The estimation variance was found to be approximately 2.5 to 2.8 times less than the input variance.

For the second dimension scenario (the length side equal to 10 m) the results are shown in Figure 2.11. It can be observed that the estimation variance does not vary significantly with the assumed height for the sides 1 and 3, which are the 5 m sides. Furthermore, the results are very close to the results from the previous scenario. On the other hand, for sides 1 and 4, the estimation variance decreases as the assumed height increases. The reason for this difference is because the base of the formed triangle is now twice as big as the other cases, causing the height estimation to be more sensitive to changes in the pulse's traveled distance because of the different assumed slopes of the reflection surface. Those fluctuations have less effect as the height of the formed triangle increases. In short, the estimation variance depends on the base to height ratio of the formed triangle.

Moreover, Figure 2.12 shows the estimation variance vs the input variance for the 5 m and 10 m height cases which, for sides 1 and 3, are found to be almost identical between each other and to the graphs shown in Figure 2.10. On the other hand, the 5 m height case, on the 10 m length sides (2,4), was found to have its estimation variance to be approximately 1.58 to 1.66 times less than the input variance. On the contrary, the 10 m height case was found to be almost identical to cases in the 5 m length sides. This observation supports the conclusion that the estimation variance depends on the base to height ratio of the formed triangle. Furthermore, as the ratio decreases the effect of the changes is reduced as shown in the 5m length sides in which the 5 m and 10 m height cases are almost identical.

From the simulation results it can be concluded that the estimation algorithm can effectively use four ranging measurements (one on each side of the crate) to estimate the height and orientation of a crate relative to a ship's deck. Furthermore, it was found that when the height is short compared to the base of the formed triangle the estimation variance is increased. However, in an actual application the reduced height will probably cause a reduced input variance because the received UWB pulse is likely to be stronger, thus providing more accurate acquisition.

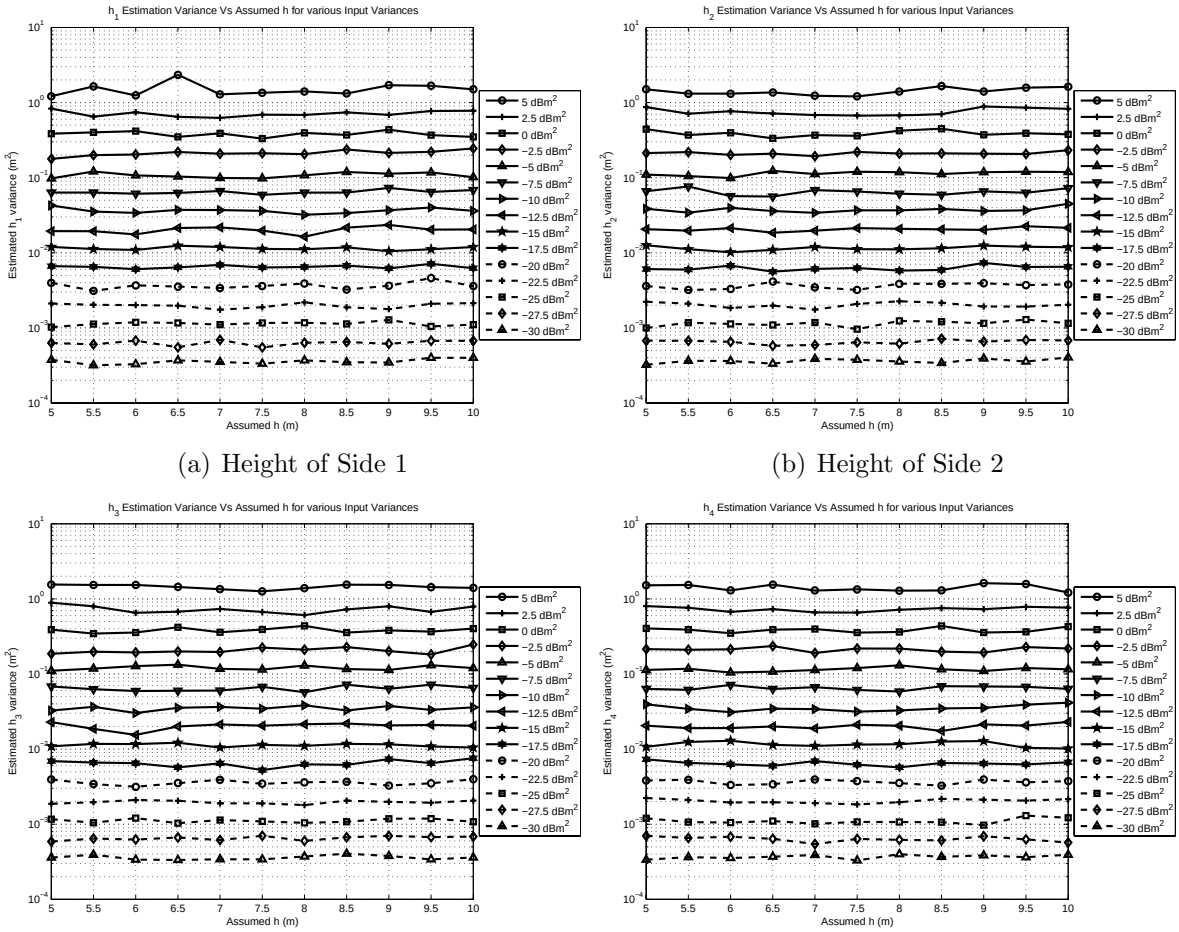

(a) Height of Side 1

(b) Height of Side 2

(c) Height of Side 3

(d) Height of Side 4

Figure 2.9: Estimation Variance Vs Assumed Height (Crate Dimensions $d_w = 5m$, $d_l = 5m$)

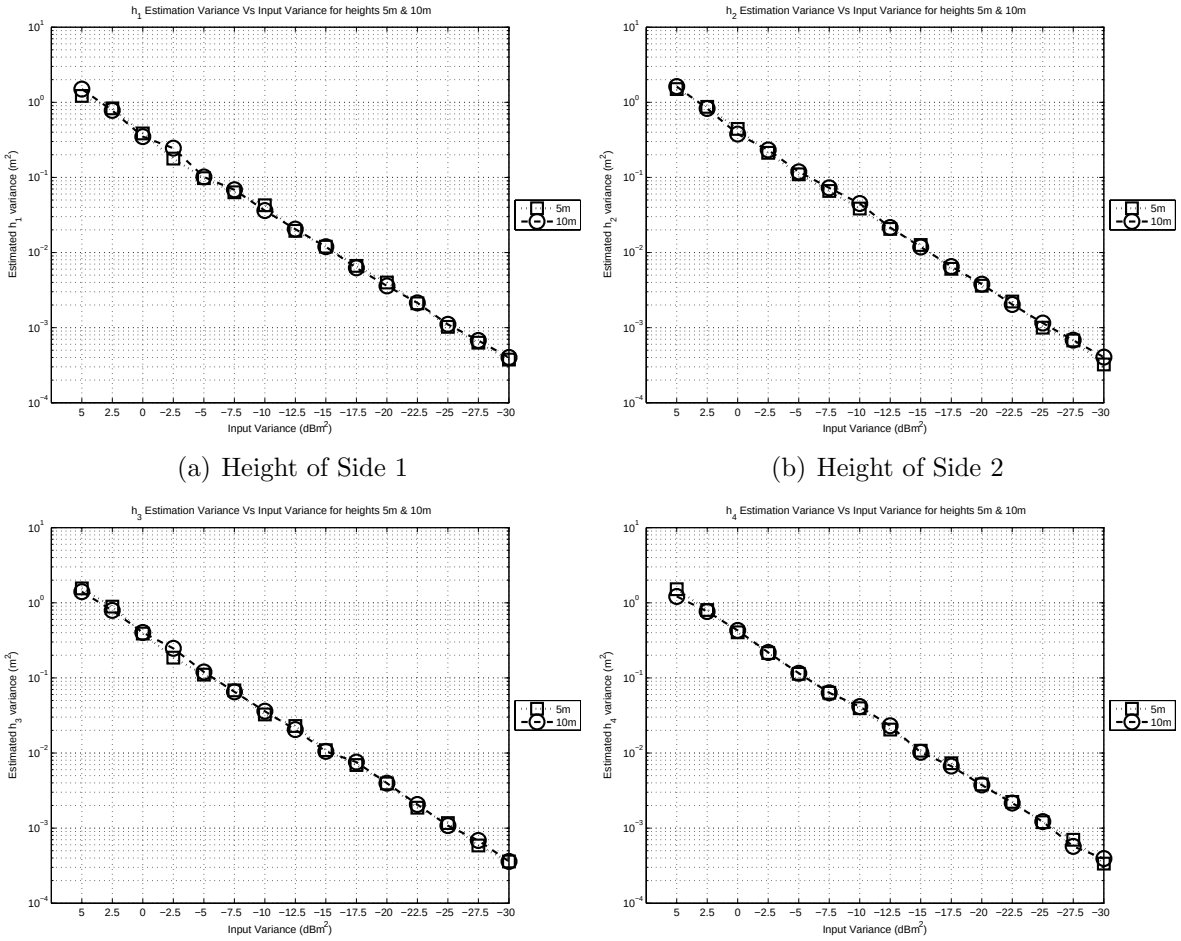

(a) Height of Side 1

(b) Height of Side 2

(c) Height of Side 3

(d) Height of Side 4

Figure 2.10: Estimation Variance Vs Input Variance (Crate Dimensions $d_w = 5m$, $d_l = 5m$)

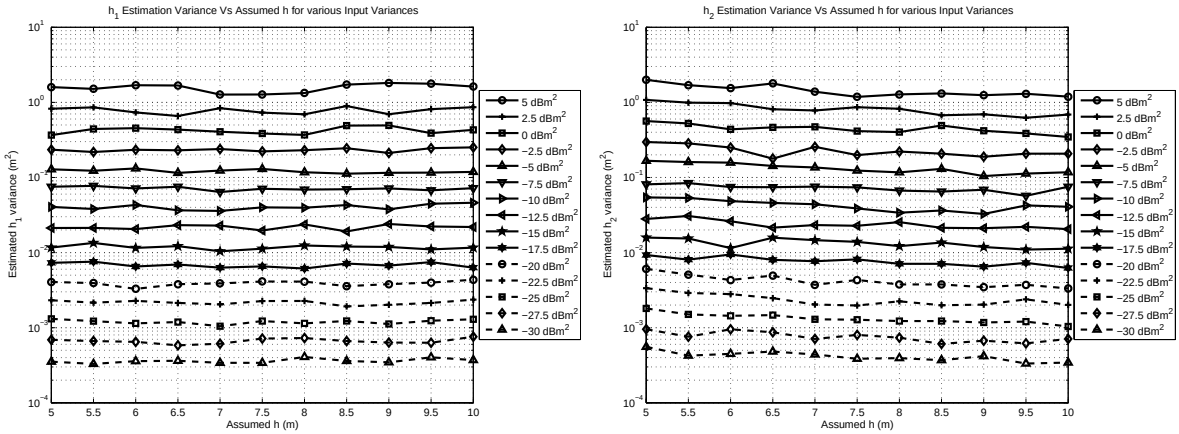

(a) Height of Side 1

(b) Height of Side 2

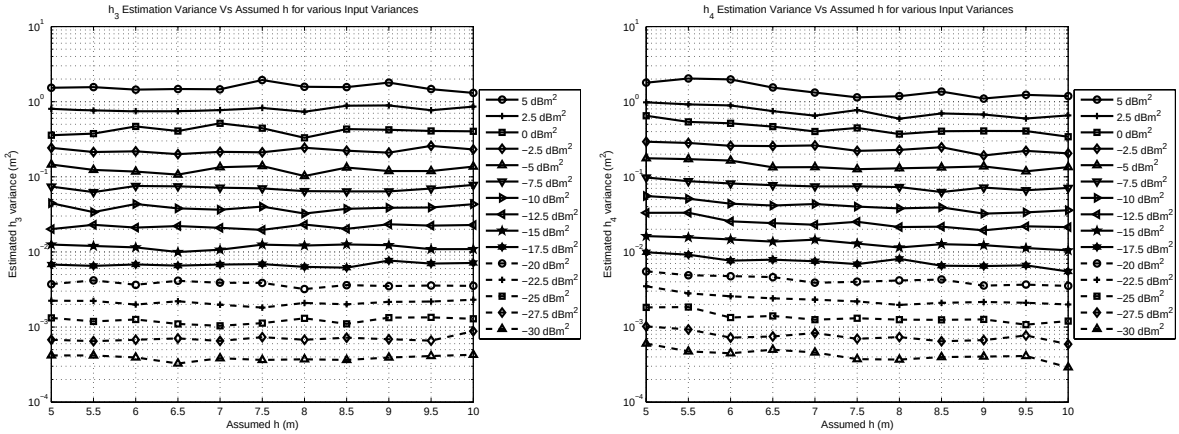

(c) Height of Side 3

(d) Height of Side 4

Figure 2.11: Estimation Variance Vs Assumed Height (Crate Dimensions $d_w = 5m$, $d_l = 10m$)

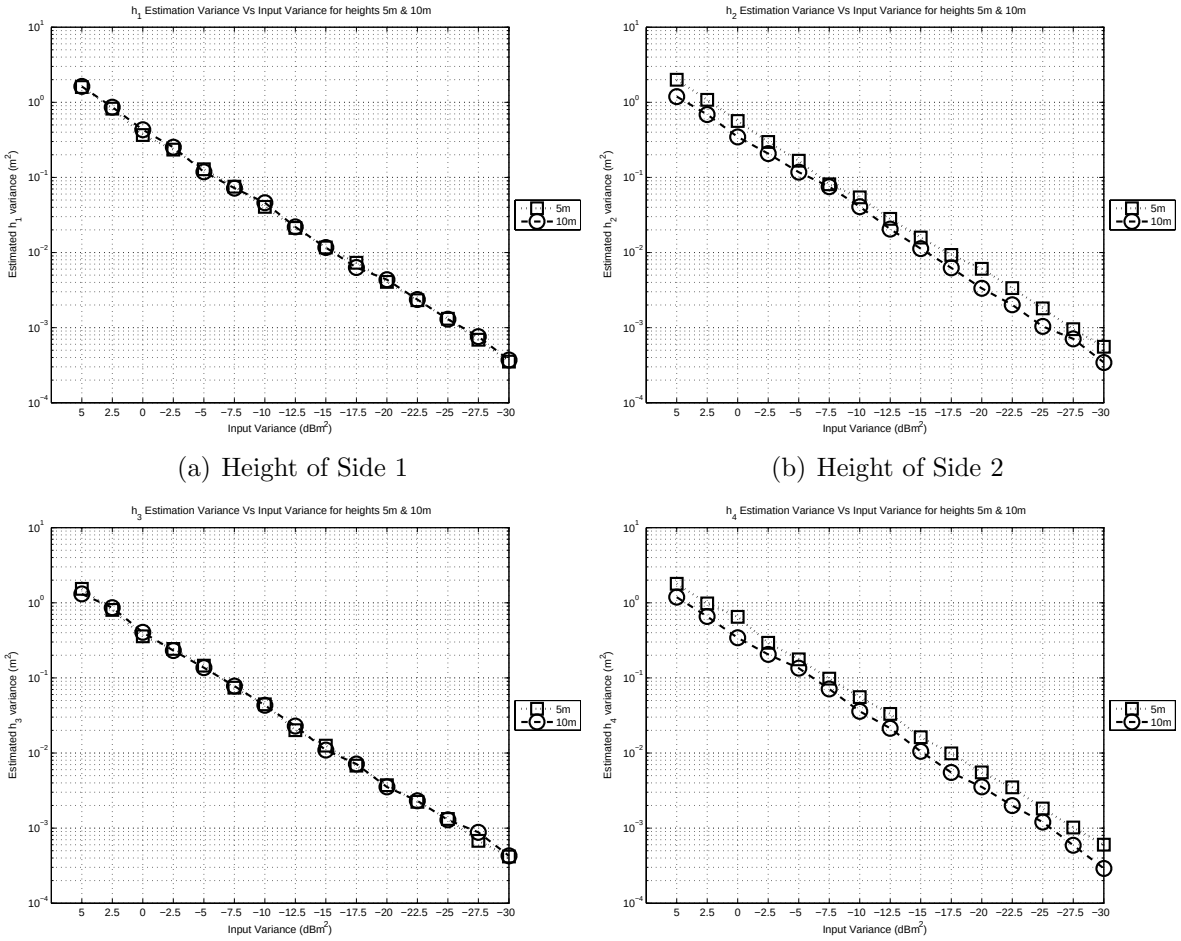

(a) Height of Side 1

(b) Height of Side 2

(c) Height of Side 3

(d) Height of Side 4

Figure 2.12: Estimation Variance Vs Input Variance (Crate Dimensions $d_w = 5m$, $d_l = 10m$)

2.5 Arrival Time Estimation Accuracy

The Cramer-Rao Lower Bound (CRLB) sets a lower bound on the variance of any unbiased estimator. This can be useful on evaluating the performance and feasibility[1] of a possible estimator.

The estimator we consider here (Figure 2.13) observes the matched filter output of the received signal for a time interval and then it estimates the time of the maximum peak (assuming LOS and no significant unwanted reflections).

The CR lower bound of the variance for this estimator was derived in [8] and is given by:

$$\sigma_{\hat{\tau}}^2 \geq \frac{1}{8\pi^2 SNR\beta_f^2} \tag{2.23}$$

where $\sigma_{\hat{\tau}}^2$ in seconds squared is the lower bound of the estimation variance of time delay τ, SNR is the signal-to-noise ratio, and β_f the bandwidth of the signal in Hz.

To express the estimation variance in meters squared Equation (2.23) only needs to be multiplied by the speed of light.

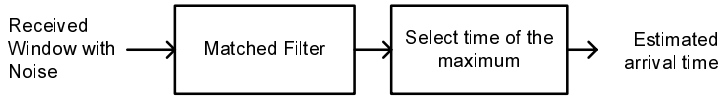

Figure 2.13: Acquisition Process

Using the proposed acquisition procedure the CRLB was calculated assuming a Gaussian pulse with pulse width $\tau_p = 2\pi\sigma$ [5] equal to 100 ps, 500 ps, 1 ns, and 2ns. The same pulses were used in a simulation of the proposed scheme. Figure 2.14 shows the result of the evaluation of the CRLB and the simulation. It can be observed that the proposed estimation scheme needs 10 dB higher SNR in order to perform as well as the theoretical lower bound suggested by the CRLB.

2.6 Sample Link Budget using Radar Equation

For further insight, it was decided to explore the requirements for archiving a certain accuracy from the ranging scheme. We assume a desired estimation variance of $6.25\times10^{-4}m^2$ (σ=0.025 m=1 inch), for which the input variance must be less than -29 dBm^2 (rounded up from Figure 2.9), therefore the input variance to the estimation algorithm must be less than

[1] if it is better than the CLRB is not feasible

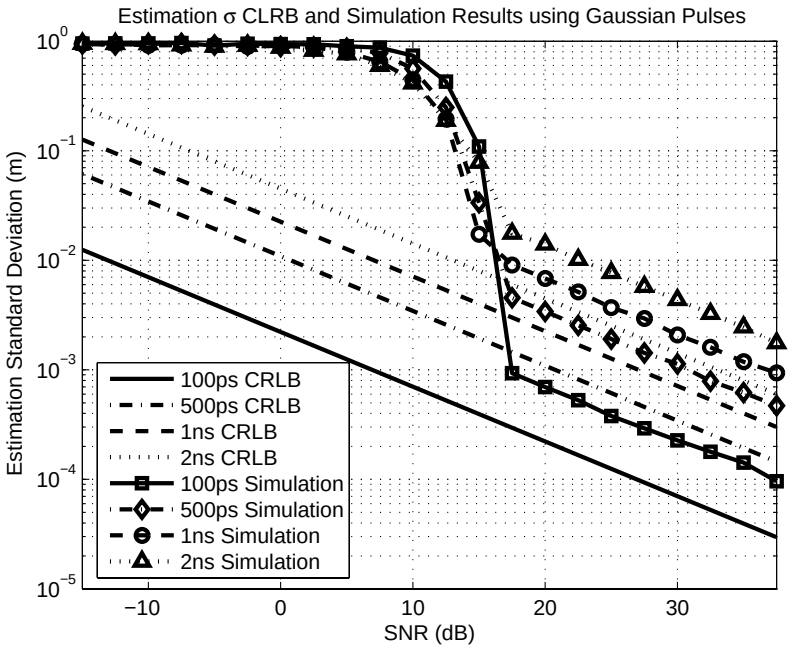

Figure 2.14: Estimation σ CRLB and Simulation Results Using Gaussian Pulses

$< 1.25 \times 10^{-3} m^2$. From Figure 2.14 the SNR required for this accurancy is at least 26 dB using a 500 ps pulse.

Assuming the crate dimensions of Figure 2.8(a) the transmitter was assumed to send a pulse every 150 ns both to the ground and to receiver. As soon as the receiver receives the first pulse (in 16.67 ns, 5 m distance), it starts looking for the ground reflected pulse over a 150ns window. The pulse for the maximum likehood range estimation (for a height 10 m, the traveled distance is 21 m) is expected to arrive in 53.3 ns, in addition to the 16.67 ns that have already elapsed. The additional 80 ns in the window is to avoid InterSymbol Interference (ISI) due to late arriving paths.

At this point we have an estimate for the SNR needed for the required estimation accuracy (σ=0.025 m=1 inch.) The last part of this section is to calculate a link budget in order to get a feel for what system parameters are needed, such as antenna gains, interleaving factor (how many pulses are needed for a complete waveform), and update rate that will archive the required SNR. The link budget is evaluated for two cases, case 1 when the crate is at the maximum ranging height (5 m above the ship deck, 10 m for the tx/rx), and case 2 when the crate is half way to the ship's deck (2.5 m.) The link budget is evaluated by estimating the received power using the radar equation [4] (Equation (2.24).) The radar equation is used even though might not be the optimal method for a UWB system as explained in Part II of this thesis. However, it provides an estimate of the needed parameters.

The radar equation is

$$P_R = \frac{P_T G_T G_R \alpha \lambda^2}{(4\pi)^3 R^4} \tag{2.24}$$

where P_R is the received power reflected from a target a distance R meters, P_T is the transmitted power, G_T and G_R are the gain of the transmit and receive antennas respectively. α is the target (floor) reflectivity, and λ is the transmission wavelength. The received SNR is given by:

$$SNR_{Rx} = \frac{P_R N_a T_w}{N_0 F} \tag{2.25}$$

where N_a is the number of waveforms averaged, T_w is the length of the received window, N_0 is the Noise Power Spectral Density, and F is the noise figure of the system.

Combining and rearranging Equations (2.24) and (2.25):

$$R_{\max} = \left(\frac{N_a P_T G_T G_R \alpha \lambda^2}{(4\pi)^3 N_0 SNR_{req}} \right)^{1/4} \tag{2.26}$$

For the link budget calculations some parameters had to be assumed, such as the interleaving factor, which is how many pulses are required for a practical receiver to construct a full waveform. The maximum number of pulses sent is $1/T_w$, this number divided by the desired update rate yields the maximum available pulses per update. Finally, dividing the maximum available pulses per update with the interleaving factor the total number of waveforms available for averaging is estimated. The two cases to follow trade update rate for more waveforms to average at the higher height case for improved SNR.

Link budget parameters for case 1 and 2
Detection Algorithm required SNR (for an Est $^2 < 1.25 \times 10^{-3} m^2$): 27 dB
Transmit Power (P_T): 1 mW
Tx,Rx Antenna Gain: 4 dBi
Floor Reflectivity(α): 0.5
Noise Figure (F): 1.25
Noise PSD (N_0)=$4 \times 10^{-21} W/Hz$
Pulse Width=500 ps
Detection Window(T_w): 150 ns
Interleaving factor: 250
Center frequency (f_c): 4GHz

Using the above parameters, the following cases are calculated:

Case 1
Max Traveled Distance (R): 21/2=10.5 m (Height= 10 m)
Update Rate:2.2 Hz

Max Allowed Pulses (N_a)= 3×10^6
Waveform Averaging (N_w):12×10^3
Evaluating Eequations (2.24), (2.25) and (2.26):
SNR_{Rx} =27.23 dB Rmax = 10.64 m

The values calculated by the link budget suggest the received SNR is 27.2 dB and the maximum working range is 21.24 m. Those values agree with the desired SNR and working range which are 27 dB and 21 m, respectively.

Case 2
Max Traveled Distance (R): 16/2= 8 m (Height=7.5 m)
Update Rate:6.67 Hz
Max Allowed Pulses (N_a)= 1×10^6
Waveform Averaging (N_w):4×10^3
SNR_{Rx}=27.19dB Rmax =8.09 m

For this system to work, the link budget suggests high antenna gains, and a low interleaving factor which was assumed to be 250, the Tektronix CSA8000B can interleave up to 4000 waveforms. However, these values might not reflect typical equipment parameters, therefore, further study of actual equipment parameters is required, and an improved acquisition scheme that will perform with as low SNR as possible is needed. Furthermore, it can be seen that we can increase the update rate as the crate approaches the deck (SNR increases). The latter observation suggests that we can trade range for update rate which is very useful for a practical system that the crane controller when the crate is too high does not need accurate and fast updates of the range. The need for more accurate and faster range updates increases as the crate approaches the ship's deck were care must be taken for its safe landing. Again, these calculations were done to determine the factors that affect the system's performance.

2.7 Another Crane Application

Besides the problem presented in this chapter, there is another problem involving a horizontally moving crane on parallel tracks as shown in Figure 2.15 that is of interest.

As the crane moves the crate which is hanging below sways back and forth. The crate's oscillation is unwanted because of the danger that it might hit something, and because the operator can not unload the crate unless it is fully still. An automatic crane controller can eliminate the sway if the exact position of the crate is known. Therefore, an electronic system needs to be designed to estimate the location of the crate. An initial idea is to have transmitters on the top of the crate and receivers on the bottom of the crane. The receivers will obtain ranging information from the known transmitting points, and by mathematically manipulating the ranging information, obtain the location of the crate (Figure 2.16). The transmitters can be replaced by transceivers that will transmit after receiving a trigger signal from a transmitter on the crane system to avoid the need of RF cables running all the way

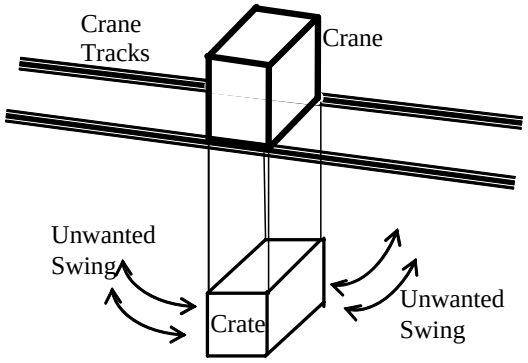

Figure 2.15: Crane Illustration (not to scale)

down to the crate.

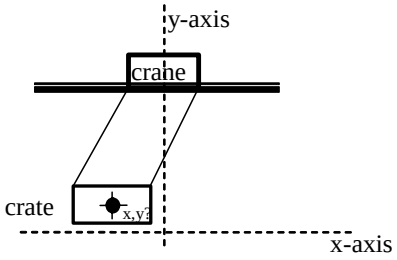

Figure 2.16: Required Crane Location

The major swaying occurs along the direction of the track, and any sway that happens in the other direction (perpendicular to the tracks) for the time being is assumed to be negligible.

2.7.1 Initial Development

As a starting point, the system can be examined in its simplest form, which assumes two receiving points and one transmitting point. This will also allow, if so desired, an initial demonstration for a proof of concept with the equipment that is currently available at MPRG, which include a two channel Digital Sampling Oscilloscope (Tektronix CSA8000B) and a 30 ps pulser made by Geozandas. The range of movements that can be examined will be determined by the antennas used for this demo. If common available large UWB antennas are used the ability of the system to estimate the position can be demonstrated but the range of motion might be limited.

Operation Description

Again, it is assumed that the crate moves only in one plane. A transmitter is placed on the crate that will send a UWB pulse. There will be two receiving points on the crane. From the time needed for the signal to travel from the transmitting position to the receiving positions the distance between each of the receiving positions to the transmitting point will be estimated. The exact position of the transmitting point will be estimated by simple trigonometry. In an actual system the transmitter can be replaced with a transceiver that will send the pulse when signaled. More transceivers and receivers can be added for additional accuracy and 3D information.

Transmit Location Estimation

The transmit location can be estimated by knowing the location of the two receive points and their distances from the transmit location as illustrated in Figure 2.17.

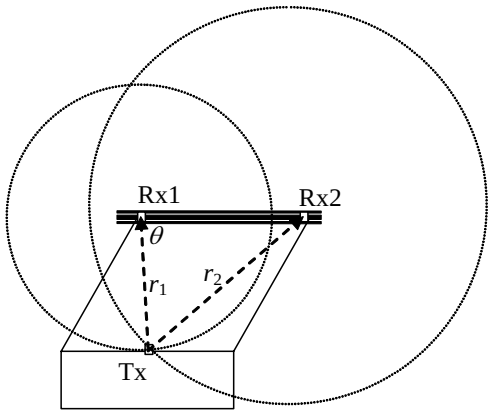

Figure 2.17: Tx Location Estimation

Let
r_1: The distance from Rx1 to Tx
r_2: The distance from Rx2 to Tx
d: The distance between Rx1 and Rx2
θ: The angle between the line Rx1-Rx2 and the line Rx1-Tx

Then, it can be shown that the Tx coordinates can be given by the following equations:

$$a = \frac{r_1^2 - r_2^2 + d^2}{2d} \tag{2.27}$$

$$\theta = \arccos\left(\frac{a}{r_1}\right) \tag{2.28}$$

$$x_{tx} = x_{Rx_1} + r_1 \cos(\theta) \tag{2.29}$$

$$y_{tx} = y_{Rx_1} - r_1 \sin(\theta) \tag{2.30}$$

2.7.2 Future Development

Future development will include simulations of the scheme as initially proposed, as well as more scenarios in which additional antennas and transmitting points can be evaluated.

Chapter 3

UWB-based Ranging:Hardware Demonstration

3.1 Description

After investigating the proposed ranging scheme in theory and via simulation, it was desired to put it to a real test. Therefore, a demonstration was planned for December 2005. The demonstration's purpose was to show that using UWB the range below a cargo crate can be estimated and an automatic crane controller can make use of the ranging information to land the crate on the platform with minimal impact. Furthermore, a real demonstration might give insight to conditions not considered during the theoretical development.

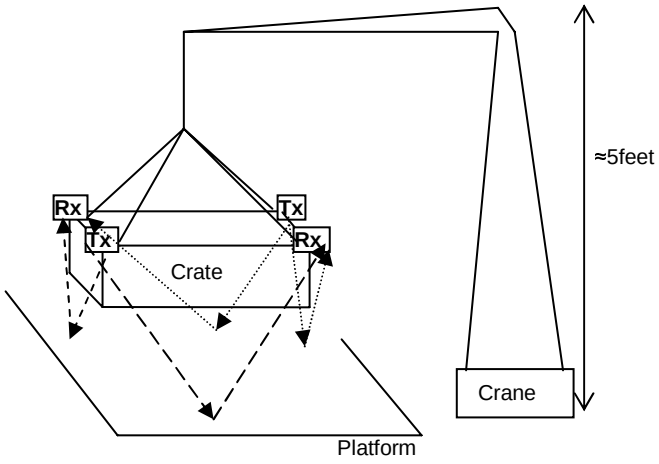

Figure 3.1: Demonstration General Layout (not to scale)

The demonstration called for a 1/24 scale demonstration using a 5 foot boom crane (Figure

3.1) in the ESM's Non-linear Dynamics Lab. Originally, the system was supposed to give 10 updates/second for all sides to the crane's control system. However, as it will be explained later, that requirement could not be met with the available equipment.

3.2 Setup and Specifications

The demo was based around the major equipment comprising the demo, the transmitter, and the receiver that were already available in MPRG's radio lab. Only the minimal equipment had to be purchased and constructed such as the crate with the antennas, an antenna switch, the four antenna dividers/combiners, a switch driving circuit, a USB Digital I/O interface, and cables.

3.2.1 Equipment List

The following equipment was used to make the demonstration possible:

- Geozondas Pulser $T_{0.5} < 30ps$, $V_{out} > 30V/50\Omega$ (GZ1106DL1 & GZ1117DN-25)
- HP33120A Function Generator
- Tektronix CSA8000B Digital Sampling Oscilloscope (DSO)
- Tektronix PS280 DC Power Supply
- National Instruments USB 6501 Digital I/O interface
- Custom made (by the author) Switch Driving Circuit
- Gateway M460 Laptop computer with LabVIEW (2.0GHz Pentium-M, 1GB RAM)
- Crate with UWB antennas made by Randall Nealy (Virginia Tech Antenna Group)
- United Microwave cables Micropore 190 (3x8ft)
- United Microwave cables Microflex 150 (3x10ft)
- Crossover Ethernet cable for direct connection between the laptop computer and the DSO
- 9dB attenuator
- Generic cables for trigger connections

Figure 3.2 shows how the equipment was connected, and Figure 3.3 presents an actual photo of the equipment. The Geozondas pulser was used as the transmitter generating a -30V 30ps pulse (time width measured at half-amplitude.) The pulser was triggered by the the HP function generator using a TTL signal of 200KHz. From the pulse the TTL triger signal was attenuated by a 9dB attenuator in order to safely trigger the Tektronix CSA8000B DSO that was used as the receiver. The DSO and the Switch Driving Circuit (for the antenna switch in the crate) were controlled by the laptop. The laptop communicated with the switch driving circuit and the crane control by the NI USB Digital I/O interface. The only information sent to the crane controller was the current range information. The crane control software was developed by Nader A. Nayfeh.

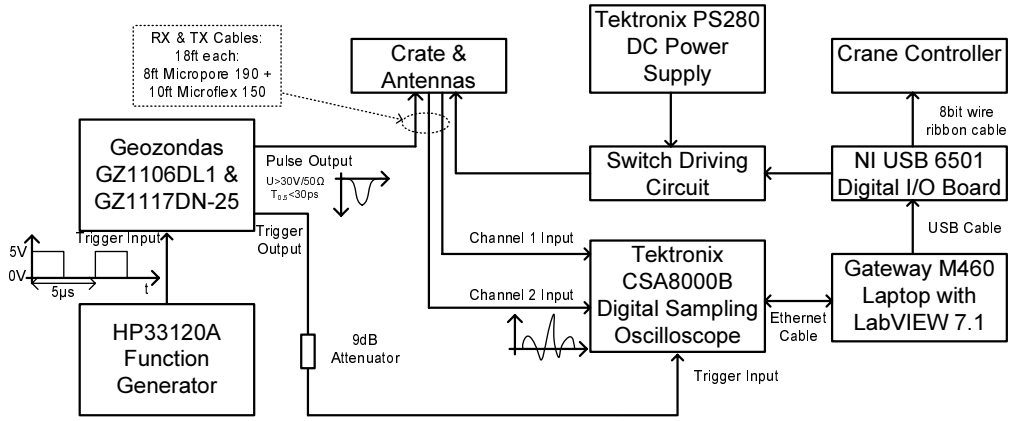

Figure 3.2: Demonstration Setup Block Diagram

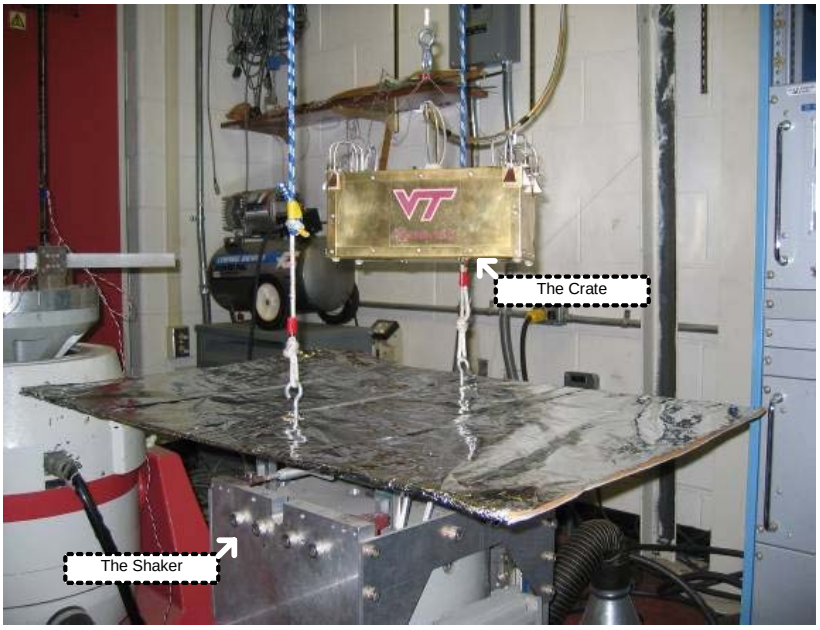

(a) Crate and Shaker

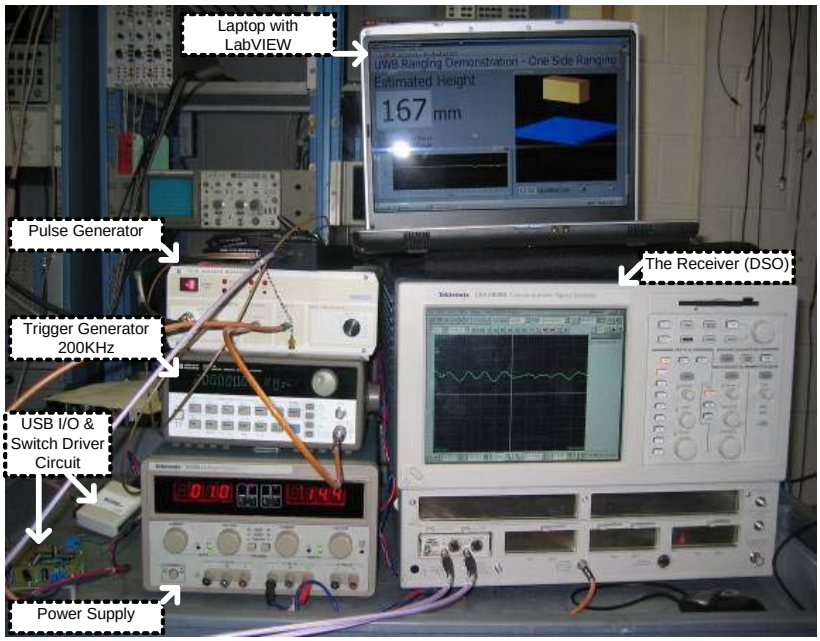

(b) Equipment

Figure 3.3: Demonstration Setup Photos

3.2.2 Transmitter and Receiver

As was previously mentioned the transmitter was a simple pulser that produces a -30V 30ps Gaussian pulse. Because of the availability of only one transmitter and the fact that the crate had two transmitting sides on the crate, an antenna switch was installed inside the crate in order to switch between transmitting sides.

The receiver was a Tektronix CSA8000B Digital Sampling Oscilloscope, capable of receiving 50, 4000 sample, waveforms per second when triggered with a 200KHz signal. Unfortunately, the DSO was not designed for real time transfer of the acquired data to an external device. The effective rate was at least 16 waveforms when it was continuously receiving the same signal without interruptions or 3 waveforms per second when it was forced to clear the acquired data and start receiving anew (which was required every time the transmission side was changed). This limitation on update rate caused the demonstration to be done in two ways, one with fast update rate using only one side for ranging, and one with the slow update rate fully utilizing the four sides and the orientation estimation algorithm which was developed in the previous chapter.

3.2.3 Crate & Antennas

(a) The Crate (b) Antennas

Figure 3.4: Crate Photo

For the demonstration one of the major components was the crate with the UWB antennas. Both, the crate and the UWB antennas (Figure 3.4) were designed and built by Randall Nealy, staff engineer of VTAG. Furthermore, inside the crate additional components (antenna switch and power dividers/combines) had to be installed, those were installed by the author with the help of Randall Nealy.

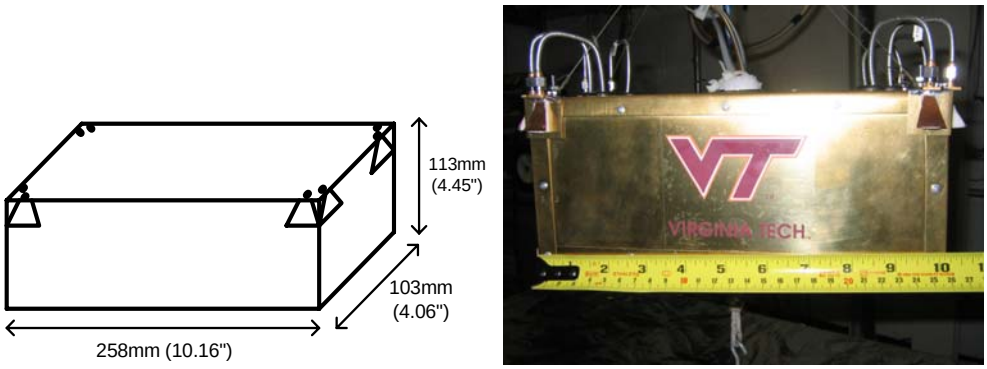

(a) Diagram (b) Photo

Figure 3.5: Crate Dimensions

The crate as shown in Figure 3.5 had dimensions of 103 mm (4.06") wide, 258 mm (10.16") long, and 113 mm (4.45") high. The dimensions are approximately 1/24 scale of a real container.

Regarding the antennas, an antenna design that will be as directive as possible was desirable. However, due to the size limitations, the actual antennas were most directive and effective in frequencies above 10 GHz. This caused reduced received signal levels because most of the pulse's energy was below 10 GHz. Also, because of the reduced directivity in the low frequencies in some cases unwanted reflections were present. However, with the choice of good quality cables and DSP the only direct effect to the demonstration was to reduce the range from 5ft to 2ft.[1] The sample pulse used for the matched filter detection process is shown in Figure 3.6(c) and was obtained after applying a bandpass filter of 8 to 18 GHz to the received signal.

Antenna Coupling

Due to the small dimensions of the crate, the transmitting and receiving antennas were very close to each other, causing a signal to be directly received from the transmit antenna (coupling). This coupling was very strong compared with the desired reflected signal. The coupling was mitigated by recording it during calibration and subtracting it from the received signal. The received signal and coupling are shown in Figures 3.6(a) & 3.6(b).

[1]The range was also limited to 255mm (10") because only 256 different values could be communicated to the crate controller and a resolution of 1mm was desired.

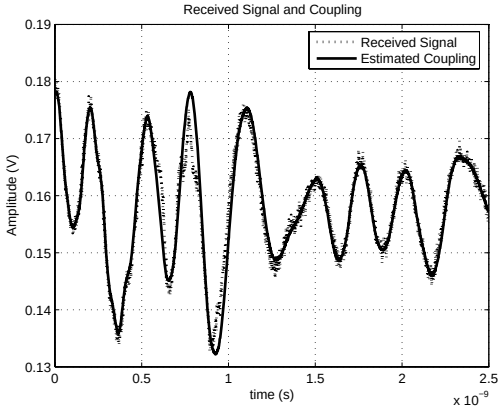

(a) Coupling

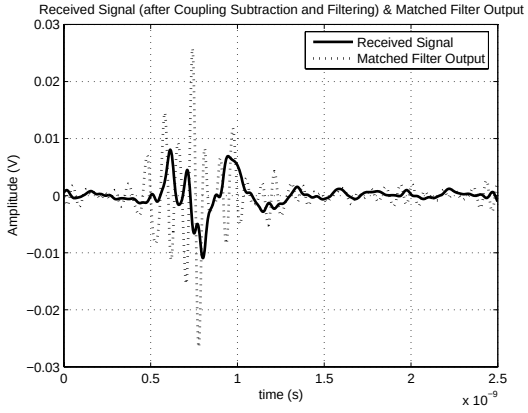

(b) Received signal with coupling subtracted and matched filter output

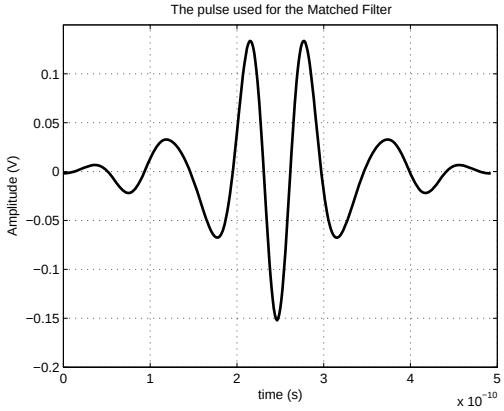

(c) The pulse used for matched filtering

Figure 3.6: Received Signals

Crate's Inside Configuration

The crate had four antenna pairs, one pair at each corner. Two of the pairs were designated transmitting pairs and the other two pairs were designated receiving pairs. The transmit and receive pairs were located on alternate corners as shown in Figure 3.7. The signals from the receiving antennas on each corner were added via RF combiners and the signals to the transmitting corner antennas were distributed via RF dividers as shown in Figure 3.7.

The parts used insise the crate included:

- 4 × Narda 4456-2 2-Way Power Dividers/Combiners 2-18GHz.
- Microwave Communications Laboratories K2-8-LIS/12P Latching Electromechanical Switch, SPDT, DC to 26.5GHz.

- 4 × 8.5” United Mircowave Microform 139 Cables.
- 4 × 9.5” United Mircowave Microform 139 Cables.

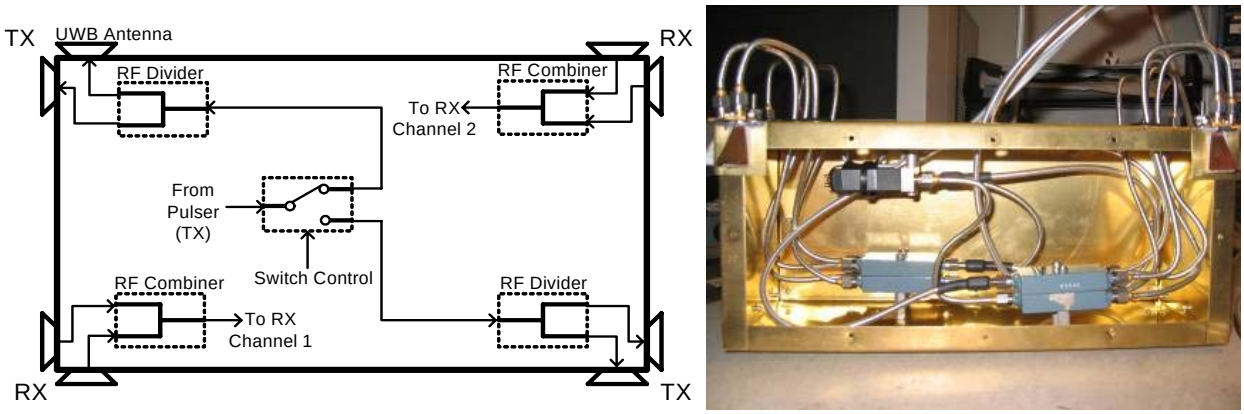

(a) Diagram (b) Photo

Figure 3.7: Crate Inside Configuration

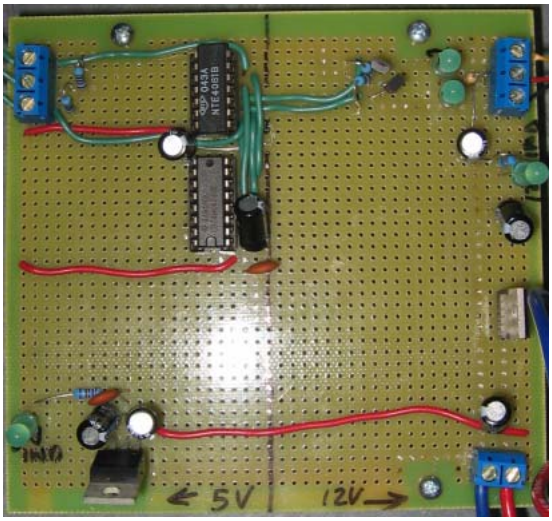

Figure 3.8: Switch Driver Circuit Photo

3.2.4 Supporting Circuitry

The antenna switch used inside the crate required a driving voltage of 12 V and 100 mA peak current. The USB I/O card used was not able to meet these requirements. For that reason,

a simple driving circuit was designed. The circuit shown in Figure 3.9 consists of three parts. First, the power supply's input voltage is regulated to 12 V using a standard regulator IC providing power to the 12 V part of the circuit, and then it is further regulated to 5 V for the 5 V components of the circuit. Second, a simple logic circuit was designed to prevent the combination "1 1" which means both sides are transmitting. That state is undesired and must be prevented to avoid potential damage to the driving transistors and to the switch itself. Third, two high speed switching transistors were used to drive the switch which only draws current when it is changing state (latching switch.) Furthermore, for additional safety the current supplied to the circuit from the external Tektronix power supply was limited to the minimum required for the proper operation of the circuit.

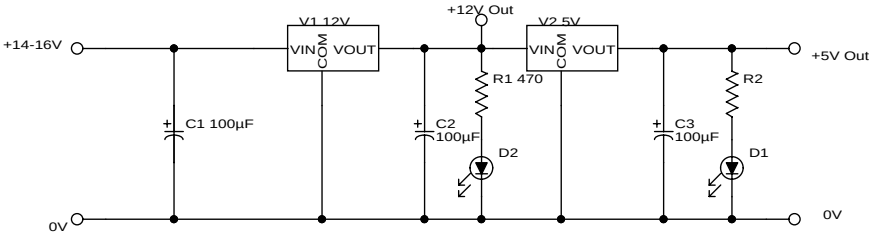

(a) Power Supply

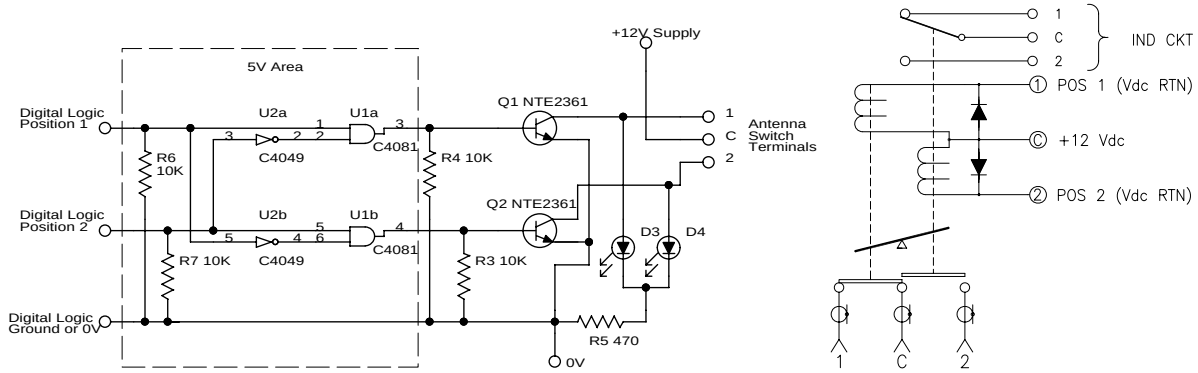

(b) Logic and Driver Part (c) Switch

Figure 3.9: Switch Driver Circuit Schematic

3.3 Software Application (LabVIEW)

The application that will read the waveforms, control the switch, process and display the required information was developed in LabVIEW because it provided all the necessary DSP functionality and the ability to connect with external peripherals such as the DSO and the USB I/O interface. Two applications were developed: first, an application utilizing the one side for ranging; and second, after the one side was perfected, the application was expanded

to four sides. Figure 3.10 shows screenshots from the two applications, one for single-side ranging, and three samples from four-side ranging. As can be seen from the screen shots the results were not limited to numbers, a 3D visual representation was also developed. Figure 3.11 shows a sample screen shot of an actual LabVIEW block diagram.

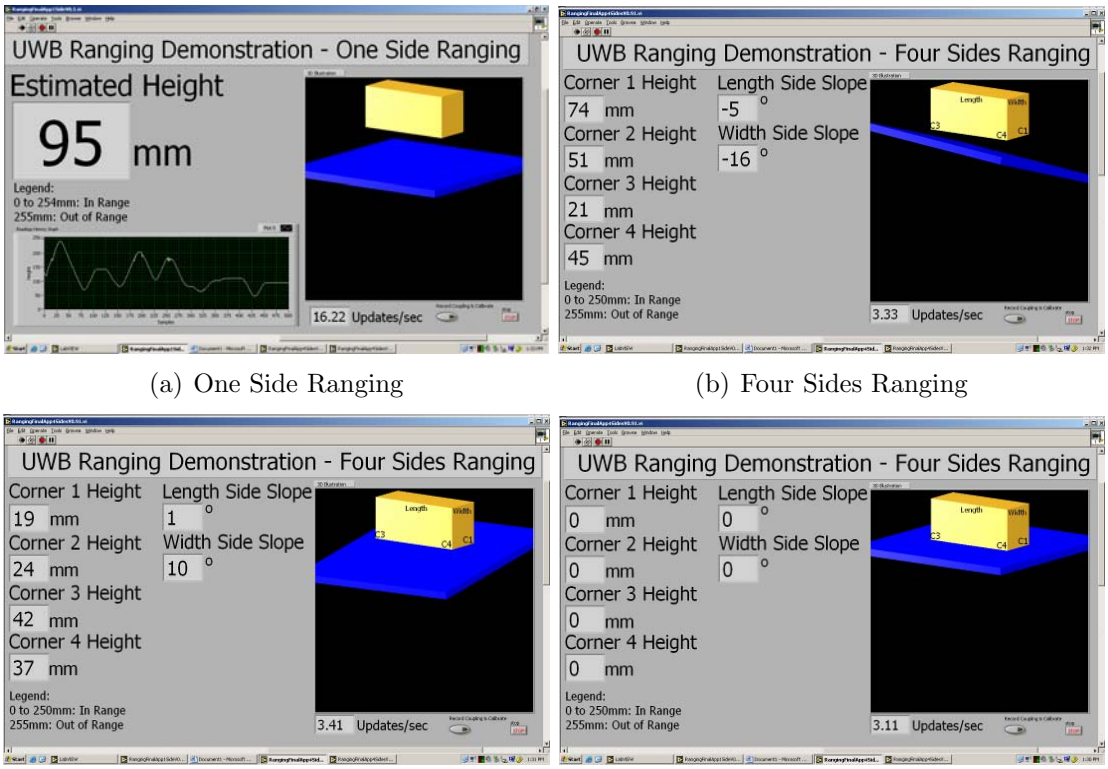

(a) One Side Ranging

(b) Four Sides Ranging

(c) Four Sides Ranging

(d) Four Sides Ranging

Figure 3.10: LabVIEW Application Screen Shots

3.3.1 Single-Side Ranging

This is a description of the single-side ranging application referring to the application's block diagram shown in Figure 3.12.

The `Initialize` sub-block establishes connections with the external devices (DSO, USB Digital I/O), reads the reference pulse to be used for the matched filter process, and initializes all the necessary variables. The main program starts with `Get waveform` that communicates with the DSO and gets the latest acquired waveform. Then, `Subtract coupling` subtracts the current estimate of the coupling from the received waveform. Furthermore, the `Filter waveform` sub-block applies a 0.8-20 GHz bandpass filter to remove out-of-band noise in the received signal. Additionally, `Find pulse's location and traveled distance` ap-

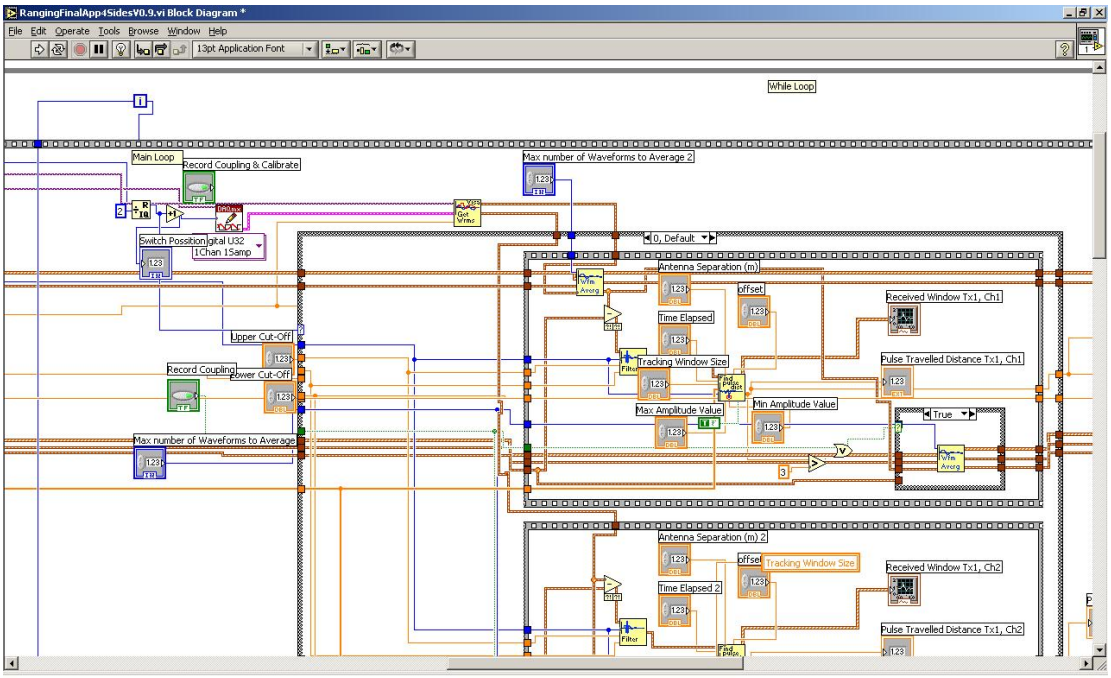

Figure 3.11: Actual LabVIEW Block Diagram Sample Screen Shot

plies the acquisition method in order to find the pulse's location and estimate the distance traveled by the pulse.—This will be discussed in more detail in its own section.—Moreover, `Estimate distance` applies the Pythagorean theorem to find the height based on the traveled distance assuming a right triangle with a base equal to the half antenna separation and a hypotenuse half the traveled distance. Finally, `Non-linear filtering` smooths the output by eliminating sudden output changes that might occur due to incorrect estimation. The operation of this block will be also discussed in more detail in its own section.

The `Add waveform to coupling database` function helps update the coupling database which is being maintained for the coupling estimation. Initially, the database is filled during the calibration process, but later it is continuously updated with new waveforms. When a new waveform is received and the pulse's location is estimated, a half window waveform centered in the pulse's location is replaced with the current coupling estimation, and the rest of the waveform is included in the database. This allows active coupling estimation without recording the actual pulse.

3.3.2 Four-Side Ranging

The block diagram of the four-side ranging application is shown in Figure 3.13. The basic components are the same as the single-side application repeated four times, however, there

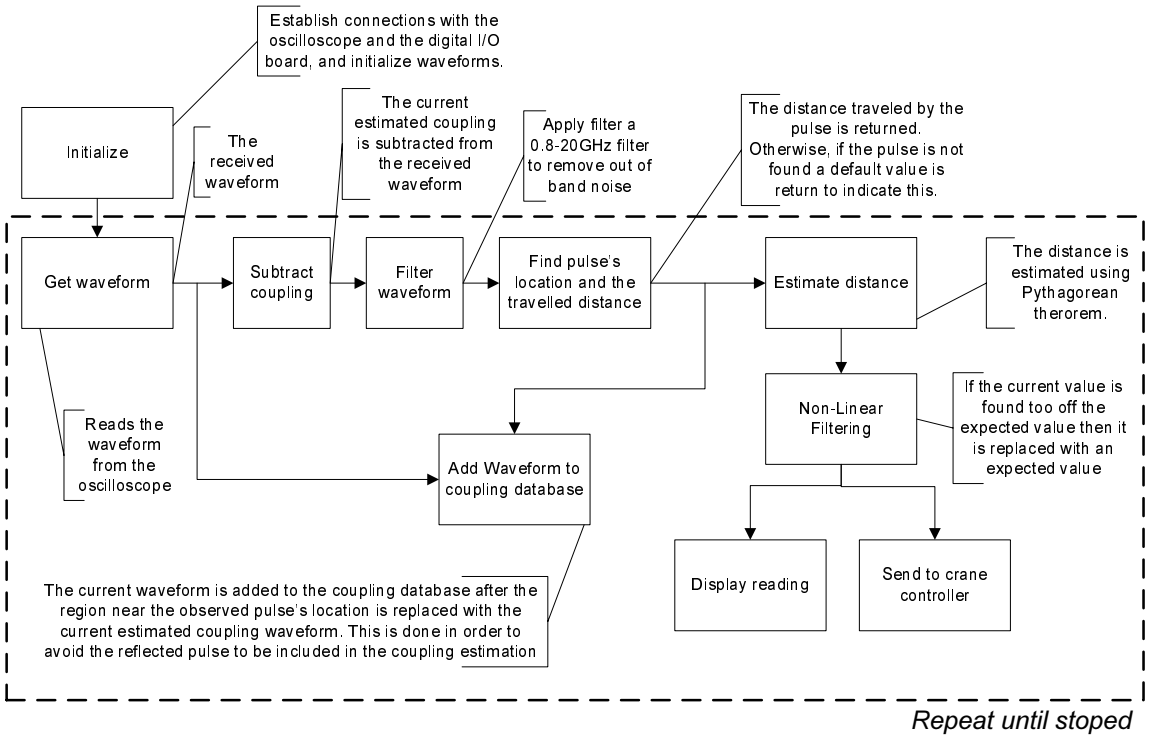

Figure 3.12: Single-Side Ranging Application Block Diagram

are some differences. First, at each iteration the transmit side alternates. Second, because of the transmit side alternation at each iteration only two waveforms are processed, therefore, only two sides have updated values. For the other two sides the last known values are used. Third, in this application no data are sent to the crane controller. And fourth, the estimation algorithm for full orientation estimation (as described earlier in this thesis) is utilized.

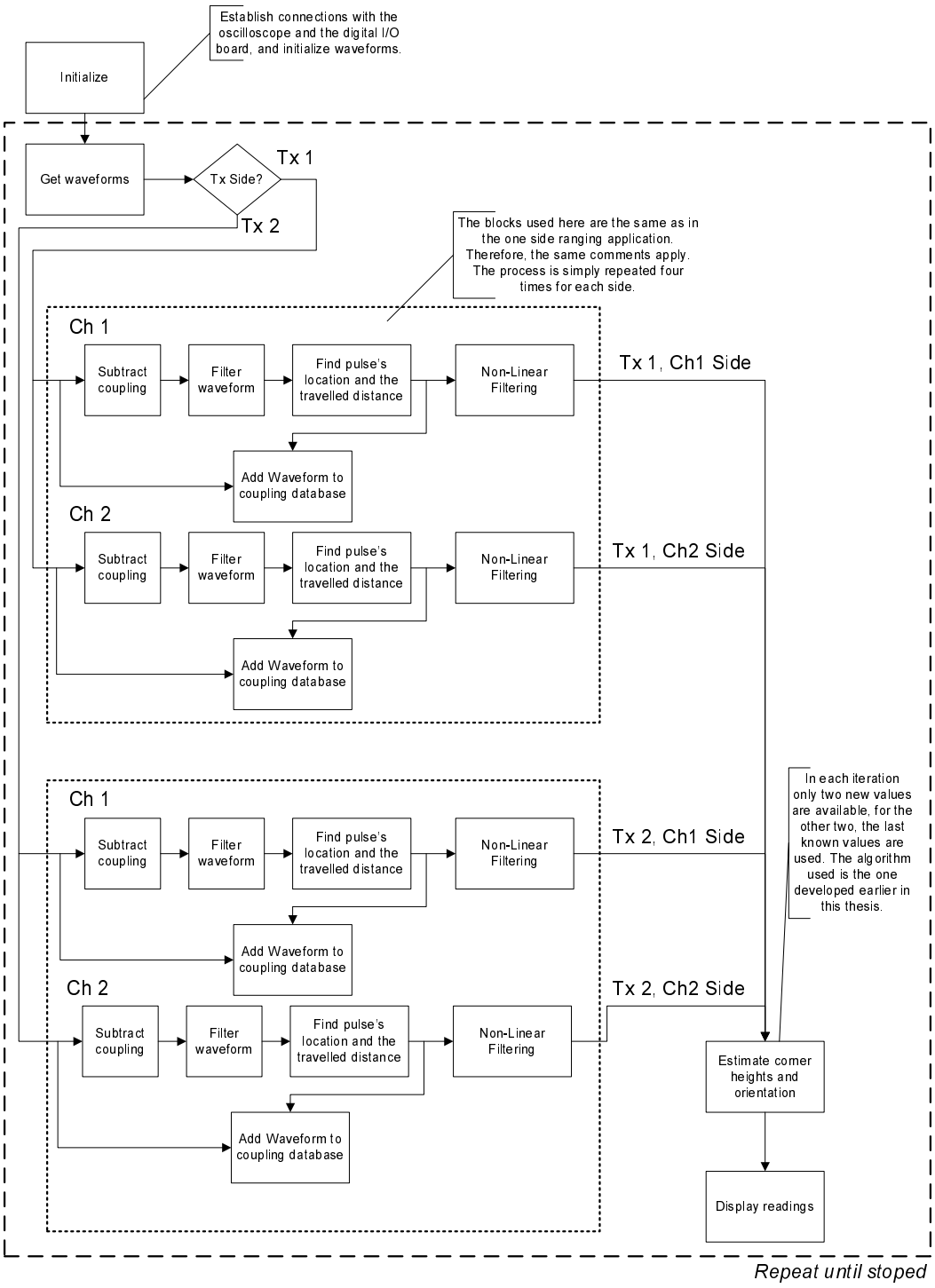

Figure 3.13: Four-Side Ranging Application Block Diagram

3.3.3 Sub-blocks Used

Record Coupling & Calibrate Procedure

Find Pulse's Location

This sub-block gets the input waveform from the main program, then it applies an exponential threshold to received signal. The exponential threshold is applied knowing that the signal's level decreases exponentially. This was found to eliminate wrong detections due to imperfect coupling cancellation. Furthermore, in parallel a match filter with a threshold is also applied to the received waveform, then both results are combined to get a waveform that will meet both the exponential threshold and the matched filter threshold.

After the above criteria are applied to the received waveform, if the last location of the pulse is known, the detection is limited around the last observed location. This provides a simple tracking knowing the pulse should be near the detected location. However, if no pulse is found satisfying detection criteria, then the whole received window is considered for detection. Finally, if no pulse is found in the whole window then the sub-block returns some default values that indicate that the pulse was not found, and probably was out of range.

If a pulse is found, the second strongest peak is also found and if it is at least 90% as strong as the first peak then it is also considered. It was observed for some cases that near the desired pulse will be another pulse consistently before or after the pulse, depending on the side. For that reason the program was instructed to give priority to one of them. The second pulse was given priority when the pulse was received on the short sides.

The two separate arriving pulses was due different cables inside the crate. The cables inside the crate where calculated thus the pulses will start arriving at the same time on the receiver, therefore, will use the most of the received window. The cables of the short side of the crate were in total two inches longer that the cables of the long side (one inch for the receiving antenna, and one inch for the transmitting antenna). This caused the pulse for the long side to be sent earlier and to be received before the intended pulse on the short side. Usually, this pulse was attenuated, put there were cases that caused some instability on the detection, and selecting the second strongest pulse mitigate this problem.

Figure 3.14 shows a screen shot of the received window that was used for troubleshooting purposes. On the screen shot some of the detection features discussed are visualized: the exponential threshold (blue), the matched filter output (yellow), and the matched filter region that was considered for detection (red).

Figure 3.14: Received Window Sample Screen Shot

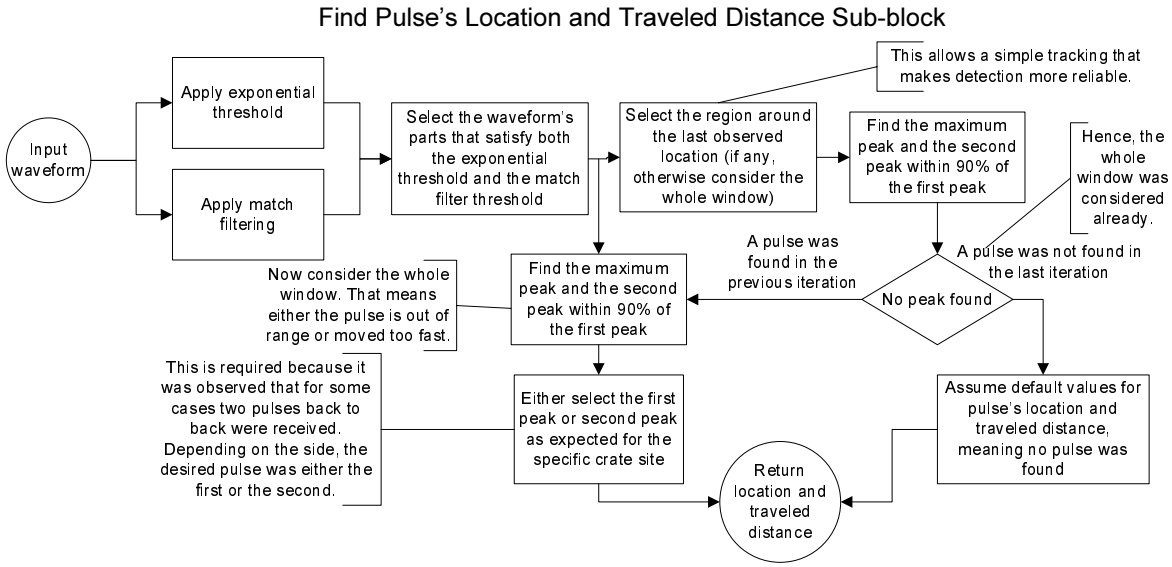

Figure 3.15: Find Pulse's Location Sub-block

Non-linear Filtering

Occasionally, the detector momentarily might assume detection far from the actual pulse's location and then return back to the correct reading. This can cause unwanted spikes on the output of the program. For this reason the program keeps history of the last two values. Before a value is given for an output, first, the values before and after that value are compared, and if they are found to be within a percentage of each other, then their average is computed. Furthermore, the percentage of the current value is compared to that average value and if it is found to have more than a 40% diffence then it is replaced with the average of its surounding values.

In addition, to the the procedure above, a moving average filter further smooths the output based on a longer history record that is also kept for that reason.

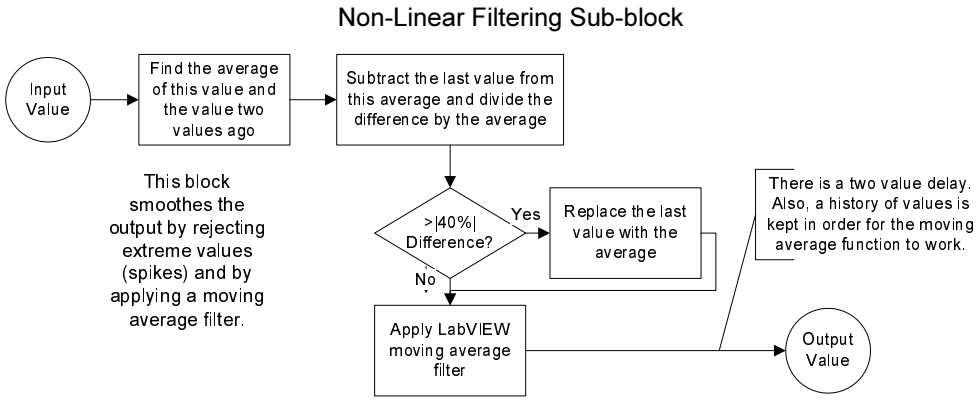

Figure 3.16: Extreme Value Rejection Sub-block

3.3.4 Other Techniques Used

Keeping a waveform database with minimum processing

A waveform database had to be maintained for the coupling estimation. Keeping a number of waveforms requires memory and processor time. The former was not an issue for this application: however, the latter was a problem because whenever a new waveform was added (to the database) and one was removed at the same time, all the waveforms had to be averaged. That caused significant delays. However, a technique was employed that used the minimum processing time: in addition to the waveforms, their sum was maintained as well, and when a waveform was added to the database it was also added to the total sum. Furthermore, the waveform that was removed was subtracted from the sum. This procedure, for the averaging, only required one addition, one subtraction and one division, compared to N additions and one division, where N is the number of the waveforms kept in the database.

Ethernet: A GPIB replacement

GPIB (General Purpose Interface Bus) is a standard interface for communication between instruments from different sources. The Tektronix CSA8000B DSO is also equipped with a GPIB interface. The problem was that the GPIB's version used has limited data transfer capabilities. The GPIB was successfully replaced by an Ethernet connection between the DSO and the laptop used for the DSP.

The replacement was made possible by installing the updated National Instruments VISA[2] driver (replacing the Tektronix VISA driver) to the DSO. The updated driver provides the NI-VISA server which allowed the laptop to connect using a TCP/IP network connection to the DSO. This allowed faster data transfer and network access to the DSO folders.

Custom GetWaveform Routine Implementation

The DSO had a LabVIEW driver for issuing commands and transferring waveform data from the DSO to the laptop running LabVIEW. However, the `GetWaveform` implementation of the driver was found not to be optimized for transfer speed. It is speculated that it issues commands that might be redundant and that opens and closes the connection to the DSO each time a waveform is requested which causes some delays. For that reason a new `GetWaveform` was written in LabVIEW that sends only the necessary commands for obtaining the current waveform. Furthermore, the connection to the DSO was kept open during the acquisition process; therefore no unnecessary time was lost for opening and closing the connection. Finally, the transfer mode was in binary instead of ASCII which yielded fewer bits to be transfered, hence a faster response.

Despite the customization of the `GetWaveform` the delay introduced by the DSO when clearing the acquired data, required when changing tx sides, could't be overcome. That slowed the transfer rate for the Four-side application.

3.4 Demo Outcomes

3.4.1 Single-Side Ranging

The demo was able to provide 1 mm resolution and 16 Updates/second of the estimated height of the the crate. At first the system was demonstrated with a stationary floor. The crate was moved up and down to demonstrate the abilities of the system to accurately

[2]The Virtual Instrument Software Architecture (VISA) is a standard for configuring, programming and troubleshooting instrumentation systems comprising GPIB, VXI, PXI, Serial, Ethernet, and/or USB interfaces.

estimate the height between the crate and the floor. A sample of the system's output is shown at Figure 3.17 where the crate is raised from the floor to the maximum range of the system and then is landed back to the floor. Table 3.1 shows a sample set of height measurements. Because of the 1 mm resolution of the system obtaining good estimates of the system's accuracy was a hard task. In order to improve measurement accuracy and minimize measurement errors, the measurements were taken by resting the crate in wooden blocks of known height, instead of the crate being suspended by string wire. Nevertheless, the sample measurements demonstrate that system is accurate in most cases within 1 mm, and the maximum error recorded being 2 mm from 0-191 mm heights. The accuracy for these measurements appears to be independent of height. This is due to the fact that for the heights evaluated the accuracy is within the resolution of the system because of the good SNR observed at these heights. The SNR for these measurements was 29.9 dB and 17.5 dB for the 0 mm and 191 mm case respectively. For a 250 mm case the SNR was 16.8 dB. The system could potentially range up to 2 ft (600 mm) but for this to happen several changes are needed to the LabVIEW application in order to accommodate for the longer receive time window (more points per waveform) and estimation of good threshold values, furthermore, unlike the first foot (0 - 300 mm), the second foot will experience lower SNR's that will challenge the accuracy of the system. Finally, keep in mind that 1 foot translates to 24 feet in an actual scale system.

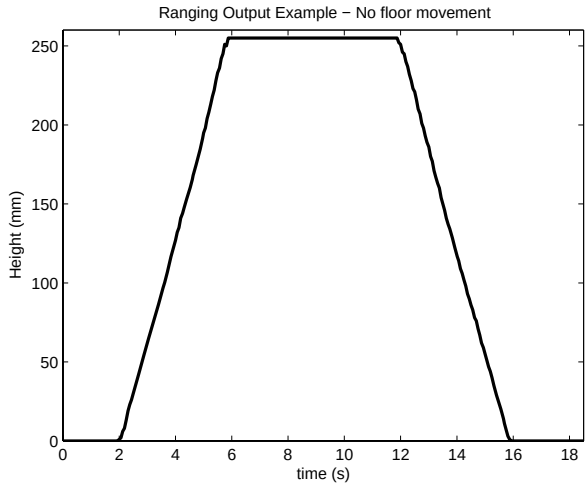

Figure 3.17: Sample Ranging Output: Motion all the way up and then down

After the ability of the system to provide fast and accurate range information was demonstrated, the floor was set to oscillate with 1 Hz and the crate control system was demonstrated, which was able to successfully land the crate on the oscillating floor with minimum impact. The range output to the crane control system is shown on the Figure 3.18, from which three main regions can be observed: the oscillating region, the landing region, and the landed region.

Table 3.1: Single-Side Sample Measurements (mm)

Actual	Measured										σ	mean	mean % error
	Trial												
	#1	#2	#3	#4	#5	#6	#7	#8	#9	#10			
0	0	0	0	0	0	0	0	0	0	0	0.00	0	0.00
19	20	20	20	20	20	19	19	19	19	18	0.70	19.4	2.11
38	38	38	40	39	39	38	38	38	37	38	0.82	38.3	0.79
57	57	57	58	58	57	57	56	57	57	57	0.57	57.1	0.18
76	77	77	77	77	76	77	76	76	75	76	0.70	76.4	0.53
95	97	96	96	96	95	96	95	95	95	96	0.67	95.7	0.74
115	114	115	115	115	114	115	114	115	114	114	0.53	114.5	-0.43
134	133	135	134	134	134	135	134	134	133	134	0.67	134	0.00
153	153	153	153	153	153	154	153	153	153	154	0.42	153.2	0.13
172	172	173	173	173	173	174	174	173	172	173	0.67	173	0.58
191	191	192	191	192	192	193	192	191	191	192	0.67	191.7	0.37

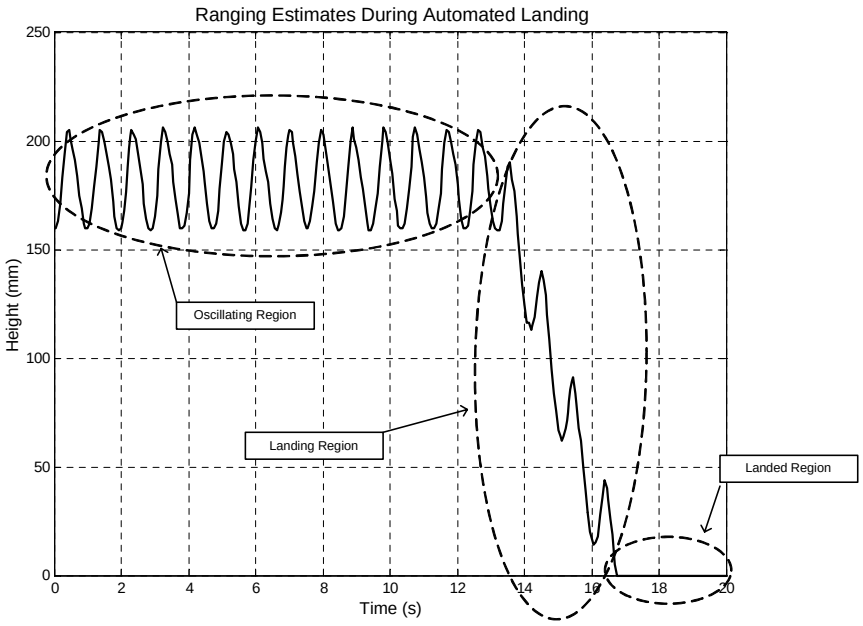

Figure 3.18: Automatic Landing

3.4.2 Four-Side Ranging

The full implementation of the system was demonstrated in a slow motion manner because of the low update rate of the system (3 updates/second). The orientation capabilities of the

algorithm were demonstrated by tilting the floor and by visualizing the tilt on the laptop's screen. Furthermore, because two sides were estimated at a time this caused the effective update rate to be 1.5 updates/second, which further limited the speed of this part of the demo. Also for this case a few sample measurements were taken which are shown in Table 3.2. These measurements were taken with the crate suspended using string wire, which makes the measurements subject to measurement errors. The slopes were calculated using Equations 2.21 and 2.22. Nevertheless, the system was found to have the same accuracy as the single-side case.

Table 3.2: Four-Side Sample Measurements

	Corner Height (mm)				Slope (^{o})	
	C1	C2	C3	C4	Length Side	Width Side
Actual	0	0	0	0	0	0
Meas.	0	0	0	0	0	0
Actual	79	78	74	75	0	-2
Meas.	78	78	74	75	0	-2
Actual	48	46	36	39	0	-5
Meas.	49	47	37	38	0	-8
Actual	25	53	55	28	6	-1
Meas.	24	52	54	27	6	-1
Actual	35	59	52	26	6	-4
Meas.	36	61	53	27	6	-5

Chapter 4

UWB Ranging Conclusions

The first part of the thesis addresses the problem of unloading cargo crates to ships, either from a port's crane or a crane on another ship. The problem in unloading is due to the fluctuations of the ship's deck due to sea waves. For this problem a scheme was proposed that estimates the height and the orientation of the ship in reference to the cargo crate being unloaded. The scheme uses UWB antennas at each corner of the crate, from each side an UWB pulse was sent to the deck and received back; from the pulse's traveled path the distance from the crate was estimated. In this thesis an algorithm was developed that can estimate both the height and the orientation of the deck just using the traveled distances of the four sides.

The proposed algorithm was evaluated by means of simulation and was found to accurately estimate the deck's height and orientation given valid data. Furthermore, it was found that the estimation variance at the output of the algorithm is less than the input variance by a factor of 1.5 to 2.8, depending on the ratio of the crate side's length and the height to be estimated.

After the scheme was verified analytically and via simulation, a demo was planned to demonstrate its accuracy. For the demo a 1/24 scale crate was used with small UWB antennas. The demo was first performed using a single side for ranging which provided 16 updates/second to the cranes controller to test the system with the crate landing algorithm developed by Nader A. Nayfeh. The crate landing algorithm was able to land the crate, using the input from the UWB system developed with minimum impact at an oscillating surface (1 Hz.)

In the second part of the demo, the orientation capabilities of the algorithm were demonstrated at a slower rate. In the demo the algorithm only received the update information of two sides at a time, also limited the update rate of the system by an additional factor of two. It is suggested that the final application will have four receiving channels.

Because the antennas were very close to each other there was a direct received signal (coupling) which was successfully mitigated. This is something that will be a lesser issue in a

real-world system in which the antennas will be separated by several meters and the coupling will be attenuated.

For future development an acquisition technique can be employed which will allow more robust acquisition and more sophisticated pulse tracking. Furthermore, pulse shapes might be investigated as some pulses might be more suitable than others for this application because of their different spectrum characteristics. Moreover, the application's environment can be further investigated for making potential suggestions and additions to the system. Finally, the ranging information of the crate can be potentially used for other purposes such as detecting nearby objects to the crate and predict possible collisions.

Part II

Ultra Wideband Link Budget Design

Chapter 5

Ultra Wideband Link Budget Design

5.1 Introduction

In a communications link the transmitter sends a signal and a receiver at some distance attempts to detect that signal. Since the early days of wireless communication, engineers have devised different signals with different properties to send the information to the receiver. Some signals are better than others; simpler or more complex to implement. However, regardless of the signal used, a communications engineer has to be able to estimate the performance of the link based on many parameters that have to do with the link. The performance of the link, regardless of the type of signal sent is directly related to the ratio of received signal power to noise power. The procedure of estimating the signal-to-noise ratio of the link is often referred to as calculating a link budget.

A link budget is a set of calculations aimed at estimating the power of the signal received by the receiver and the noise power seen at the receiver. The received power is estimated by knowing the transmit power, the separation distance, propagation conditions, frequency of operation, and the antenna parameters. From the received power other parameters of the communication link such as the ratio of energy per bit to noise power spectral density (E_b/N_0) can be estimated, which directly determines the achieved bit error rate of the link. Furthermore, not only do path loss and noise affect the link, other parameters such channel fading and system losses must be considered for an even more accurate prediction.

For most signals that are narrow in bandwidth, a procedure for calculating the link budget exists which accurately predicts the receive signal's power. That link budget is based on the Friis transmission formula which estimates the received power by considering the transmit power, the antenna gains, the frequency of operation, and the distance between the antennas.

The FCC's decision in 2002, to allow UWB operation in a broad range of frequencies (3.1-10.6 GHz) stimulated research in UWB based communication systems. One way to implement

a UWB system is to use very short duration pulses that are wide in bandwidth, a technique commonly termed Impulse-UWB (I-UWB). Analysis of I-UWB systems requires the examination of the impulse response of the system as opposed to the steady state response. [5].

An I-UWB system is very different from narrow band systems because of its bandwidth that often occupies a few GHz. Attempting to use a link budget that is based on the Friis transmission formula which assumes a single frequency of operation and is based on steady-state sinusoidal signals is not the most accurate procedure. In other words, the assumption that the link behaves the same at all frequencies of operation no longer holds because of the complex spectrum characteristics of both the pulse and the antennas used. Furthermore, besides the estimation of the received power, the whole approach of the link budget much be reconsidered because of the channel and the receiver structures used.

In this chapter, the traditional narrowband link budget will be introduced. Furthermore, a proposed I-UWB link budget that first appeared in [5] will also be introduced and explained. The purpose of the remainder of the chapter is to demonstrate, mainly by measurements done with four different UWB antennas, that the proposed I-UWB link budget is much more accurate and suited for I-UWB systems than the link budget based on the Friis transmission formula. Furthermore, the proposed approach is primarily defined in the time domain as opposed to the frequency domain which simplifies the process and the data required for the link budget calculations.

5.2 The Traditional Narrowband Link Budget

As already mentioned, a link budget for narrowband systems already exists that is based on the Friis transmission formula which is going to be derived and explained. We will now briefly derive and explain this link budget approach.

5.2.1 The Friis Transmission Formula

It is assumed that the transmit antenna of a communication link radiates isotropically in free space a power P_T Watts, such that the power flux density at distance r, P_D is given by [6]

$$P_D(r) = \frac{P_T}{4\pi r^2} \quad (W/m^2) \tag{5.1}$$

The term $4\pi r^2$ is the surface area of a sphere of radius r. This isotropic antenna does not really exist. Practical antennas do not radiate equally in all directions and thus have higher gain in a particular direction, which is assumed to be used for the link. That gain is denoted

by G_T and Equation (5.1) becomes

$$P_D(r) = \frac{P_T G_T}{4\pi r^2} \quad (W/m^2) \tag{5.2}$$

where P_D is the power received in the the direction of the peak gain G_T of the transmit antenna.

The term $P_T G_T$ is called the *Effective Isotropic Radiated Power* (EIRP). The received power P_R can be found by multiplying Equation (5.2) with the effective aperture of the receive antenna A_e. The effective aperture is a measure of the antenna's ability to collect electromagnetic (EM) energy which is given by

$$A_e = \frac{G_R \lambda^2}{4\pi} \quad (m^2) \tag{5.3}$$

where G_R is the gain of the receiving antenna, and λ is the wavelength of the transmit frequency in meters. The multiplication of Equations (5.2) and (5.3) results in:

$$P_R(r) = \frac{P_T G_T G_R \lambda^2}{(4\pi r)^2} \quad (W) \tag{5.4}$$

where $P_R(r)$ is the received power at distance r[1] and the formula above is the standard Friis transmission formula.

The factor $L_s = \left(\frac{4\pi r}{\lambda}\right)^2$ is referred to as the *free-space path loss*. The λ in the path loss suggests that path loss is frequency dependent. However, it must be noted that this is an antenna effect as shown in Equation (5.3) and not a propagation effect. Furthermore, it is shown [5], that by using a constant aperture transmit and a constant gain receive antenna, the effects of this term are canceled. These observations will be useful for the UWB link budget development.

5.2.2 Link Budget

The received power of a narrowband signal can be estimated using the Friis transmission formula. However, the received power is only a part of a link budget. Another important term is the thermal noise at the receiver which is a function of the operating temperature. For a signal that only experiences noise due to the receiver, its link is modeled as an Additive White Gaussian Noise (AWGN) channel. The noise power spectral density N_0 is given by

$$N_0 = kT_0 \quad (W/Hz) \tag{5.5}$$

[1]Note that this assumes that the antennas are oriented such that their maximum gains are directed along the link.

where k is Boltzmann's constant and T_0 is the nominal system noise temperature in Kelvin. Since most receivers amplify this noise based on the quality of its components, we typically also include a term called the noise figure N_F which accounts for the increase in thermal noise:

$$N_0 = N_F k T_0 = k T_s \tag{5.6}$$

where $T_s = N_F T_0$ is the effective system noise temp.

The SNR per bit $\left(\frac{E_b}{N_0}\right)$ is given by dividing the received power with the noise spectral density and the number of bits sent per second:

$$\left(\frac{E_b}{N_0}\right) = \frac{P_R}{N_0 R_b} \tag{5.7}$$

where R_b is the bit rate in $bits/sec$

In addition, a fading margin M_F or safety margin can be added to account for deviation in the received power due to fading. This will ensure that the received $\frac{E_b}{N_0}$ will be above a threshold some % of the time. The desired SNR per bit will now be equal to:

$$\left(\frac{E_b}{N_0}\right) = \frac{P_R}{N_0 R M_F} \tag{5.8}$$

The link budget also can be also expressed in dB terms:

$$\left(\frac{E_b}{N_0}\right) = (P_R)_{dB} - (N_0)_{dB} - (R)_{dB} - (M_F)_{dB} \tag{5.9}$$

$$(P_R)_{dB} = (P_T)_{dB} + (G_T)_{dB} + (G_R)_{dB} - (L_s)_{dB} \tag{5.10}$$

If desired, the above can be rearranged to find the maximum achievable bit rate.

Table 5.1 provides a sample conventional free space link budget calculation.

Table 5.1: Conventional Free Space Link Budget

Term	Value (example)	Comment
P_T	-55dBW	Transmit power in dB relative to a W
G_T	3dBi	Transmit antenna gain relative to isotropic radiator at operating frequency.
L_s	86dB	$(4\pi r/\lambda)^2$ - Free space path loss given constant gain antennas at a distance r (assume f_c=4.6GHz and r=100m)
G_R	3dBi	Receive antenna gain relative to isotropic radiator at operating frequency.
P_R	-140dBW	$(P_T + G_T - L_s + G_R)$
k	-228.6dbW/Hz/K	Boltzman's constant
N_F	7dB	Noise Figure
T_0	24.6dBK	System Noise Temperature (290K)
N_0	-197dBW/Hz	Noise PSD= $N_F k T_0$
R_b	50dB	Bit Rate (100kbps)
E_b	-190dB	$P_R - R_b$
E_b/N_0	7dB	$E_b - N_0$
M_F	0	Fading Margin
E_b/N_0	7dB	E_b/N_0 achieved

5.3 The Proposed I-UWB Link Budget

This section presents the proposed link budget for UWB mostly as it appeared in [5].

It is natural to want to apply the previous link budget to UWB systems. However, there are several problems with that approach. The development of the previous link budget assumes a frequency of operation and everything is calculated based on that frequency. It is assumed that the estimated power approximately holds for all the nearby frequencies around the selected frequency which is usually referred to as the carrier or center frequency of the link.

Using the center or carrier frequency for evaluating the link budget, as is usually the case for narrowband systems, is a challenge in I-UWB systems since the transmit pulse usually has a bandwidth of a few to several GHz. Some might suggest to use the center frequency of the bandwidth spectrum of the transmit pulse. Still, using a formula that takes into account only a single frequency out of a bandwidth of few GHz is not optimal. Furthermore, the formula can not take into account pulse distortion due the antennas' and channel's frequency response. In addition, usually a link budget is calculated in terms of average power. However, in an I-UWB system because of the the low duty cycles one might want to define the link budget in terms of energy or peak power (The Friis formula does not really apply to energy).

Going back to the Friis transmission formula and arranging it into parts in order to examine potential modifications we have:

$$\begin{aligned} P_R &= \frac{P_T G_T G_R \lambda^2}{(4\pi r)^2} \\ &= P_T \frac{G_T G_R \lambda^2}{4\pi} \frac{1}{4\pi r^2} \end{aligned} \tag{5.11}$$

The formula has three components: the transmit power P_T, the spherical spreading factor $4\pi r^2$, and a term due to the antennas $\frac{G_T G_R \lambda^2}{4\pi}$. The first two terms can't be changed. In contrast, the antenna effects term, which consists of the antenna gains and the effective aperture of the receive antenna, can be replaced by an "antenna-pulse coupling gain," or G_{AP}. For comparison purposes in the validation section lets call the old term $G_{Friis} = \frac{G_T G_R \lambda^2}{4\pi}$ with units m^2.

The new G_{AP} term captures the gain in either energy or peak power in the received pulse with respect to the generated pulse. Whether energy or power is examined depends on the modulation scheme used, as will be discussed shortly. In some cases the two measures may be equal, but not in general. It should be clear that this gain is very different from the traditional antenna gain. It is different because it defines an antenna *pair* as opposed to a single antenna, and because it is *pulse specific*. Just as the traditional "gain" of an antenna is frequency specific, G_{AP} is pulse specific. Additionally, it captures the receive antenna aperture which is normally lumped into path loss. As a result, the "gain" actually has a negative dB value in general and has units of meters squared (m^2).

A second modification to the traditional link budget is that path loss now accounts only for spreading loss, not effective aperture at the receive antenna. Thus, we can define path loss as

$$L_p = 4\pi r^2 \tag{5.12}$$

where r is the distance between the transmitter and the receiver. This simply represents the power distributed over the area of a sphere of radius r; thus, it has units of square meters (m^2).

Another difference in the I-UWB link budget is that it should be in terms of either pulse energy or peak pulse power. In traditional link budgets, we deal with *average* power. However, average power may not be useful in UWB because low duty cycle pulses are possible. Also, we are interested in the impact of the antenna as well. Since peak power could be affected by the antennas, we allow for G_{AP} to be defined either in terms of peak pulse power or pulse energy. The former would be more applicable to threshold detector receivers, while the latter would be more applicable to correlator receivers.

The term G_{AP} can either be determined directly from a time domain line-of-sight measurement or derived from an antenna S_{21} measurement. Specifically, for a pulse energy-based

link budget, the gain should be determined as

$$\begin{aligned} G_{AP} &= 4\pi r^2 \frac{\varepsilon_p^{rx}}{\varepsilon_p^{tx}} \\ &= 4\pi r^2 \frac{\int_{-\infty}^{\infty} b_r^2(t)dt}{\int_{-\infty}^{\infty} a_t^2(t)dt} \end{aligned} \tag{5.13}$$

where ε_p represents the pulse energy, $a_t(t)$ is the generated pulse, and $b_r(t)$ is the received pulse measured at a distance r meters in free-space or calculated as

$$b_r(t) = \frac{1}{4\pi r}\frac{\mu}{50}\frac{d}{dt}\left\{a_t(t) * h_{tx}\left(t - \frac{r}{c}\right) * h_{rx}(t)\right\} \tag{5.14}$$

where the combined response of $h_{tx}(t)$ and $h_{rx}(t)$ (the impulse responses of the transmit and receive antenna respectively) can be determined for the antenna pair of interest using an S_{21} measurement. Additionally, note that we have neglected the vector nature of the general problem. We have assumed that Equation (5.14) is calculated with both antennas aligned for maximum response. This is analogous to narrowband antenna gain, which is typically defined as the maximum gain versus azimuth and elevation angles. Additionally, traditional link budget designs assume proper polarization alignment or include a polarization loss factor.

Thus, G_{AP} represents the energy gain of the pulse due to the antennas. Note that this term *is not waveform independent.* **That is, it is not merely a factor of the antenna, unlike the traditional antenna gain.** It is *waveform specific.* As such, care must be taken in its use. Alternatively, the received pulse can be determined in the frequency domain

$$B_r(j\omega) = (j\omega) \cdot H_{tx}(j\omega) \cdot H_{rx}(j\omega) \cdot A_t(j\omega) \cdot \frac{e^{-j\omega\frac{r}{c}}}{4\pi r}\frac{\mu}{50} \tag{5.15}$$

where $A_t(j\omega)$ is the Fourier Transform of the generated pulse and the combined term $H_t(j\omega)H_r(j\omega)$ is the transfer function of the transmit and receive antennas which can be determined from network analyzer measurements.

Assuming that the S_{21} measurement is the combined frequency response of the link and the antennas at a reference distance r_0, then the frequency response of the link is equal to:

$$S_{21}(j\omega) = \frac{B_r(j\omega)}{A_t(j\omega)} = (j\omega) \cdot H_{tx}(j\omega) \cdot H_{rx}(j\omega) \cdot \frac{e^{-j\omega\frac{r_0}{c}}}{4\pi r_0}\frac{\mu}{50} \tag{5.16}$$

Rearranging Equation (5.16), the combined antenna frequency response $H_{tx}(j\omega) \cdot H_{rx}(j\omega)$ can be determined using the S_{21} parameter of the two antennas using:

$$H_{tx}(j\omega) \cdot H_{rx}(j\omega) = \frac{4\pi r_0}{(j\omega)}\frac{50}{\mu} \cdot S_{21}(j\omega) \cdot e^{+j\omega\frac{r_0}{c}} \tag{5.17}$$

Substituting Equation (5.17) into Equation (5.15) we arrive at

$$B_r(jw) = \frac{r_0}{r} S_{21}(jw) \cdot A_t(jw) \cdot e^{-\frac{j\omega}{c}(r-r_0)} \tag{5.18}$$

In the time domain this becomes

$$b_r(t) = \frac{r_0}{r} s_{21}\left(t - \left(\frac{r-r_0}{c}\right)\right) * a_t(t) \tag{5.19}$$

The received pulse $b_r(t)$ is the convolution of the time shifted $s_{21}(t)$ parameter of the link, adjusted for the spherical path loss according to the desired distance r with the transmit pulse $a_t(t)$.

The received pulse energy in dBJ (that is, dB relative to one J) is then calculated as

$$E_R(dBJ) = E_T(dBJ) + G_{AP}(dBm^2) - L_p(dBm^2) \tag{5.20}$$

The noise power spectral density N_0 is calculated as before, and E_R/N_0 dB is simply $E_R(dB) - N_0(dB)$. Of course, this is the energy per pulse, not necessarily per bit. In many systems multiple pulses may be transmitted per bit. Thus, this value must be multiplied by the number of pulses per bit N_s (added in dB) to obtain the energy per bit. The result then represents the available E_b/N_0 or the SNR per bit of a matched filter output.

Due to pulse mismatch, which is much more likely in UWB due to both the channel and limitations in replicating the received pulse, we must include a factor ρ (negative in dB or less than unity in linear), which represents the fraction of the energy captured by the receiver. This factor can either be due to per path distortion or overall temporal dispersion of the channel. For example, consider a Rake receiver that uses only two to three correlators. As discussed in [5] it is known that in many environments, such a receiver only captures $\sim 20\%$ of the total energy. Thus, a factor of $\rho = 0.2$ (-7dB) should be included in this case, provided the path loss value implies total energy capture. Various receiver structures will have different values of ρ. The final result is the E_b/N_0 available to the detector. Table 5.2 presents a sample set of calculations based on the trasnmitted pulse and the "TimeDomain" antenna from the validation section.

5.3.1 Receiver Structure Dependence

This development has been specifically in terms of energy because we are typically interested in the received energy per bit.Traditional link budgets can obtain E_b from the average received power as $E_b = P_r T_b$, where T_b is the bit period. However, this is not necessarily true for UWB; thus, we have set up the budget in terms of the energy per pulse. If the receiver is based on threshold detection or is otherwise concerned only with the peak power of the pulse, the link budget should be worked in terms of peak power. In that case, we should

Table 5.2: Proposed UWB Free Space Link Budget — Correlator Detector

Term	Value (example)	Comment
E_T	-108dBJ	Transmit energy in dB relative to a J
G_{AP}	$-38dBm^2$	Energy gain of the link for the specific antenna pair and pulse used.
L_p	$31dBm^2$	$4\pi r^2$ - Free space spreading loss at a distance r=10m
E_R	-177dBJ	$(E_T + G_{AP} - L_p)$
k	-228.6dbJ/K	Boltzman's constant
N_0	-197dBW/Hz	Noise PSD= $N_F k T_0$
T_0	24.6dBK	System Noise Temperature (290K)
N_0	-197dBJ	Noise PSD= $N_F k T_0$
N_s	0dB	Pulses per bit (1 pulse/bit)
E_b	-177dBJ	$E_R + N_s$
E_b/N_0	20dB	$E_b - N_0$
M_F	0	Fading Margin
ρ	-7dB	Energy capture loss (20% Capture)
E_b/N_0	13dB	E_b/N_0 achieved

define the pulse antenna coupling gain G_{AP} as

$$\begin{aligned} G_{AP} &= 4\pi r^2 \left.\frac{P_p^{rx}}{P_p^{tx}}\right|_{rm} \\ &= 4\pi r^2 \frac{max\left\{b_r^2(t)\right\}}{max\left\{a_t^2(t)\right\}} \end{aligned} \tag{5.21}$$

where again $b_r(t)$ is the received signal at a distance of r meters, P_p^{rx} and P_p^{tx} are the peak power of the received pulse measured at r meters and the generated pulse respectively. Note that the notation $[]|_{rm}$ signifies that the gain is measured at r meters. This should coincide with the reference distance used for the path loss calculations.

An example set of link budget calculations for a peak detector receiver is presented in Table 5.3.

As a final note, we should mention again that the preceding analysis is more applicable to pulse-based (I-UWB) rather than Multi Carrier UWB (MC-UWB). With MC-UWB, we can resort to traditional narrowband approaches for each carrier.

Table 5.3: Proposed UWB Free Space Link Budget — Peak Detector

Term	Value (example)	Comment
P_T	-10dBW	Transmit peak power in dBW
G_{AP}	$-44dBm^2$	Peak power gain of the link for the specific antenna pair and pulse used.
L_p	$31dBm^2$	$4\pi r^2$ - Free space spreading loss at a distance r=10m
P_R	-85dBW	$(P_T + G_{AP} - L_p)$
k	-228.6dbW/Hz/K	Boltzman's constant
T_0	24.6dBK	System Noise Temperature (290K)
N_0	-204dBW/Hz	Noise PSD= kT_0
N	-104dBW	Noise Power (9.2GHz BW)
SNR	19dB	$P_R - N$
M_F	0	Fading Margin
ρ	-10dB	Capture loss (10%)
SNR	9dB	SNR achieved

5.4 Link Budgets for Systems Other than Free-Space

The analysis in the previous section considered only free-space propagation. For non-free-space environments, a traditional approach is to model the average received power using a log-distance power decay law. We can represent the average received signal power at distance r as

$$\overline{p_r(r)} = \overline{p_0(r)} \left(\frac{r_0}{r}\right)^n \tag{5.22}$$

where $p_0(r)$ is the pulse power received at a reference distance assuming free-space. This is the traditional log-distance path loss model [7]. Note that the average is a spatial average. If we define our reference distance as 1m (typical for indoors), we would redefine total path loss as

$$L_p = 10log(4\pi) + 10nlog(r) \tag{5.23}$$

where n is the path loss exponent defined as the path loss relative to a 1 m free space measurement. Additionally, we must include a fade margin in non-free space environments because of multipath combining and other parameters which cause the received power to deviate around the predicted power.

5.5 Validation

For validation purposes measurements were taken both in the frequency domain and the time domain. The frequency domain measurements were taken to estimate the S_{21} parameters and the nominal gains of the four antenna pairs used. From the S_{21} parameters the G_{AP} values were calculated as well.

From the time domain measurements, G_{AP} was also calculated by using reference LOS measurements. Furthermore, LOS and NLOS propagation measurements were taken for link budget verification purposes.

Finally, the G_{AP} was calculated for various pulses in order to demonstrate that it's pulse dependent and precisely captures the spectrum characteristics of the pulses. On the other hand, the Friis transmission formula is not able to fully capture all the characteristics of the pulses.

5.5.1 Vector Network Analyzer (VNA) Measurements

One of the methods of calculating G_{AP} is by using the S_{21} parameter of the antenna pair of interest and the UWB pulse to be used. However, the exact data (digital form) for the antennas used were not available. Therefore, the author had to estimate them using a Vector Network Analyzer (VNA).

Method

For the measurements, an HP8510C Vector Network Analyzer (VNA) was used. Ideally, the measurements should have been placed inside an anechoic chamber that provides a reflection free environment. However, because of the lack of easy access to such an environment the measurements were taken in the MPRG Radio Lab at 471 Durham Hall. The measurements were taken at a reference distance of 1 m (Figure 5.1). The antennas were facing each other with their boresight side. Because of the non-ideal environment it is expected that a strong reflection from the floor and probably one strong reflection from the ceiling would be present in the measurements. The antennas were 1.2 m above the floor and about the same from the ceiling. As it will be explained later, multipath reflections from the surrounding objects were removed during post-processing.

The frequency range of the measurements was set from 50 MHz to 18.05GHz. 50 MHz was chosen since it is the lowest frequency that the VNA could measure, and 18.05GHz was chosen because the connectors were not rated to be used at higher frequencies. To increase the frequency resolution, two measurements of 9 GHz per antenna were taken, one between 50 MHz to 9.05 GHz and one between 9.05 GHz to 18.05 GHz.

Before taking the measurements the VNA was calibrated to the cables used in order to remove their effects. An averaging factor of 10 was used during the measurements.

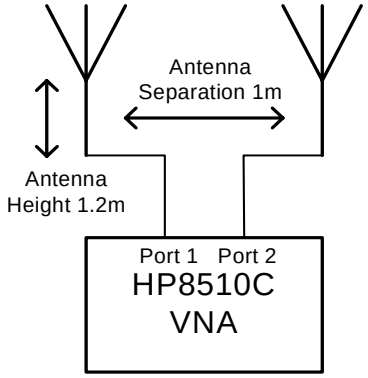

Figure 5.1: VNA Setup

From the measurements there were a total of 1601 points in the selected frequency range (50 MHz to 18.05 GHz). This resulted in a frequency resolution of 11.25 MHz. The resulting frequency resolution could not allow exact zeropading to DC. For that reason the measurements were interpolated by a factor of 9 using Matlab, then decimated by a factor of 8 which made the frequency resolution 10 MHz. The measurements were then zero padded to DC and converted to the time domain using the IFFT.

In the time domain the main pulse was identified, and the rest of the signal was zero padded and converted back to the frequency domain using the FFT to get the final S_{21} parameters. This allowed the removal of multipath reflections. The results were compared and found to be in agreement with [5] that has S_{21} measurements of the same and similar antennas from an anechoic chamber.

Results — Antenna Characterization

The following antennas were characterized and used for the measurements in this section:

1. Ridged TEM Horn — Commercially made.
2. Bicone Antenna — Commerciallly made, repaired/modified[2] at Virginia Tech.
3. Vivaldi Antenna — Manufactured[2] at Virginia Tech as part of a past project investigating the Vivaldi antenna design for UWB systems.

[2]The author was just a user of these antennas and had no involvement in any development or modifications of the antennas.

4. "TimeDomain" — This antenna was made by Time Domain Corporation and was supplied with their PulsON 200 UWB Development system.

Using the method described, the characterization results of each antenna Tx/Rx pair at a reference distance of 1 m are shown in Figures 5.2 to 5.5.

Figure 5.2 shows a photo, impulse response, and frequency response of the the Ridged TEM Horn antenna. From the frequency response of this antenna it can be observed that it is a wideband antenna which is officially rated, by the manufacturer, to operate in the range of 0.7 to 18 GHz.

In Figure 5.3 the same information is shown for the Bicone Antenna which has a wide but narrower frequency response compared to the Ridged TEM Horn antenna. In addition, the Bicone antenna has an attenuated frequency response because it has a uniform azimuth radiation pattern, compared to the Ridged TEM Horn which is a directional antenna.

Furthermore, the Vivaldi antenna shown in Figure 5.4 is also a directional antenna with a similar bandwidth range as the Ridged TEM Horn. Finally, in Figure 5.5 the "TimeDomain" antenna is shown, which has an almost uniform azimuthal radiation pattern. It is slightly directional to the front and the back of the antenna, but for practical purposes it can be assumed to have an omni-directional pattern. In addition, this antenna has a significantly narrower bandwidth compared to all the antennas mentioned.

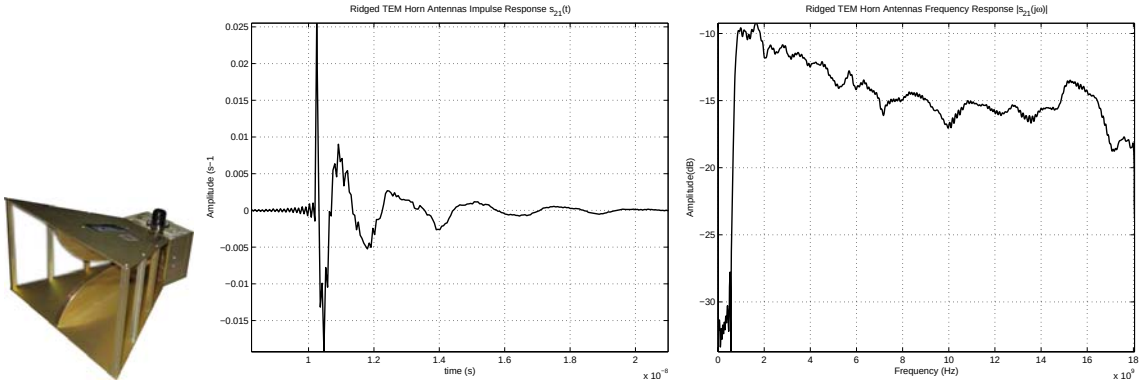

(a) Photo (b) Impulse Response (c) Frequency Response

Figure 5.2: Ridged TEM Horn Antenna

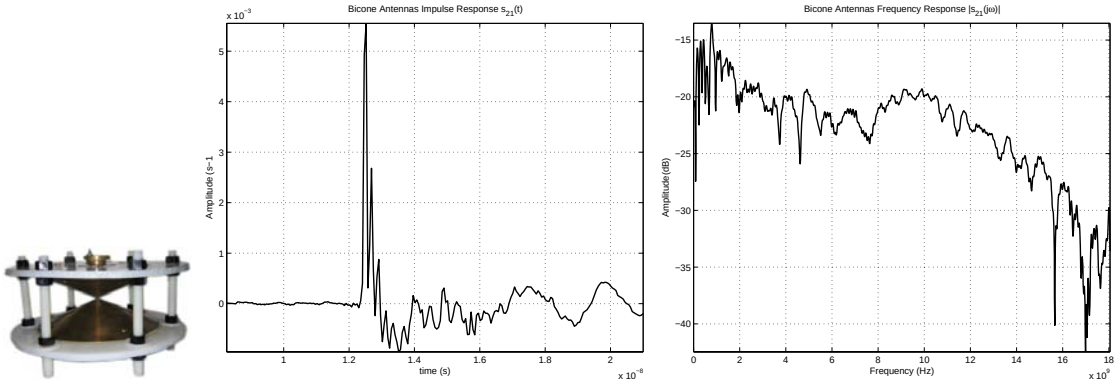

(a) Photo (b) Impulse Response (c) Frequency Response

Figure 5.3: Bicone Antenna

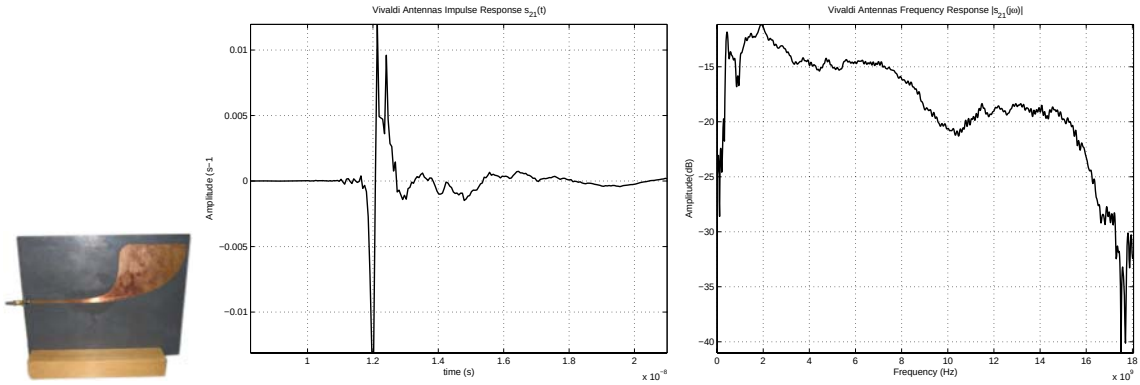

(a) Photo (b) Impulse Response (c) Frequency Response

Figure 5.4: Vivaldi Antenna

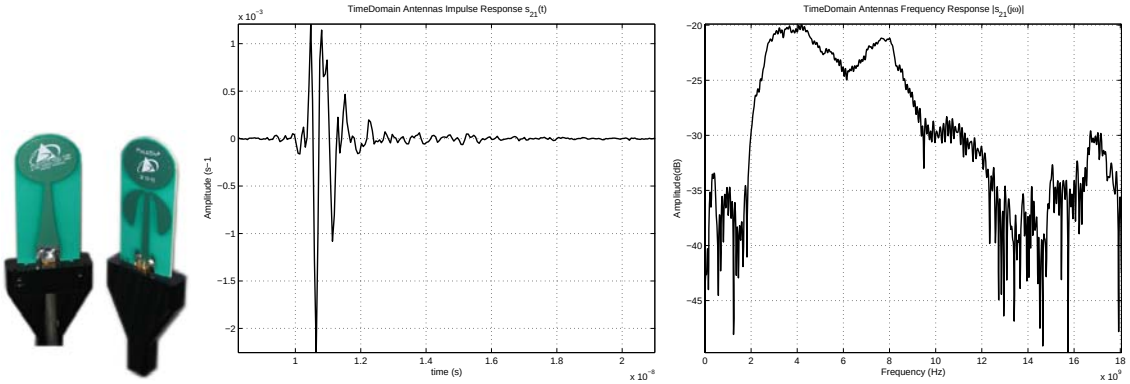

(a) Photo (b) Impulse Response (c) Frequency Response

Figure 5.5: TimeDomain Antenna

Results — Calculated Pulses

Using the S_{21} parameters and the generated pulse (Figure 5.6) the received pulse at 1m was calculated using Equation (5.19) for each antenna. However, the effects[3] of the cables are not included in the S_{21} parameters, therefore, for consistency with the measurements done in the time domain in which the cables affect the measurements, the effects of the cables were added after calculating the received pulse using Equation (5.19). Furthermore, G_{AP} is also calculated before and after adding the cable effects.

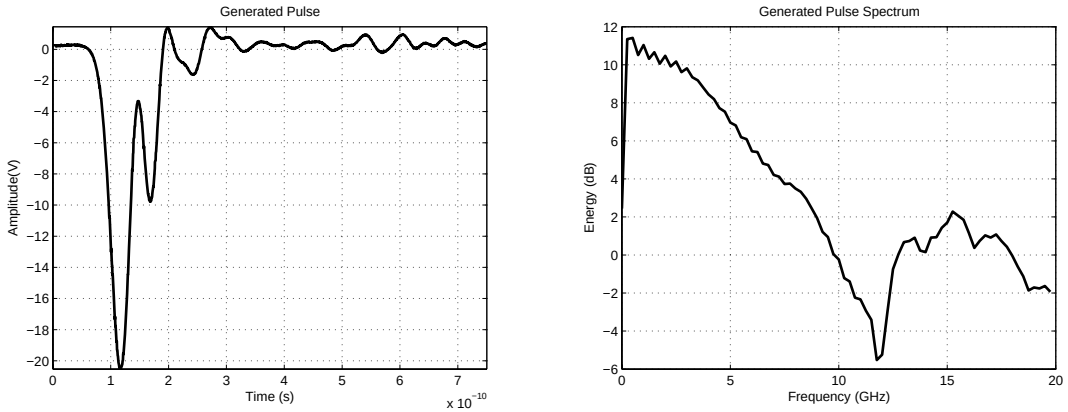

(a) Time Domain (b) Energy Spectrum

Figure 5.6: The Generated Pulse

Figure 5.7 shows the calculated pulses using the procedure described above (with the cable effects added). It may be noticed that the pulses are very similar to the impulse response of the antennas. This is because a very wide bandwidth pulse was used (9.2 GHz 10 dB bandwidth), which approximates an impulse.

[3]The transmit cable effects are a part of the generated pulse, therefore, only the effect of the receive end cable had to be included. The effect of the cable per foot was a loss of 0.1 dB at DC linearly increasing to 0.45 dB at 18 GHz. The calculated pulse was converted to the frequency domain in which the cable's frequency dependent attenuation effect was added and then the signal was converted back to the time domain.

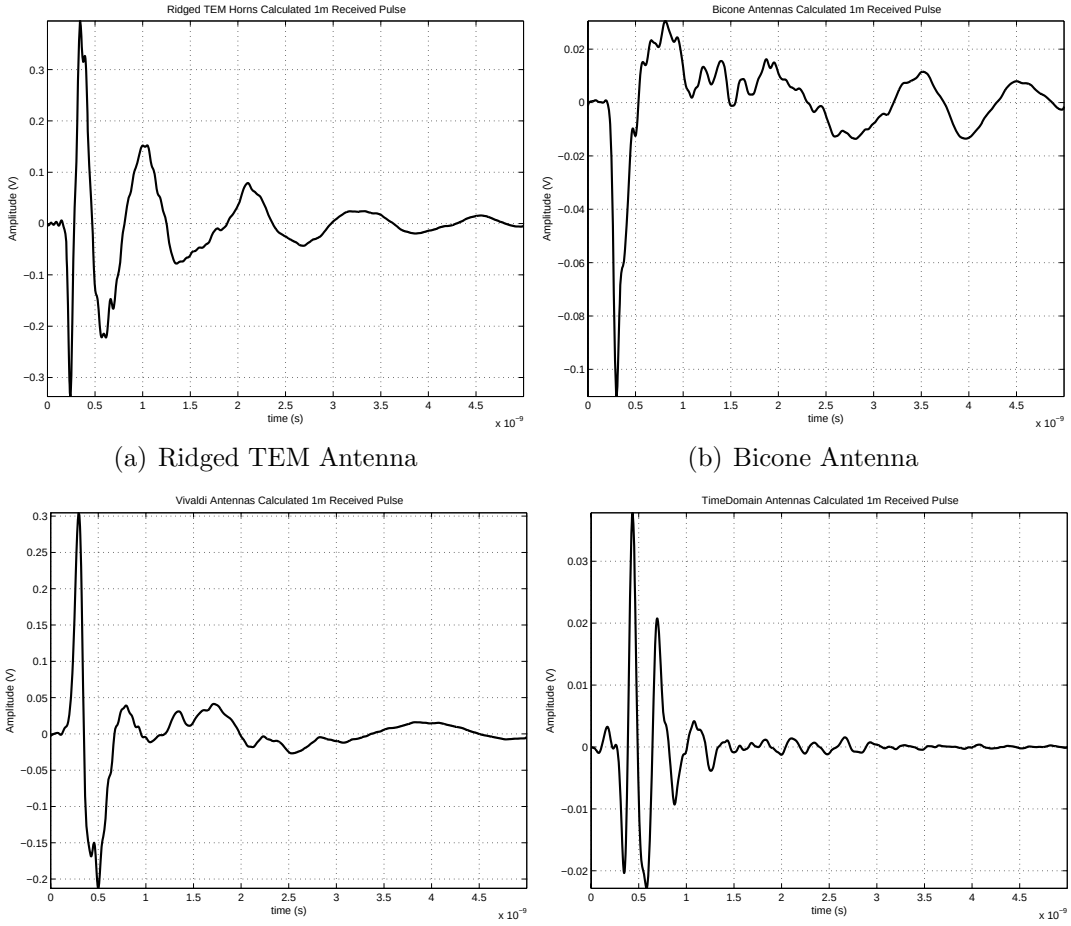

(a) Ridged TEM Antenna

(b) Bicone Antenna

(c) Vivaldi Antenna

(d) TimeDomain Antenna

Figure 5.7: Calcuated 1m Received Pulses

Results — G_{AP} Calculations

G_{AP} was calculated using the calculated pulses (Figure 5.7) from the S_{21} parameters, and from time domain measurements at 1m. G_{AP} was found using the two different methods which were found to be very close, and the largest deviation is 0.5dB.

It must be noted that G_{AP} is consistent with the antenna characteristics. The Ridge TEM Horn and Vivaldi antennas have the highest G_{AP} because these are directional antennas. Furthermore, the Bicone has a lower G_{AP} because it is an omni directional antenna. Finally, the TimeDomain antenna has the lowest G_{AP} both because its radiation pattern is omni-like and because its bandwidth is significantly narrower than the other antennas. The narrow antenna bandwidth negatively affects G_{AP} because the pulse had a wide bandwidth of which a small fraction was received, hence the ratio of the transmitted pulse energy over the received

Table 5.4: G_{AP} for Energy (dBm^2)

Antenna	Method		
	S_{21}	S_{21} (with cable effects)	Time domain
Ridged TEM Horn	-13.02	-15.42	-15.50
Bicone	-26.79	-28.92	-28.57
Vivaldi	-17.04	-19.42	-19.39
TimeDomain	-35.38	-38.22	-37.99

Table 5.5: G_{AP} for Peak Power (dBm^2)

Antenna	Method		
	S_{21}	S_{21} (with cable effects)	Time domain
Ridged TEM Horn	-20.30	-23.32	-22.82
Bicone	-31.58	-34.41	-34.66
Vivaldi	-22.72	-25.51	-25.57
TimeDomain	-40.49	-43.69	-43.82

energy was smaller.

Results — Antenna Gain Estimation Measurements

It is desirable to compare the narrowband approach with the proposed one. In order to be able to calculate the traditional link budget using the Friis transmission formula the gain values of our antennas had to be estimated.

In order to estimate a gain value for our antennas a standard gain horn was used which is rated to have an 18dBi gain in the frequency range of 3.3-4.9 GHz. The frequency response of a pair of these antennas is plotted in the same figure with the frequency response of one of these antennas and one of the other unknown gain antennas, and with the frequency response of a pair of the unknown gain antennas. The difference in dB between each plot should match the gain difference between the unknown gain and the gain of the horn antenna. These measurements were also taken at a separation distance of 1 m^2.

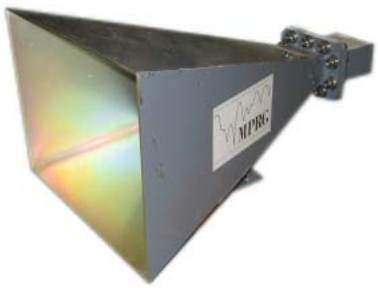

Figure 5.8: The Standard Gain Horn

Looking at the results in Table 5.6, as expected the Ridged TEM Horn and the Vilaldi have the higher gain values. Furthermore, it may be noticed that the Bicone performs better than a dipole[4] (2.1 dBi) at most frequencies examined. Finally, the TimeDomain antenna for some frequencies (4-4.6 GHz) performs better than a dipole, but for other frequencies its performance is worse than a dipole.

[4]The gain of a dipole is used solely for comparison purposes, it is acknowledged that a dipole can only optimally work to the frequency that it was designed

Table 5.6: Estimated Antenna Gains

Antenna	Est. Gain (dBi) at Frequency (GHz)						
	1	2	3.3	4	4.6	5	9
Ridged TEM Horn	13	11	11.4	10.5	10.5	9.5	9.25
Bicone	6.75	4	5	3	3	4	2.5
Vivaldi	9.25	11.25	8.5	8	8	7.25	4.5
TimeDomain	-12	-8.5	2	3	3	1	-2.5

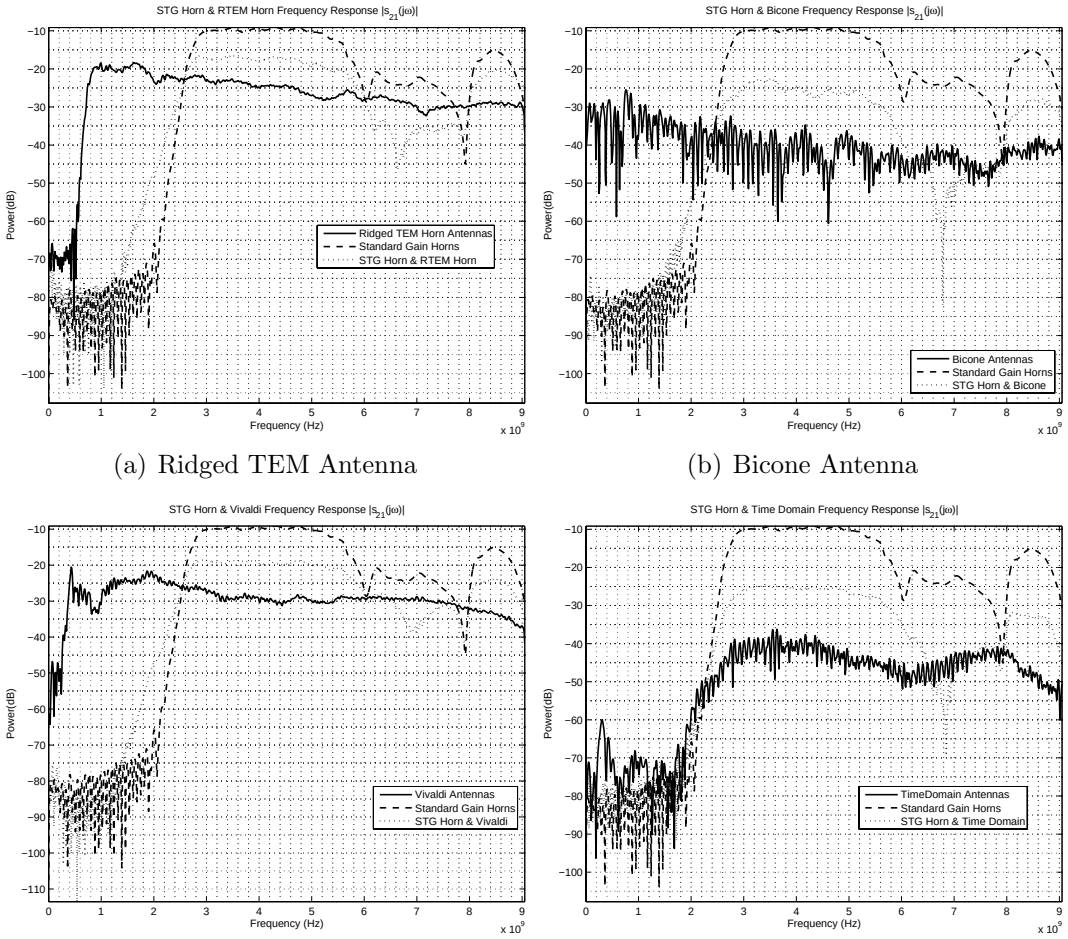

(a) Ridged TEM Antenna

(b) Bicone Antenna

(c) Vivaldi Antenna

(d) TimeDomain Antenna

Figure 5.9: Antenna Gain Measurements

Results — Link Budget Comparison

From the estimated antenna gains, the traditional Friis transmission formula link budget is to be compared to the proposed link budget. The Friis transmission formula is presented again:

$$\begin{aligned} P_R &= \frac{P_T G_T G_R \lambda^2}{(4\pi r)^2} \\ &= P_T \frac{G_T G_R \lambda^2}{4\pi} \frac{1}{4\pi r^2} \\ &= P_T G_{Friis} \frac{1}{L_p} \end{aligned} \tag{5.24}$$

From the above it can be shown that the Friis formula G_{AP} equivalent term is:

$$G_{Friis} = \frac{G_T G_R \lambda^2}{4\pi} \ (m^2) \tag{5.25}$$

In terms of received power or energy, the only difference in the two link budgets is the terms G_{AP} and G_{Friis}. Therefore, any difference between the two will be reflected in those two terms.

One might argue that a gain defined in terms of energy (G_{AP}) can not be compared with a gain defined in terms of average power (G_{Friis}). Assuming that a pulse $p(t)$ is repeated every T seconds, that the duration of the pulse is less than T seconds, and that only a single instance of the pulse can always be found in the time interval $(0, T)$, the energy of that single instance of the pulse can be defined as:

$$E_p = \int_{-\infty}^{\infty} p^2(t)dt = \int_0^T p^2(t)dt \tag{5.26}$$

The average power when the same pulse is repeated every T seconds will be:

$$P_p = \frac{1}{T}\int_0^T p^2(t)dt = \frac{1}{T}E_p \tag{5.27}$$

The power ratio R_{12} of two pulses $p1$ and $p2$ that repeat themselves every T seconds will be:

$$R_{12} = \frac{P_{p1}}{P_{p2}} = \frac{\frac{1}{T}E_{p1}}{\frac{1}{T}E_{p2}} = \frac{E_{p1}}{E_{p2}} \tag{5.28}$$

The above result indicates that the ratio of the energy of a single instance of two pulses is the same as the ratio of the average power of the two pulses when they are repeated every

T seconds. Therefore, G_{AP} and G_{Friis} should be comparable either when the UWB pulse repeats every T seconds or when just a single pulse is being sent.

Using the gains in Table 5.6, G_{Friis} was calculated and presented to Table 5.7, which also presents the calculated G_{AP} from the S_{21} parameters with no cable effects added.

Comparing G_{Friis} and G_{AP} (without the receive cable effects) it can be observed at some frequencies, for example 4.6 GHz, which is the center frequency of the 10 dB bandwidth of the generated pulse, the two gains are close to each other. This should be treated as a coincidence, since G_{AP} is pulse dependent and will be different for different pulses with different spectrum characteristics. On the other hand, G_{Friis} will remain the same with any pulse used, if it is evaluated at the same frequency.

Table 5.7: Calculated G_{Friis}

Antenna	G_{Friis} (dBm^2) at Frequency (GHz)						G_{AP} (S_{21})
	2	3.3	4	4.6	5	9	(dBm^2)
Ridged TEM Horn	-5.48	-9.03	-12.5	-13.71	-16.44	-22.04	-13.02
Bicone	-19.48	-21.83	-27.5	-28.71	-27.44	-35.54	-26.79
Vivaldi	-4.98	-14.83	-17.5	-18.71	-20.94	-31.54	-17.04
TimeDomain	-44.48	-27.83	-27.5	-28.71	-33.45	-45.54	-35.38

Results — G_{AP} for different pulses

To further demonstrate that G_{AP} is pulse dependent, G_{AP} was calculated using different pulses. The chosen pulses are a 100 ps and a 500 ps Gaussian pulse and their first derivatives (Gaussian Monocycle.) The pulse width, in seconds, for these pulses is defined as $\tau_p = 2\pi\sigma$, where σ is the standard deviation of the pulse, also in seconds. The pulses and their spectrum characteristics are shown in Figure 5.10. The resulting G_{AP}'s and the spectrum characteristics (10 dB Bandwidth and center frequency) of the pulses are shown in Table 5.8. If the G_{AP} is compared between the 100 ps and 500 ps cases, for both the Gaussian and Gaussian Monocycle, it may observed that the 500 ps cases have higher gains compared to the 100 ps cases, this is because the 500 ps pulses have narrower bandwidth which makes use of the higher gain portions of the antennas' frequency response.

In addition to the above pulses, G_{AP} was calculated for two Gaussian Pulses (1ns & 5ns) which were used to modulate a sinusoidal wave in order to change the center frequency of the pulses. The results are displayed in Figure 5.11. It can be seen that for a very few cases the resulting G_{AP} might be close to G_{Friis}, but for most cases is not. Furthermore, it can be noticed, especially for the TimeDomain antennas that as the bandwidth of the pulse is

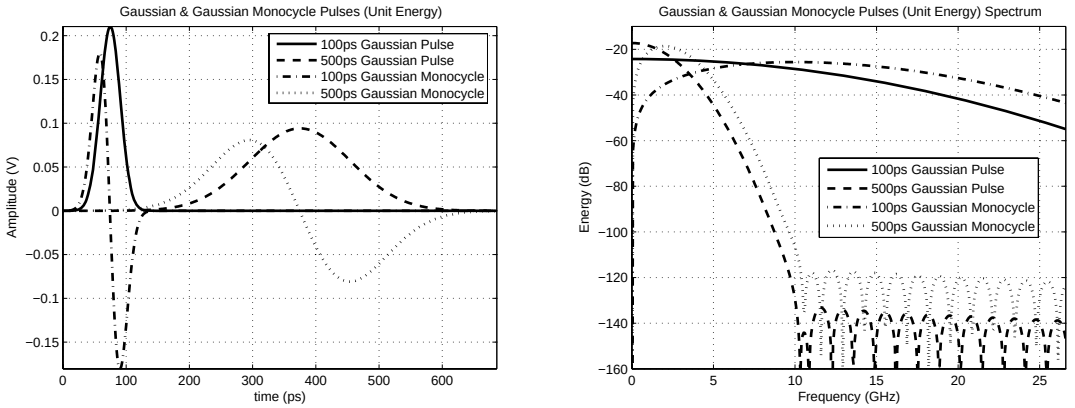

(a) Time domain

(b) Energy Spectrum

Figure 5.10: Gaussian & Gaussian Monocycle Pulses

Table 5.8: Sample G_{AP} for different pulses

Property	Pulse			
	Gaussian		Gaussian Monocycle	
	100ps	500ps	100ps	500ps
10dB BW (GHz)	15.2	3.1	20.1	4.1
10dB BW Center Freq. (GHz)	7.6	1.53	12.1	2.4
Ridged TEM Horns G_{AP} (dBm^2)	-13.84	-11.79	-18.37	-10.60
Bicones G_{AP} (dBm^2)	-27.81	-23.79	-32.56	-25.83
Vivaldis G_{AP} (dBm^2)	-17.77	-15.95	-22.76	-14.59
TimeDomains G_{AP} (dBm^2)	-35.09	-42.21	-37.99	-35.21

reduced (longer pulse duration) G_{AP}'s variation follows the same fluctuations as the antenna frequency response, i.e., when the antenna has a low response at a frequency, G_{AP} will be low as well. This may observed by comparing Figures 5.5 and 5.11(d).

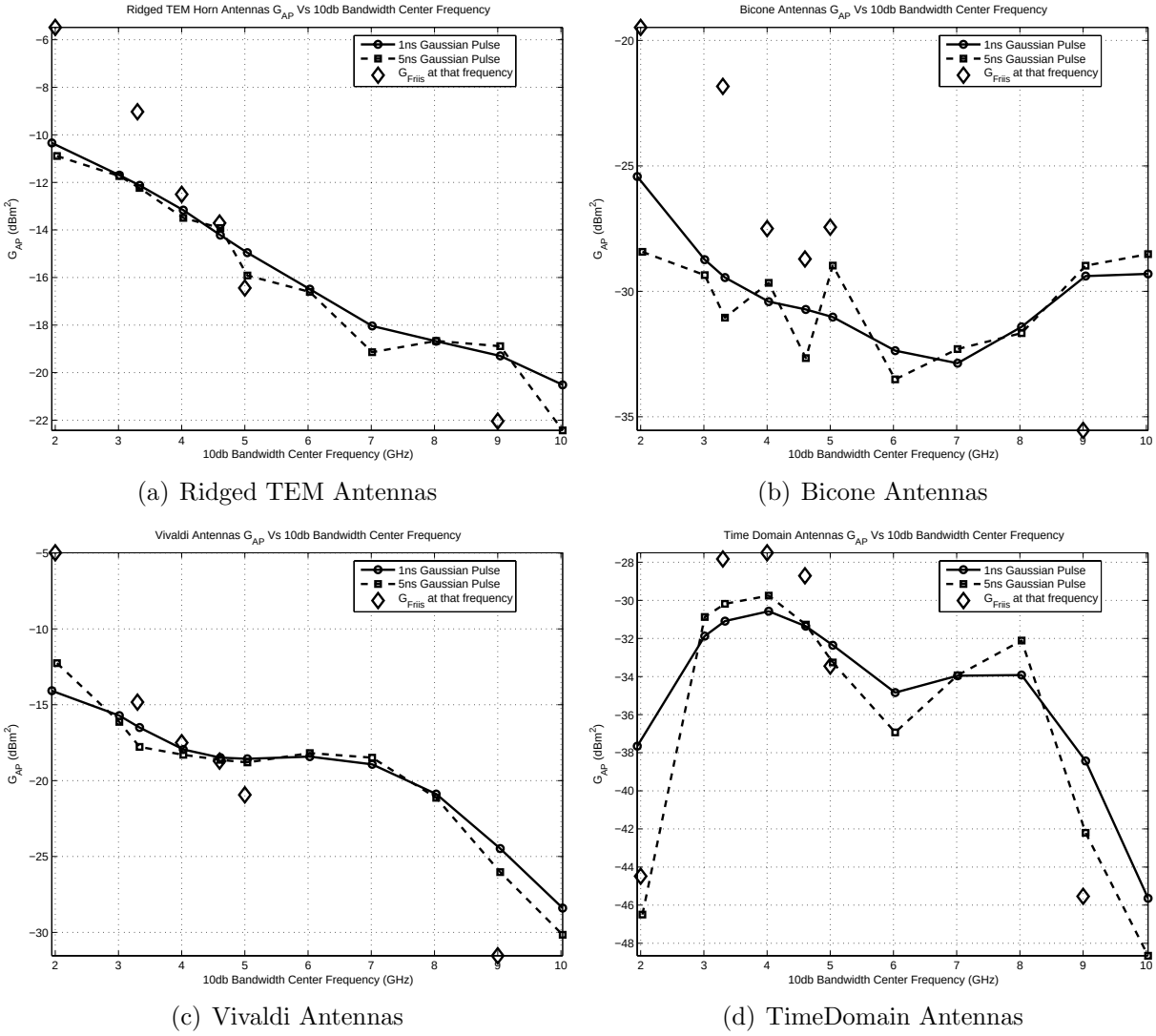

(a) Ridged TEM Antennas

(b) Bicone Antennas

(c) Vivaldi Antennas

(d) TimeDomain Antennas

Figure 5.11: G_{AP} Vs Center Frequency

5.5.2 Time Domain Digital Sampling Oscilloscope Measurements

In this section the time domain measurements taken using a Digital Sampling Oscilloscope are described and presented. The measurements include 1 m reference measurement using the four antenna pairs described earlier for calculating their G_{AP} using the time domain method. Furthermore, the received pulses were measured for additional distances up to 25 m. The additional measurements were used to evaluate the predictions of the proposed method.

Method

For the time domain measurements the following equipment were used:

- Geozondas Pulser $T_{0.5} < 30ps$, $V_{out} > 30V/50\Omega$ (GZ1106DL1 & GZ1117DN-25)
- HP33120A Function Generator
- Tektronix CSA8000B Digital Sampling Oscilloscope
- United Microwave cables Micropore 190 (10 ft for each antenna)
- Generic cables for trigger connections.

The equipment were divided into two sides: the transmit side, and the receive side (Figure 5.12). The transmit side consisted of the transmit antenna connected with a 10 ft cable to the pulser, and the function generator. On the other side, there was the receive antenna connected with another 10 ft cable to the Digital Sampling Oscilloscope (DSO). The function generator was used to trigger both the pulser and the DSO with a 200 KHz half amplitude mean square wave. In order to ensure that the DSO will not miss the pulse sent by the pulser because of the delayed triggering (caused by the trigger cable length) the trigger cable that connected the function generator to the pulser was slightly longer than the trigger cable to the DSO. That ensured that the DSO was triggered and was looking for the pulse slightly before it was sent.

Each signal measurement was taken averaging 500 waveforms in order to minimize the effects of noise. The received window duration was 5ns for the LOS case and 20 ns for the Non Line of Sight (NLOS) case. The antennas for the LOS case were placed 1.67 m high, and for the NLOS case 1.2 m high. For the LOS case a very precise measurement (in terms of separation distance) was taken at 1 m. The rest of the distances were estimated by the additional time delay.

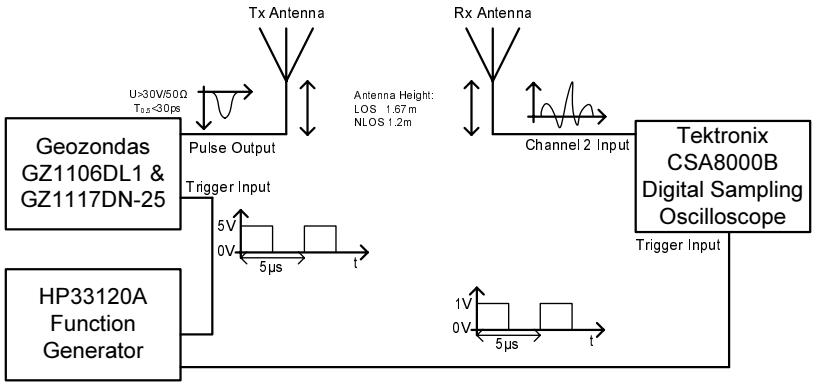

Figure 5.12: Time Domain Measurements Equipment Setup

Results — Antenna Noise

Table 5.9 presents the noise measurements done outdoors. The receive antenna was connected to the Digital Sampling Oscilloscope and the received signal was recorded without the transmitter on. Similar to the other measurements, 500 waveform averaging was used. The results show that the higher the antenna bandwidth the higher the recorded noise is. The time window for these measurements was 5 ns and the bandwidth assumed for the noise power spectral density (N_0) calculations was the noise equivalent bandwidth of the antennas.

Table 5.9: Received Antenna Noise (500 waveform average)

Antennas	Noise		
	Measured		Calculated
	Energy (dBJ)	Power (dBW)	N_0 (dBW/Hz)
Ridged TEM Horns	-187.64	-104.63	-202.56
Bicones	-191.62	-108.61	-192.56
Vivaldis	-194.49	-111.48	-205.08
TimeDomain	-213.18	-130.17	-206.77

Results — Analysis

The received waveforms were filtered using a 50 MHz to 18.05 GHz ideal bandpass filter (using the FFT and IFFT) to match the bandwidth measured by the VNA so the received waveforms can be compared to the waveforms generated with the S_{21} parameters. A reference noise measurement was taken with each antenna and the same filter was applied to the

reference noise. The noise energy and power were calculated and subtracted from the signal energy/power calculations.

Results — LOS Measurements

The LOS measurements were taken at a height of 1.67 m on the road right next to the sidewalk on the back of Durham Hall (Figure 5.13). The transmit location and the final receive location are shown in the location photo (Figure 5.13). The receive measurements were done along the receive path also shown in the same photo.

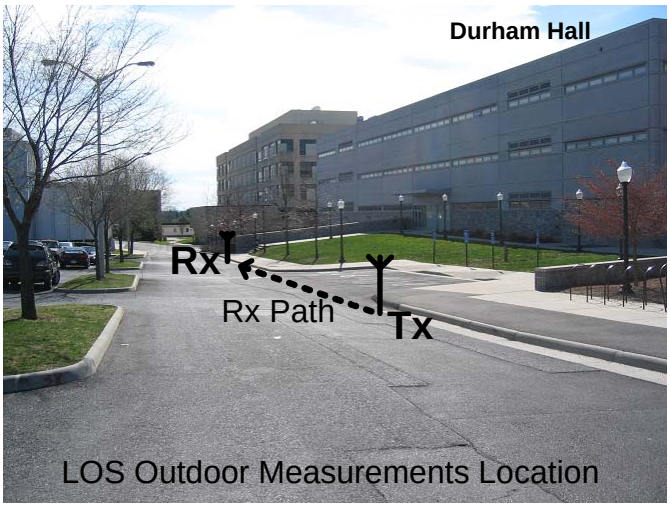

Figure 5.13: LOS Measurement Location

The results of the measurements are shown in Figures 5.14 to 5.17. Each figure:

(a) shows the received energy along with the predicted energy based on the calculated G_{AP} and a path loss exponent of 2 [Equation (5.20)]. In addition the predicted energy is also calculated using the actual observed path loss exponent which was found to vary slightly from the expected path loss exponent of 2.

(b) shows the same information as (a) for peak power.

(c) shows the received pulse at reference distance of 1 m.

(d) shows all received pulses normalized by the distances (on these pulses the ground reflection can be clearly seen and is coming closer and closer to the main pulse as the distance increases). The reflections were time gated and only the main part of the pulse (e) was used for the calculations.

(e) shows the the same information as (d) but showing only time window that was used for the energy and peak power calculations, and finally,

(f) shows the spectrum of the generated pulse along with the first and last received pulse spectra.

The path loss exponent n of the results was found to be smaller than 2. Initially this was believed to be from additional multipath (besides the main ground reflection) that could not be seen by looking at the received signal. However, by deconvolving the received signal using the CLEAN[5] algorithm [9], and reconstructing the received waveform by just using the main (strongest path) and calculating the received energy yielded results with no significant difference.

Reasons that might have contributed to a path loss exponent $n \neq 2$

- The measurements used a very small portion of the receiver's dynamic range making it prone to quantization errors.
- A high frequency triggering jitter was also observed, causing the received signal to move around its position slightly, which combined with the averaging might have contributed to additional energy level reduction.
- The TimeDomain antennas were the only pair found with a path loss slightly over 2, and were the narrowest in bandwidth of the antennas used. In a way those antennas were filtering the environmental noise before arriving at the receiver. This observation partially supports the possibility that the higher antenna bandwidth might contribute to the higher energy levels due to the additional noise.

[5]The CLEAN algorithm is a deconvolution method that correlates the received waveform with a reference pulse, finds the higher correlation, assigns a weight and subtracts the pulse from the received signal. This procedure is repeated until no correlations above specific threshold can not be found. In this report, a 15 dB threshold, referring to the stronger path, was used.

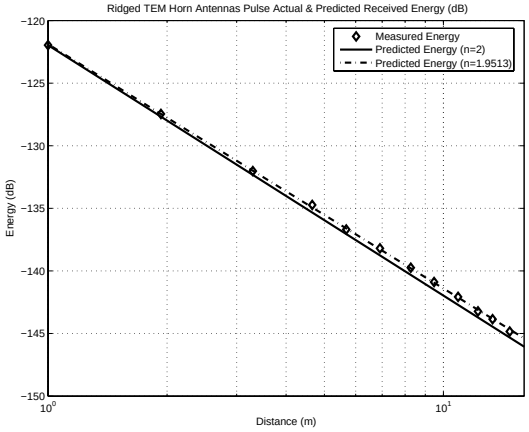

(a) Received Energy

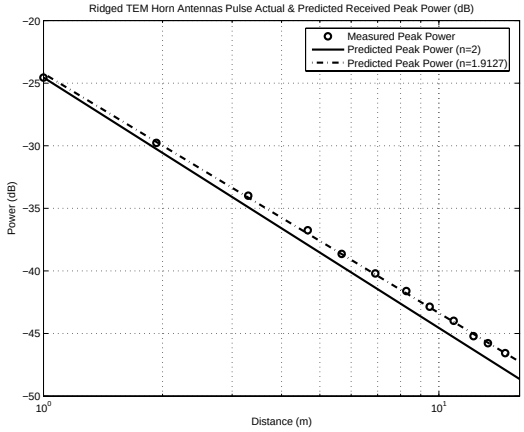

(b) Received Power

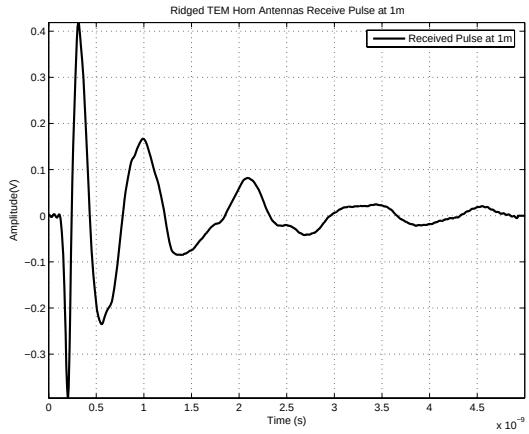

(c) Received Pulse (1m)

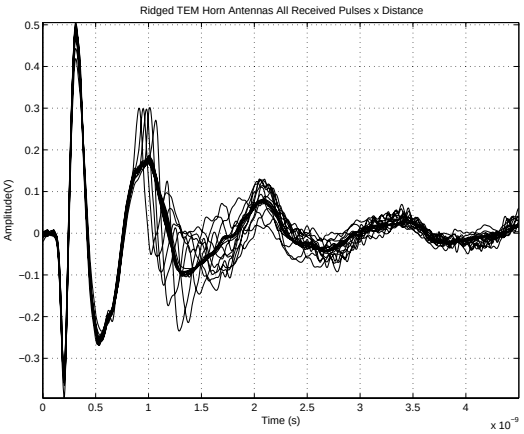

(d) All Received Pulses Normalized by the Distance

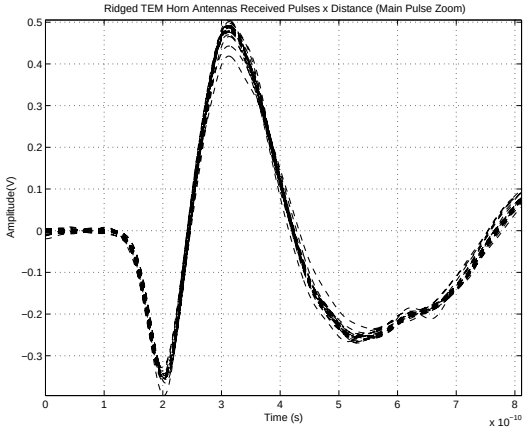

(e) All Received Pulses Normalized by the Distance (Main Pulse Zoom)

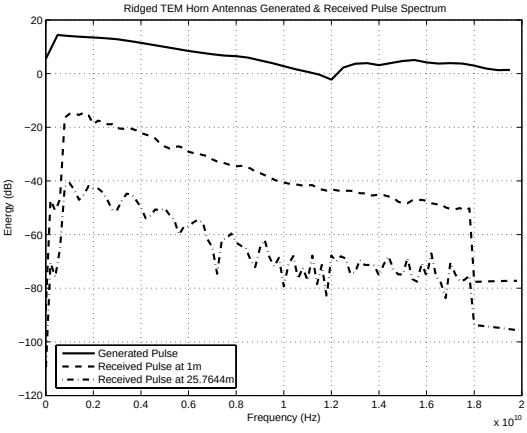

(f) Received Spectrum

Figure 5.14: Ridged TEM Antenna Results

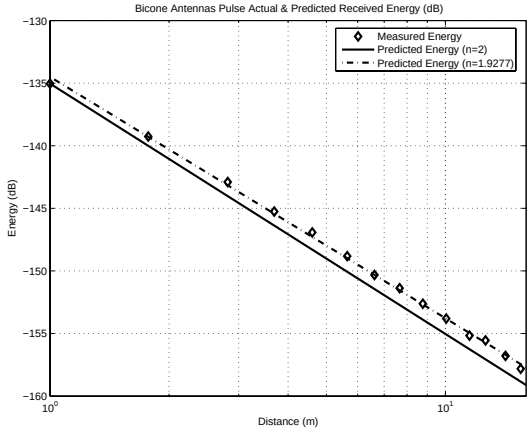

(a) Received Energy

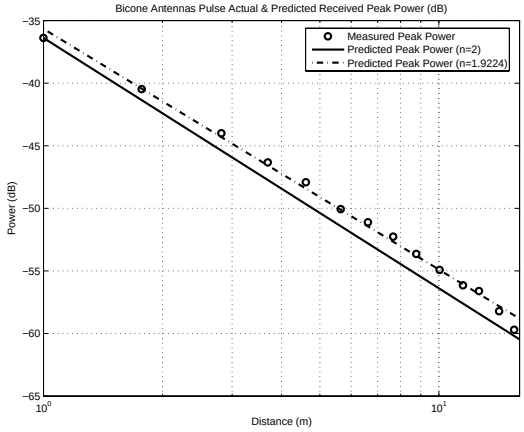

(b) Received Power

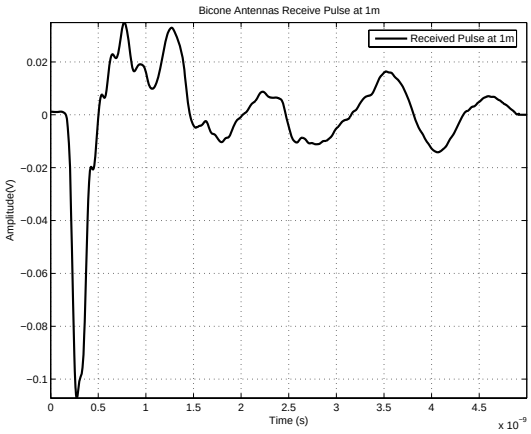

(c) Received Pulse (1m)

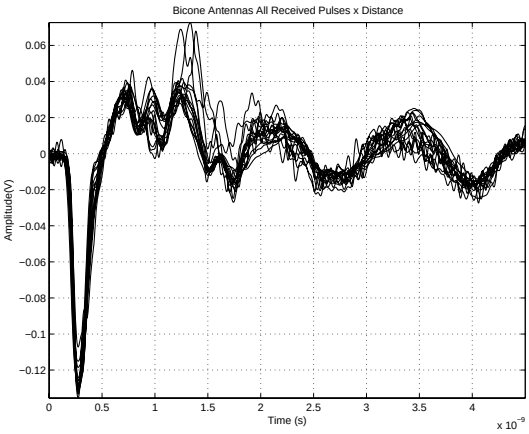

(d) All Received Pulses Normalized by the Distance

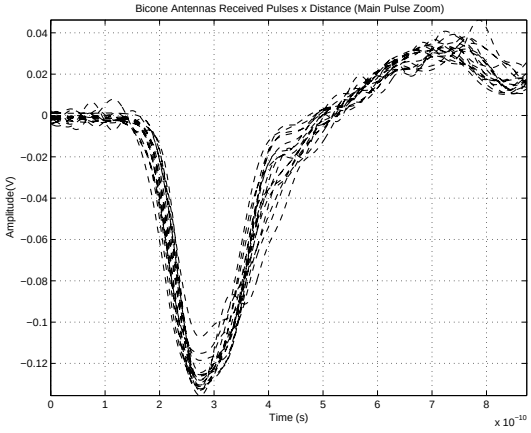

(e) All Received Pulses Normalized by the Distance (Main Pulse Zoom)

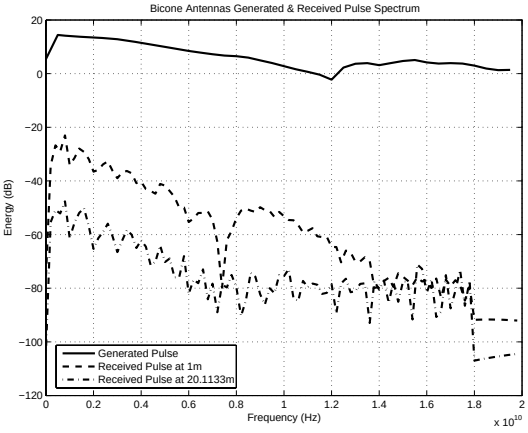

(f) Received Spectrum

Figure 5.15: Bicone Antenna Results

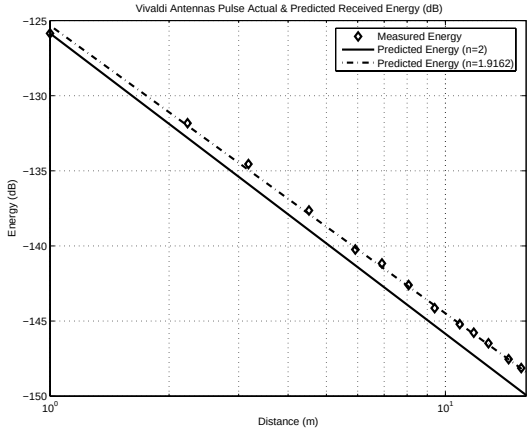

(a) Received Energy

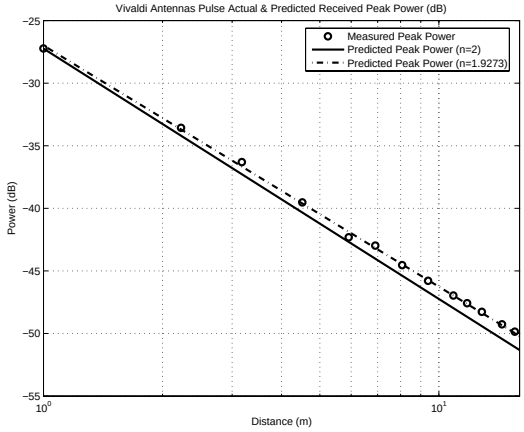

(b) Received Power

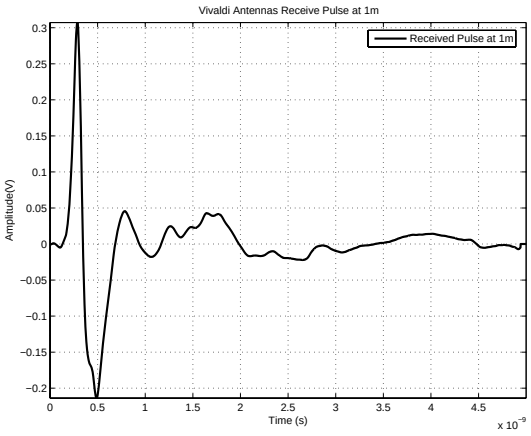

(c) Received Pulse (1m)

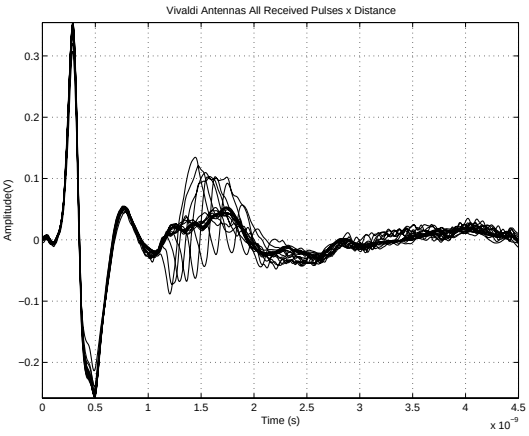

(d) All Received Pulses Normalized by the Distance

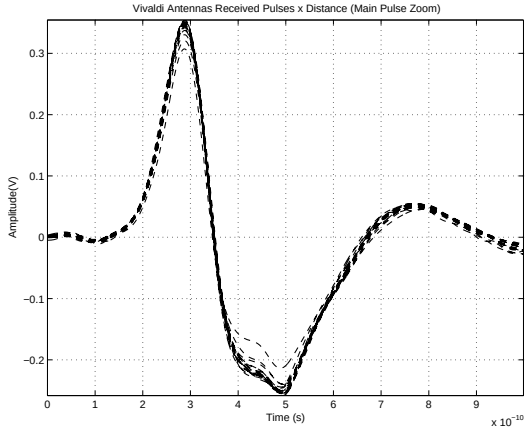

(e) All Received Pulses Normalized by the Distance (Main Pulse Zoom)

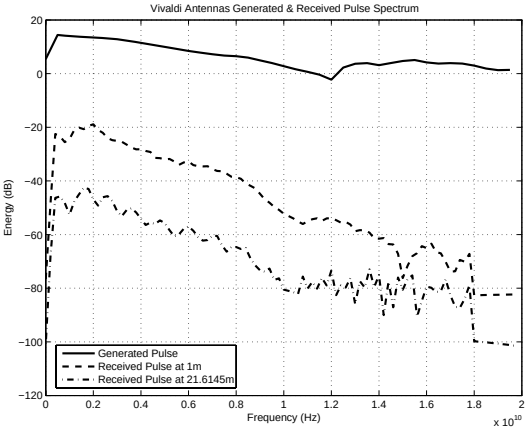

(f) Received Spectrum

Figure 5.16: Vivaldi Antenna Results

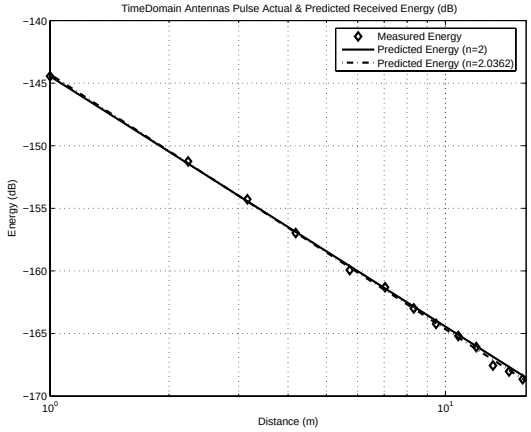

(a) Received Energy

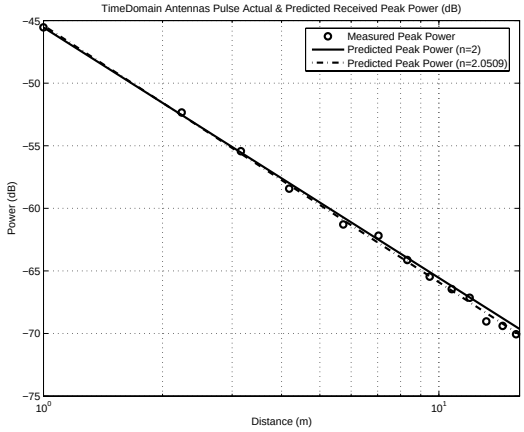

(b) Received Power

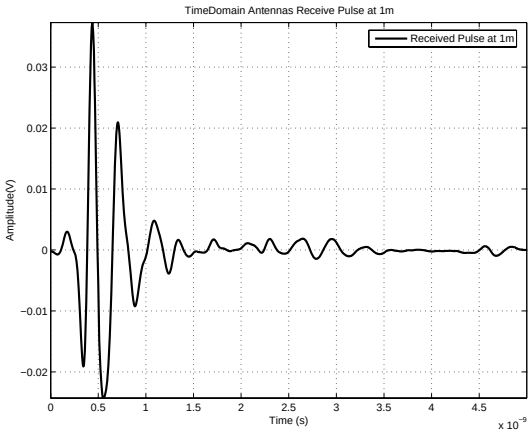

(c) Received Pulse (1m)

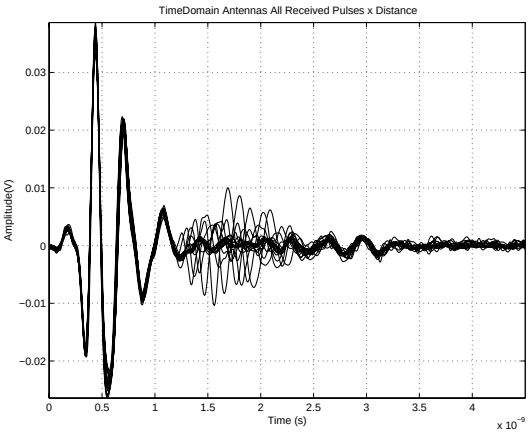

(d) All Received Pulses Normalized by the Distance

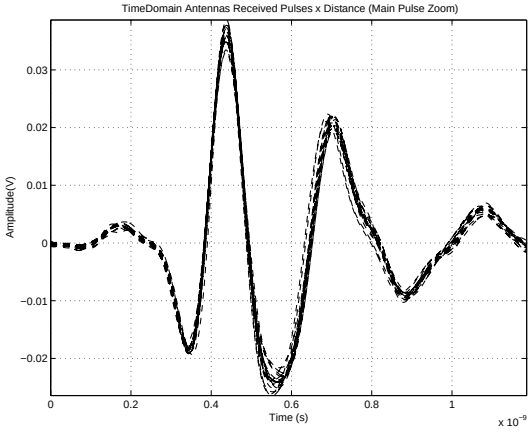

(e) All Received Pulses Normalized by the Distance (Main Pulse Zoom)

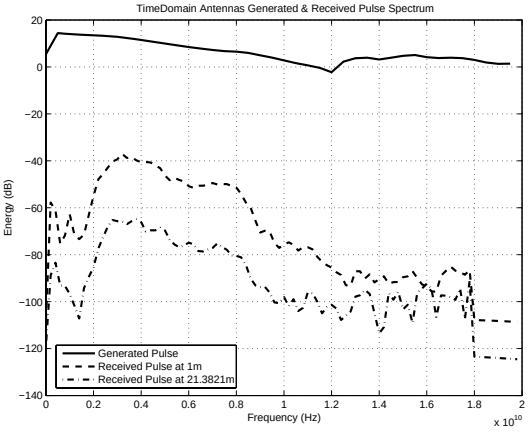

(f) Received Spectrum

Figure 5.17: TimeDomain Antenna Results

Results — NLOS Measurements

In this section the results of a sample NLOS measurement set are presented. Twelve points at MPRG's radio lab were taken (Figure 5.18). The equipment used and the setup were the same as the other time domain measurements previously presented. The same pulse was used as well. The only difference was that there was no line of sight between the transmit and receive antennas (The Bicones). In this case the received window was 20 ns.

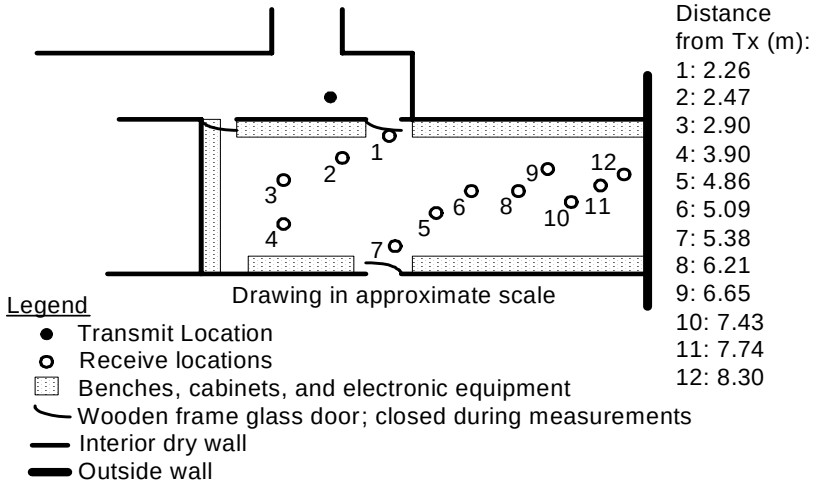

Figure 5.18: NLOS Measurement Locations

Analysis Procedure For this measurement set the distance between the trasnmit and receive antennas was not estimated from the time delay like the previous cases (LOS). Instead, it was estimated by measuring the exact location of the receive points (the transmitter location was fixed.) The received signals were bandpass filtered with a bandpass filter of 50 MHz to 18.05 GHz. Then each signal's channel impulse response (CIR) was estimated using the CLEAN algorithm

After the CIR was estimated, the received signal was reconstructed[6] by convolving the CIR with the reference pulse (of unit energy). Then the energy in the whole window was calculated. The peak power was calculated as well by using the absolute maximum peak on the received window.

Using the reconstructed received waveform the ability of a Rake receiver to capture the energy on the channel was evaluated. To simulate a Rake receiver the signal was correlated (match filtered) with a unit energy reference pulse, then using a peak detection method the first N stronger peaks were selected, where N is the number of the assumed Rake fingers.

[6]This ensured a received signal with resolvable paths and no noise present.

Furthermore, peaks closer than 1/4 of the reference's pulse width to already selected peaks were ignored. The energy on the selected peaks was calculated and divided by the total energy on the channel (energy capture of a perfect Rake,) even though it is known that such receivers do not exists. The results are presented at Figure 5.20 and are very close to results presented in [10]. The receiver's performance is required when doing a link budget in order to predict how much energy will will be captured by the receiver, therefore, making the necessary modifications to the link budget parameters for achieving the desired performance.

Observed Path loss The energy path loss exponent n observed from this set was 2.09. However, other more extensive measurements observed a path loss exponent of 2.3 ($\sigma = 2.4$ dB) for Bicones and 2.4 ($\sigma = 5.1$ dB) for Horn Antennas [5]. In addition, [11] found a path loss exponent of 2.95 to 3.12 using a Vector Network Analyzer in the range of 2 to 8 GHz. Furthermore, the IEEE 802.15.3a standards task group adopted an $n = 3.5$ with $\sigma = 0.97$ [12]. The reason for getting a small path loss exponent from the measurements presented here is because of the short distances that allow small amplitude multipath to be strong enough to be detected. Furthermore, the pulse used was narrower and combined with the higher sampling frequency (finner time resolution) these factors allow the resolution of more multipath components which contributed to the received energy. On the other hand, the path loss exponent of the peak power was found to be 3.37. Finally, high accuracy is not expected from such a small set of measurement points which were taken for link budget verification purposes and not from the channel characterization perspective. Nevertheless, Table 5.10 presents the observed channel statistics for the above measurements.

Table 5.10: Average NLOS Statistics

n	σ	$\overline{\tau}_{mean}$	$\overline{\tau}_{rms}$	$\overline{N}_p$
2.09	5.30 dB	7.52 ns	4.98 ns	53

NLOS Link Budget Considerations When doing a link budget for NLOS operation, additional factors must be taken in consideration. If the path loss exponent is defined in terms of the total energy of the channel (including multipath), then a receiver performance factor must be included, because a practical receiver will be able to capture only a fraction of the total energy as demonstrated in Figure 5.20. Furthermore, the received energy in a NLOS channel fluctuates significantly more than in the LOS case and a larger fading margin must be considered.

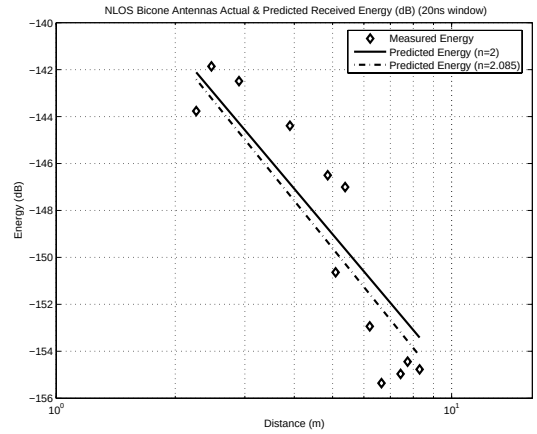

(a) Received Energy

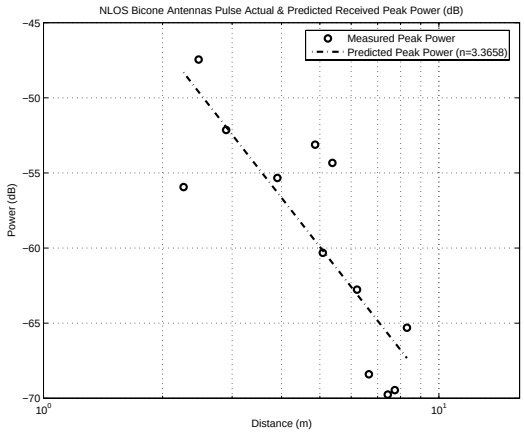

(b) Received Power

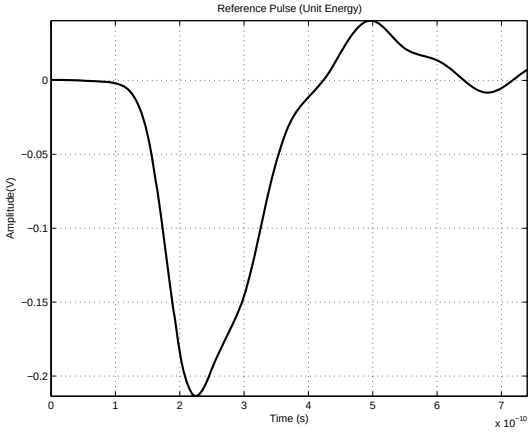

(c) Reference Pulse

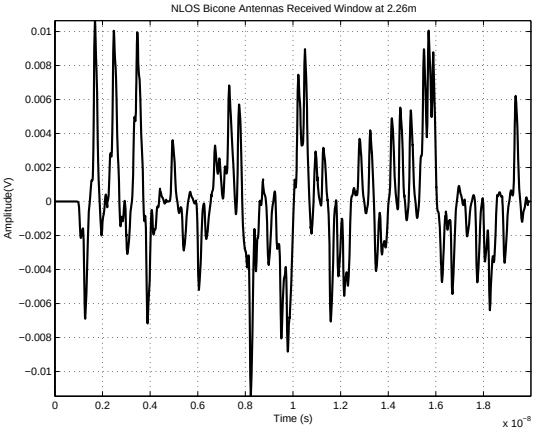

(d) 1st Received Window

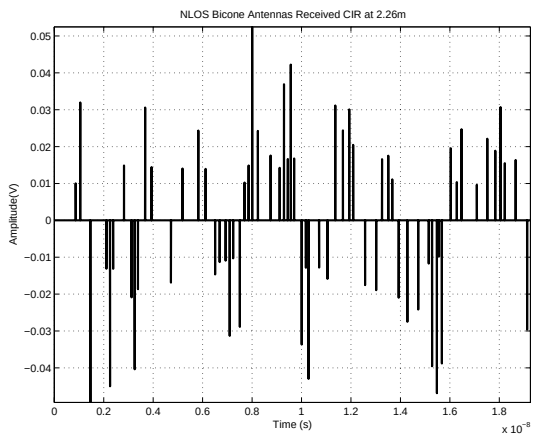

(e) 1st Received Window CIR

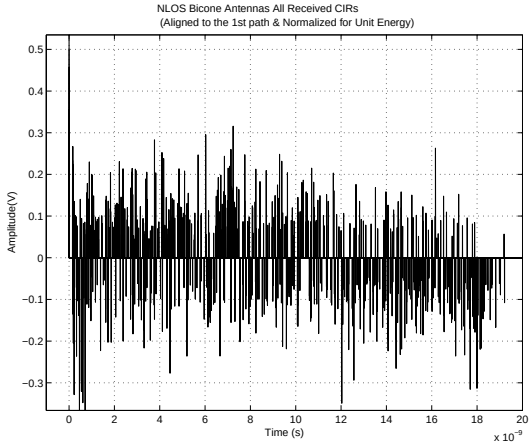

(f) All Received CIRs

Figure 5.19: NLOS Bicone Results

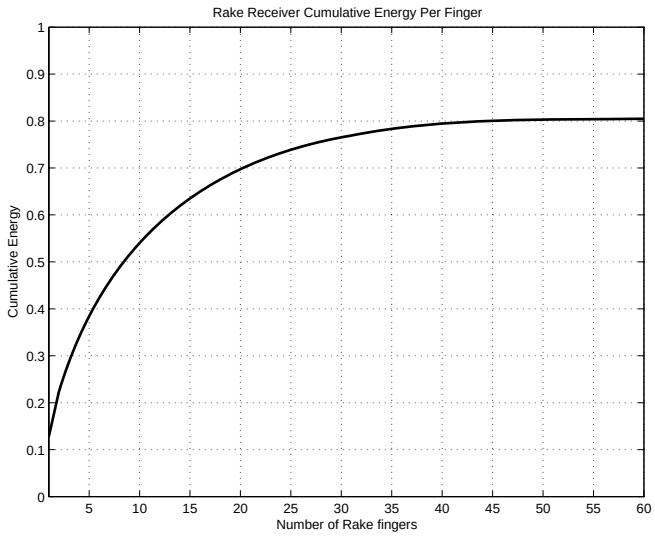

Figure 5.20: Rake Receiver Performance

5.5.3 Link Budget Calculations

Using the data collected and calculated in this section (Validation) link budget was calculated by estimating the received energy using the proposed method and the Friis transmission formula.

Figures 5.21 to 5.28 show the results for the received energy and peak power along with sample link budget calculations for the LOS cases. For the Friis formula calculations the 10 dB center bandwidth of the pulse was used which was 4.6 GHz and the received peak power frequency of each antenna pair was used as well.

LOS Example Calculations

Tables 5.11 and 5.12 show a set of actual calculations done in the same way that were performed for Figures 5.21 to 5.28.

For the TimeDomain antennas case, used in the example calculations, the most accurate way for doing link budgets based on received energy and peak power was the proposed method using G_{AP}. However, as it can be seen from Figures 5.21 to 5.26 the energy link budget (correlator) is also accurately estimated using the Friis transmission formula. On the other hand, the peak power (detector) link budget is still not accurately calculated. The results demonstrate that by using the Friis transmission formula there are cases that might be valid, but not always, on the other hand, the proposed method using G_{AP} is always very close to the observed signal levels for both energy and peak power.

NLOS Example

On Table 5.13 a sample set of NLOS link budget calculations are presented. Some of the parameters used were obtained from Section 5.5.2 were the NLOS case was investigated.

The NLOS link budget, compared to the LOS link budget, has to take in account the larger path loss experienced in a NLOS scenario. Furthermore, the path loss observed at any given point will deviate from its average value due to variations in the environment. The path loss variation has been shown to follow a log-normal distribution [5]. From a link budget perspective, a big enough fading margin must be used in order to ensure a certain performance at a % of the time. For the calculations it was assumed $n = 2.3$ with a $\sigma = 2.4$ dB [5]. The fading margin was calculated to be 6dB for providing the target E_b/N_0 at least 99.1 % of the cases. The probability that the received signal level assuming log-normal fading (in dB power units) will exceed a certain value γ can be calculated from the normal CDF using Equation (5.29) [7]:

$$Pr[P_R(r) > \gamma] = Q\left(\frac{\gamma - \overline{P_R(r)}}{\sigma}\right) \tag{5.29}$$

Table 5.11: TimeDomain Antenna Example Link Budget Calculations at $r = 15.68m$—Correlator Detector (LOS)

	Proposed Method Using G_{AP}	**Friis Formula (4.6Ghz)**	**Friis Formula (3Ghz)**	**Using Measured Energy**
Received Energy				
Transmitted Energy E_T	$-95.47dBJ$	$-95.47dBJ$	$-95.47dBJ$	$-95.47dBJ$
Antenna Pair–Pulse G_{AP} for Energy	$-37.99dBm^2$			
Antenna Gains $(G_T + G_R)$		6dBi	4dBi	
Path Loss $\frac{1}{4\pi r^2}$	$-34.9dBm^{-2}$			
Path Loss $\left(\frac{\lambda}{4\pi r}\right)^2$		$-69.61dB$	$-65.9dB$	
Received Energy E_R	$-168.36dBJ$	$-159.08dBJ$	$-157.37dBJ$	$-168.65dBJ$
Noise PSD				
Boltzmann's Constant $(dBW/K/Hz)$	-228.6	-228.6	-228.6	-228.6
System Noise Temp $(T_0 = 290K)$	$24.6dBK$	$24.6dBK$	$24.6dBK$	$24.6dBK$
Noise PSD N_0	$-204dBW/Hz$	$-204dBW/Hz$	$-204dBW/Hz$	$-204dBW/Hz$
Received Energy per Bit				
Pulses per bit $N_s = 1$	1	1	1	1
Energy/bit $E_b = E_R + 10log(N_s)$	$-168.36dBJ$	$-159.08dBJ$	$-157.37dBJ$	$-168.65dBJ$
Final E_b/N_0				
Fading Margin M_F	$0dB$	$0dB$	$0dB$	$0dB$
Energy Capture Loss (20%) ρ	$-7dB$	$-7dB$	$-7dB$	$-7dB$
$E_b/N_0 = E_b - N_0 - M_F + \rho$	*28.64dB*	*37.92dB*	*39.63dB*	*28.35dB*

Table 5.12: TimeDomain Antenna Example Link Budget Calculations at $r = 15.68m$—Peak Detector (LOS)

	Proposed Method Using G_{AP}	**Friis Formula (4.6Ghz)**	**Friis Formula (3Ghz)**	**Using Measured Power**
Received Power				
Transmitted Peak Power P_T	$9.26dBW$	$9.26dBW$	$9.26dBW$	$9.26dBW$
Ant. Pair–Pulse G_{AP} PPower	$-43.82dBm^2$			
Antenna Gains $(G_T + G_R)$		6dBi	4dBi	
Path Loss $\frac{1}{4\pi r^2}$	$-34.9dBm^{-2}$			
Path Loss $\left(\frac{\lambda}{4\pi r}\right)^2$		$-69.61dB$	$-65.9dB$	
Received Peak Power P_R	$-69.46dBW$	$-54.35dBW$	$-52.64dBW$	$-70.18dBW$
Noise Power				
Boltzmann's Constant $(dBW/K/Hz)$	-228.6	-228.6	-228.6	-228.6
System Noise Temp $(T_0 = 290K)$	$24.6dBK$	$24.6dBK$	$24.6dBK$	$24.6dBK$
Received 10db BW $(4GHz)$	$96.02dBHz$	$96.02dBHz$	$96.02dBHz$	$96.02dBHz$
Noise Power N_0	$-107.98dBW$	$-107.98dBW$	$-107.98dBW$	$-107.98dBW$
Final E_b/N_0				
Fading Margin M_F	$0dB$	$0dB$	$0dB$	$0dB$
Capture Loss (10%) ρ	$-10dB$	$-10dB$	$-10dB$	$-10dB$
$E_b/N_0 = P_R - N_0 - M_F + \rho$	*28.52dB*	*43.63dB*	*45.34dB*	*27.8dB*

Table 5.13: Bicone Antenna Example Link Budget Calculations at $r = 7.43m$—Correlator Detector (NLOS)

	Proposed Method Using G_{AP}	**Using Measured Energy**
Received Energy		
Transmitted Energy E_T	$-95.47dBJ$	$-95.47dBJ$
Antenna Pair–Pulse G_{AP} for Energy	$-28.57dBm^2$	
Path Loss $\frac{1}{4\pi r^n}$,$n = 2.3$[5], $r = 7.43m$	$-28.41dBm^2$	
Received Energy E_R	$-152.45dBJ$	$-155dBJ^*$
Noise PSD		
Boltzmann's Constant	$-228.6dBW/K/Hz$	$-228.6dBW/K/Hz$
System Noise Temp ($T_0 = 290K$)	$24.6dBK$	$24.6dBK$
Noise PSD N_0	$-204dBW/Hz$	$-204dBW/Hz$
Received Energy per Bit		
Pulses per bit $N_s = 1$	1	1
Energy per bit $E_b = E_R + 10log(N_s)$	$-152.45dBJ$	$-155dBJ$
Final E_b/N_0		
Fading Margin M_F ($Pr\{\frac{E_b}{N_0} < Target\} < 1\%$)	$6dB$	$6dB$
Energy Capture Loss ρ (40%, 5 Fingers, Figure 5.20)	$-4dB$	$-4dB$
$E_b/N_0 = E_b - N_0 - M_F + \rho$	*41.55dB*	*39dB*

* Ideally this value should be the average multiple observations for the desired distance

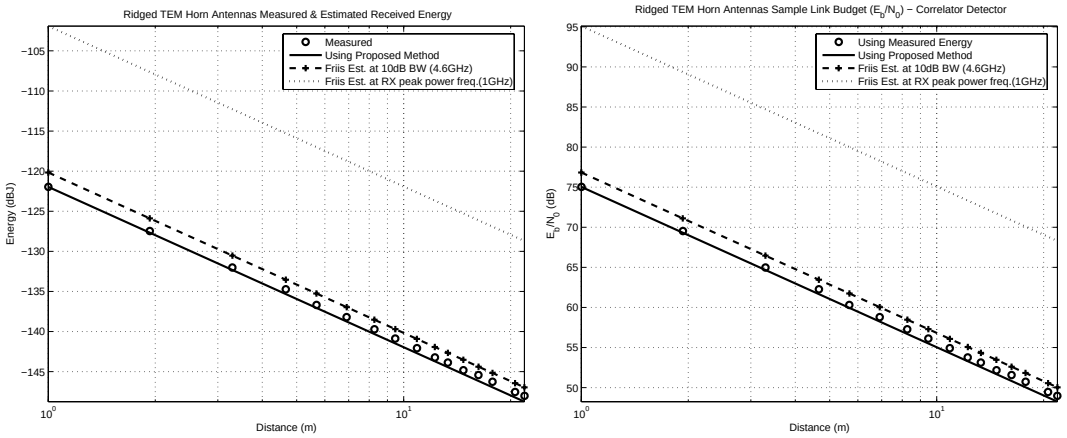

(a) Received Energy (b) Energy Link Budget

Figure 5.21: Ridged TEM Antenna Received Energy and Link Budget

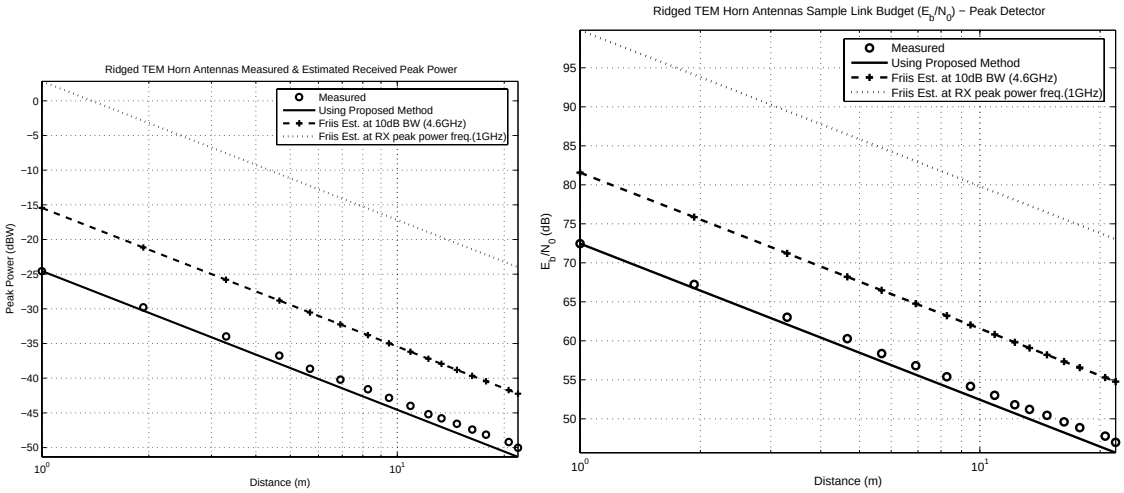

(a) Received Peak Power (b) Peak Power Link Budget

Figure 5.22: Ridged TEM Antenna Received Peak Power and Link Budget

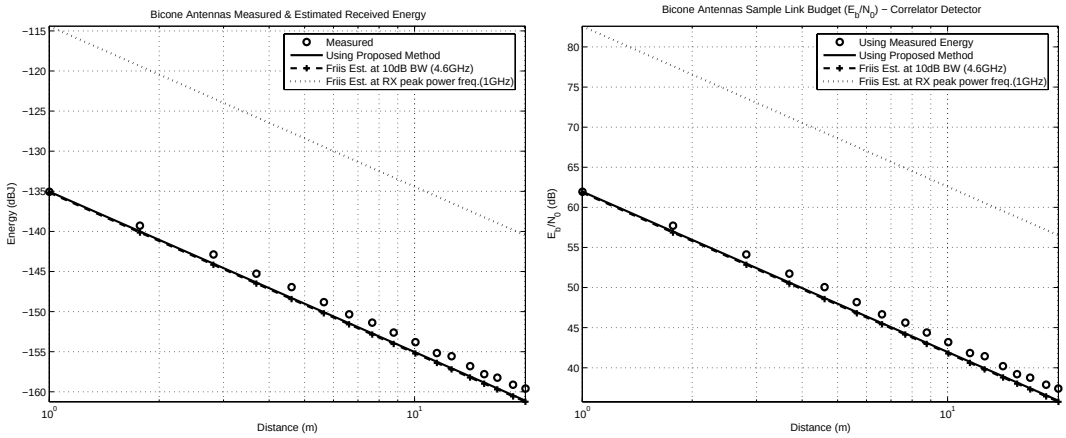

(a) Received Energy (b) Energy Link Budget

Figure 5.23: Bicone Antenna Received Energy and Link Budget

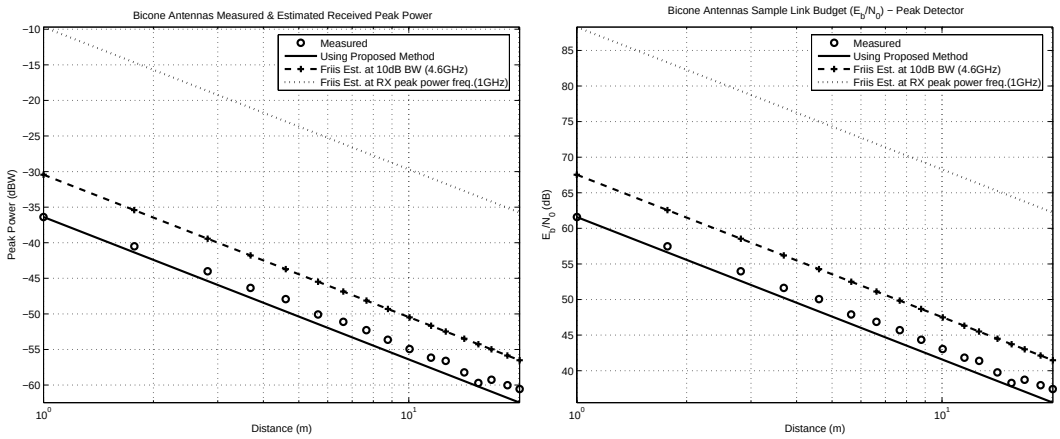

(a) Received Peak Power (b) Peak Power Link Budget

Figure 5.24: Bicone Antenna Received Peak Power and Link Budget

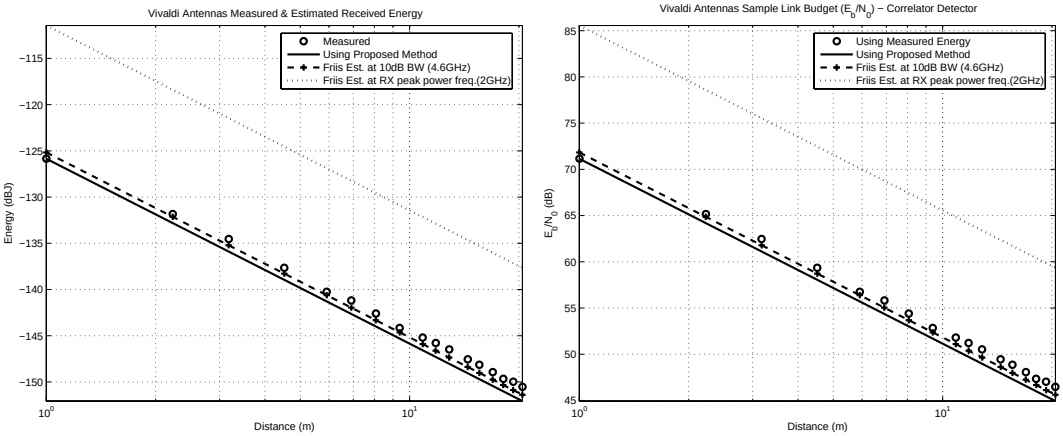

(a) Received Energy (b) Energy Link Budget

Figure 5.25: Vivaldi Antenna Received Energy and Link Budget

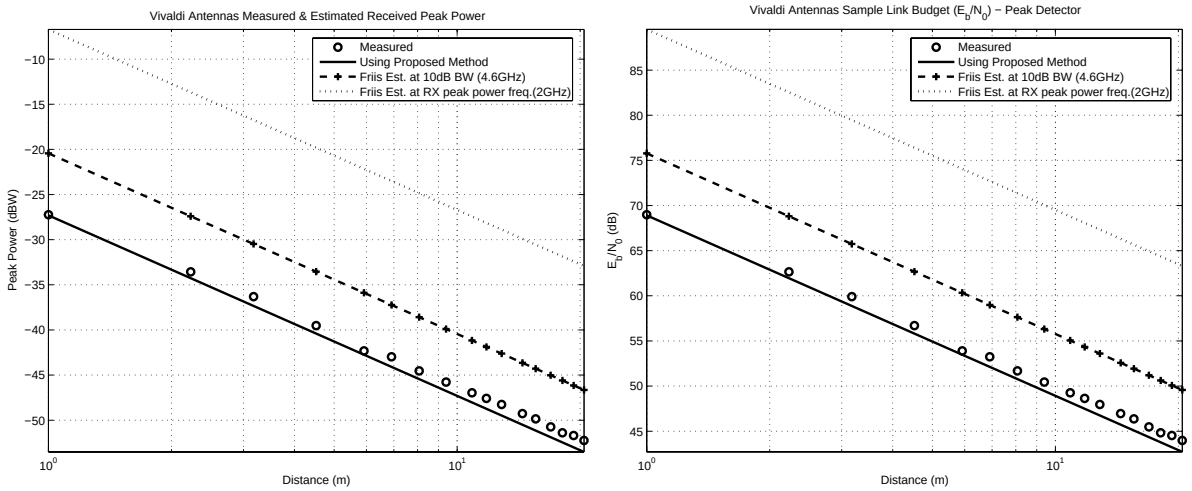

(a) Received Peak Power (b) Peak Power Link Budget

Figure 5.26: Vivaldi Antenna Received Peak Power and Link Budget

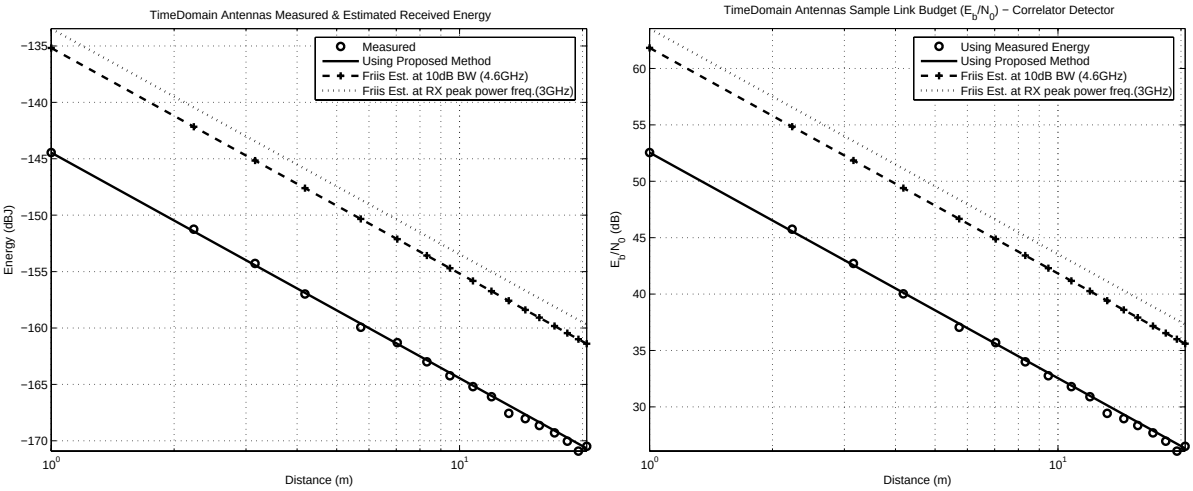

(a) Received Energy (b) Energy Link Budget

Figure 5.27: TimeDomain Antenna Received Energy and Link Budget

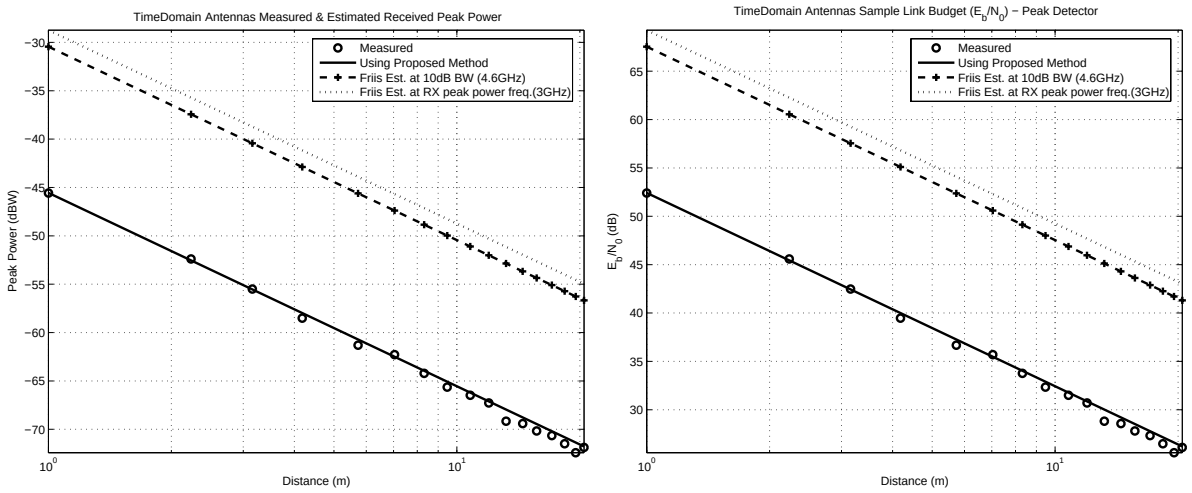

(a) Received Peak Power (b) Peak Power Link Budget

Figure 5.28: TimeDomain Antenna Received Peak Power and Link Budget

5.6 Conclusions

For narrowband systems an accurate link budget method exists based on the Friis transmission formula. However, that link budget is designed for a single frequency of operation. Using the center frequency of the transmitted I-UWB pulse along with this traditional model is not sufficient for most cases. Moreover, the Friis transmission formula is not able to capture all the spectral characteristics of the different UWB pulses and the antennas used in the communications link. For that reason all the antenna related parameters in the Friis formula were replaced with a single term called the *antenna coupling gain* G_{AP} which fully captures the pulse's spectrum characteristics and its interaction with the used antennas. Therefore, an antenna's G_{AP} is **pulse** dependent.

It was shown that G_{AP} can be easily calculated by taking a sample time domain measurement of the desired pulse and the antenna pair of the link. Furthermore, if the S_{21} parameters of the antenna pair are available the calculation of the G_{AP} for different pulses also is an easy task because the prospective pulse can be mathematically generated and by using a simple Matlab script the received pulse and G_{AP} can be calculated.

The claim that the G_{AP} is more accurate than the traditional method was verified by estimating G_{AP} for four pairs of UWB antennas both by using the time domain method and the S_{21} method which were found to be in close agreement to each other. Furthermore, it was demonstrated that the Friis formula can not capture all the cases by generating some cases of Gaussian and Gaussian monocycle pulses with different spectrum characteristics.

It was found that the proposed method of using G_{AP} consistently and accurately predicts the link budget for both energy and peak power scenarios. On the other hand, the Friis formula, though it was found for many cases involving the estimation of an energy-based link budget to be accurate, does not provide sufficient accuracy for all cases. Furthermore, using the Friis formula for the received peak power estimation was inaccurate suggesting that it can not be used for calculating a peak power (detector) link budget. The predicted link budgets were verified using the sample LOS and NLOS measurements taken in the validation section.

In this report, G_{AP} it was only measured using one pulse. However, it was calculated for several pulses. Future work can complement this work by estimating G_{AP} for different pulses using both proposed methods. This suggestion requires the availability of a pulser(s) that can generate a variety of pulses.

The main focus of this chapter was to verify the received energy/power estimation component of the proposed link budget. Future work can further investigate and verify other important parameters of the link budget, such as receiver structure dependence and losses due to pulse mismatch because of the channel distortion. In addition, it may propose a much more thorough and elaborate link budget. Finally, if the right equipment are available a complete communications link can be predicted with the link budget and be implemented for verification.

Vita

From 1999 to 2002 Haris I. Volos attended the Higher Technical Institute in Nicosia, Cyprus. Volos graduated with a Higher National Diploma (HND) in Electrical Engineering and was awarded Best Performance in both Electronic and Power Engineering subjects. In 2002 Volos was awarded an International Student Scholarship and attended Old Dominion University, where he was a graduate of the honors college with a BS (summa cum laude) in Electrical Engineering and a minor in Computer Engineering. In 2004 Volos was awarded the Cyprus America Scholarship Program CASP Scholarship for MS studies at Virginia Polytechnic Institute and State University.

Bibliography

[1] Opeermann, I.; Hämäläinen, H.; linatti, J., *UWB Theory and Applications.* West Sussex, England: John Wiley & Sons Ltd 2004

[2] Joon-Yong Lee; Scholtz, R.A., "Ranging in a dense multipath environment using an UWB radio link," *Selected Areas in Communications, IEEE Journal on*, vol.20, no.9pp. 1677- 1683, Dec 2002

[3] Chung, W.C.; Ha, D., "An accurate ultra wideband (UWB) ranging for precision asset location," *Ultra Wideband Systems and Technologies, 2003 IEEE Conference on* , vol., no.pp. 389- 393, 16-19 Nov. 2003

[4] Hahafsza, B.R., *Introduction to Radar Analysis*, Boca Raton, Florida: CRC Press LLC, 1998

[5] Reed,J. H.; Ed., *An Introduction to Ultra Wideband Communications Systems,* Crawfordsville, Indiana: Prentice Hall, 2005.

[6] Proakis, J. G., *Digital Communications.* Boston, Massachusetts: McGraw-Hill, 4th ed., 2001

[7] Rappaport, T. S., *Wireless Communications: Principles and Practice.* Upper Saddle River, New Jersey: Prentice Hall, 2002

[8] Urkowitz, H., *Signal Theory and Random Processes*, Artech House, 1983.

[9] Scholtz, R.A.; Cramer, R.J.-M.; Win, M.Z., "Evaluation of the propagation characteristics of ultra-wideband communication channels," *Antennas and Propagation Society International Symposium, 1998. IEEE* , vol.2, no.pp.626-630 vol.2, 21-26 Jun 1998

[10] Donlan, B.M.; Venkatesh, S.; Bharadwaj, V.; Buehrer, R.M.;Jiann-An Tsai, "The ultra-wideband indoor channel," *Vehicular Technology Conference, 2004. VTC 2004-Spring. 2004 IEEE 59th* , vol.1, no.pp. 208- 212 Vol.1, 17-19 May 2004

[11] Ghassemzadeh, S.S.; Greenstein, L.J.; Kavcic, A.; Sveinsson, T.; Tarokh, V., "UWB indoor path loss model for residential and commercial buildings," *Vehicular Technology*

Conference, 2003. VTC 2003-Fall. 2003 IEEE 58th , vol.5, no.pp. 3115- 3119 Vol.5, 6-9 Oct. 2003

[12] Molisch, A.F.; Foerster, J.R.; Pendergrass, M., "Channel models for ultrawideband personal area networks," *Wireless Communications, IEEE [see also IEEE Personal Communications]* , vol.10, no.6pp. 14- 21, Dec. 2003